UNIVERSIDADE ESTADUAL DE CAMPINAS

Instituto de Geociências

KEYLA THAYRINNE OLIVEIRA COIMBRA

AVALIAÇÃO DE ECOSSISTEMAS AQUÁTICOS ATINGIDOS PELA LAMA DE REJEITO DO COLAPSO DA BARRAGEM DE FUNDÃO, MARIANA-MG: UMA PERSPECTIVA VIA SENSORIAMENTO REMOTO

AN ASSESSMENT OF AQUATIC ECOSYSTEMS AFFECTED BY THE FUNDAO TAILINGS DAM COLLAPSE, MARIANA-MG: A PERSPECTIVE BY REMOTE SENSING

CAMPINAS

2020

KEYLA THAYRINNE OLIVEIRA COIMBRA

AVALIAÇÃO DE ECOSSISTEMAS AQUÁTICOS ATINGIDOS PELA LAMA DE REJEITO DO COLAPSO DA BARRAGEM DE FUNDÃO, MARIANA-MG: UMA PERSPECTIVA VIA SENSORIAMENTO REMOTO

AN ASSESSMENT OF AQUATIC ECOSYSTEMS AFFECTED BY THE FUNDAO TAILINGS DAM COLLAPSE, MARIANA-MG: A PERSPECTIVE BY REMOTE SENSING

TESE APRESENTADA AO INSTITUTO DE GEOCIÊNCIAS DA UNIVERSIDADE ESTADUAL DE CAMPINAS PARA OBTENÇÃO DO TÍTULO DE DOUTORA EM CIÊNCIAS NA ÁREA DE GEOLOGIA E RECURSOS NATURAIS

THESIS PRESENTED TO THE INSTITUTE OF GEOSCIENCES OF THE UNIVERSITY OF CAMPINAS TO OBTAIN THE DEGREE OF DOCTOR IN SCIENCIAS IN AREA OF GEOLOGY AND NATURAL RESOURCES

ORIENTADOR(A): PROF. DR. CARLOS ROBERTO DE SOUZA FILHO

COORIENTADOR(A): PROF. DR. ENNER ALCÂNTARA

ESTE EXEMPLAR CORRESPONDE À VERSÃO FINAL DA TESE DEFENDIDA PELA ALUNA KEYLA THAYRINNE OLIVEIRA COIMBRA, ORIENTADA PELO PROF. DR. CARLOS ROBERTO DE SOUZA FILHO E COORIENTADA PELO PROF. DR. ENNER ALCÂNTARA.

CAMPINAS

2020

Ficha catalográfica
Universidade Estadual de Campinas
Biblioteca do Instituto de Geociências
Marta dos Santos - CRB 8/5892

Coimbra, Keyla Thayrinne Oliveira, 1990-
C665a Avaliação de ecossistemas aquáticos atingidos pela lama de rejeito do colapso da barragem de Fundão, Mariana-MG : uma perspectiva via sensoriamento remoto / Keyla Thayrinne Oliveira Coimbra. – Campinas, SP : [s.n.], 2020.

Orientador: Carlos Roberto de Souza Filho.
Coorientador: Enner Herenio de Alcântara.
Tese (doutorado) – Universidade Estadual de Campinas, Instituto de Geociências.

1. Sensoriamento remoto. 2. Barragens de rejeitos. 3. Água - Qualidade. 4. Doce, Rio (MG e ES). 5. Abrolhos, Arquipélago dos (BA). I. Souza Filho, Carlos Roberto de, 1965-. II. Alcântara, Enner Herenio de, 1981-. III. Universidade Estadual de Campinas. Instituto de Geociências. IV. Título.

Informações para Biblioteca Digital

Título em outro idioma: An assessment of aquatic ecosystems affected by the Fundão tailings dam collapse, Mariana-MG : a perspective by remote sensing
Palavras-chave em inglês:
Remote Sensing
Tailings dams
Water quality
Doce River (Minas Gerais and Espírito Santo, Brazil)
Abrolhos (Brazil)
Área de concentração: Geologia e Recursos Naturais
Titulação: Doutora em Ciências
Banca examinadora:
Carlos Roberto de Souza Filho [Orientador]
Jurandir Zullo Junior
Marcos Cesar Ferreira
Tati de Almeida
Luciana de Resende Londe
Data de defesa: 30-09-2020
Programa de Pós-Graduação: Geociências

Identificação e informações acadêmicas do(a) aluno(a)
- ORCID do autor: https://orcid.org/0000-0001-8884-722X
- Currículo Lattes do autor: http://lattes.cnpq.br/2761055156500315

UNIVERSIDADE ESTADUAL DE CAMPINAS
INSTITUTO DE GEOCIÊNCIAS

AUTORA: KEYLA THAYRINNE OLIVEIRA COIMBRA

Avaliação de ecossistemas aquáticos atingidos pela lama de rejeito do colapso da barragem de Fundão, Mariana-MG: Uma perspectiva via sensoriamento remoto

An assessment of aquatic ecosystems affected by the Fundao tailings dam collapse, Mariana-MG: a perspective by remote sensing

ORIENTADOR: PROF. DR. CARLOS ROBERTO DE SOUZA FILHO
COORIENTADOR: PROF. DR. ENNER ALCÂNTARA

Aprovada em: 30/09/2020

EXAMINADORES:

Prof. Dr. Carlos Roberto de Souza Filho - Presidente

Profa. Dr. Jurandir Zullo Junior

Prof. Dr. Marcos Cesar Ferreira

Prof. Dr. Tati de Almeida

Dra. Luciana Resende Londe

A Ata de Defesa assinada pelos membros da Comissão Examinadora consta no processo de vida acadêmica do aluno.

Campinas, 30 de setembro de 2020.

SÚMULA CURRICULAR

Keyla Thayrinne Oliveira Coimbra

Possui bacharelado em Geologia pela Universidade Federal de Mato Grosso (2013) e mestrado em Geociências pelo programa de Geodinâmica e Geofísica da Universidade Federal do Rio Grande do Norte (2015). Sua trajetória profissional sempre foi voltada para a academia. Durante a graduação em Geologia fez dois estágios, sendo um no Departamento Nacional de Produção Mineral de Cuiabá-MT e outro supervisionado no Centro de Geologia Eschwege, em Diamantina-MG. Já os três estágios vivenciados durante a Pós-Graduação, fazem referência à carreira de docente. Durante a graduação se dedicou aos estudos sobre a evolução Neoproterozoica da Provícia Tocantins, Centro Oeste do Brasil, realizando o mapeamento geológico de uma região situada em Cocalinho-MT. A pesquisa de mestrado foi continuidade dos estudos do trabalho de conclusão de curso da graduação. No doutorado, concentrou-se no estudo de sistemas aquáticos atingidos por desastres ambientais usando dados de sensoriamento remoto. Em síntese, empenhada em desenvolver a ciência com novas abordagens e procedimentos técnicos para implementar a modelagem com dados geoespaciais. Interessa-se especialmente para questões voltadas ao estudo dos recursos hídricos, avaliação de ecossistemas contaminados por diversas fontes e mudanças climáticas.

Com amor dedico esse trabalho aos meus pais, José Ailton e Dalila.

AGRADECIMENTOS

Agradeço ao meu orientador prof. Dr. Carlos Roberto de Souza Filho que acreditou em mim e abriu espaço para que eu pudesse me juntar ao grupo de pesquisa. Gratidão pelo acolhimento, suporte, conselhos, e por todos os conhecimentos transmitidos. Ao meu Coorientador, Enner Alcântara, pelo incentivo, atenção, paciência e por todos os ensinamentos.

Minha sincera gratidão aos componentes da banca de qualificação e defesa da tese de pela grande contribuição e valiosas sugestões para melhorar o trabalho; profas. Dras. Paulina Riedel, Tati Almeida e Luciana Londe; e os profs. Drs. Jurandir Zullo Jr e Marcos Ferreira.

Agradeço à Coordenação de Aperfeiçoamento de Pessoal de Nível Superior pelo apoio financeiro e ao Departamento de Geologia e Recursos Naturais, Instituto de Geociências, Universidade Estadual de Campinas pela infraestrutura. Agradeço a todos os colaboradores do IG, em especial Valdirene, Edinalva, Cristina, e Bárbara, da secretaria; e também a Lúcia da alternativa, pela amizade e pelo carinho ao manter o ambiente da salinha de estudos tão organizado. Agradecimento em especial a equipe de Tecnologia da Informação e Comunicação (TIC) pelo importante suporte durante todo o curso do doutorado.

Agradeço aos amigos do IG pelo companheirismo e produtivas discussões científicas nos inúmeros cafés ou *happy hours*. Obrigada, João Mota, Priscilla, Saeid, Rosa, Rebecca, Alcione, Raissa, JP, Cebola.

Agradeço ao IBAMA de São Paulo, especialmente a Cláudio Dubas, pelo apoio durante as visitas de campo e por fornecer as imagens de satélite de alta resolução espacial usadas na pesquisa. Toda equipe de campo, incluindo os agentes do IBAMA de Minas Gerais e os professores da Universidade Federal de Viçosa, muito obrigada!

Agradeço minha família, que mesmo distante sempre foi tão presente em minha vida, sempre me apoiando e me dando força. Obrigada pai, mãe, irmãos, cunhada, e sobrinhos. Agradeço em especial meu irmão Kylmer, pela amizade e pela grande ajuda prestada na etapa de campo.

Agradeço a família da República Ra-tim-bum de Barão Geraldo. Ma, Bel, Syllas, Rafa, Miltiane, Rocio, Dara, Óscar, Théo e Amy. E também o Guilherme, pela amizade de sempre. Guardo no coração todos os momentos compartilhados. Agradecimento em especial para as manas Ma, Bel, e Syllas, não tenho palavras para expressar o quanto sou grata por ter vocês em minha vida.

Agradeço aos integrantes da ONG amparar pelo grande exemplo de amor ao próximo, que por meio de gestos tão nobres e bonitos que me convidaram a ter outras perspectivas sobre os problemas da vida.

Agradeço minhas amigas pantaneiras, sempre juntas desde a graduação. Obrigada Sussu e Cleide pelo carinho e apoio.

Agradeço a Deus por me guiar por caminhos que me levaram para lugares onde eu pude vivenciar inúmeras experiências que me fizeram uma pessoa melhor, e onde tive oportunidade de evoluir profissionalmente. Gratidão universo por sempre colocar pessoas queridas e amorosas em minha vida.

O presente trabalho foi realizado com apoio da Coordenação de Aperfeiçoamento de Pessoal de Nível Superior – Brasil (CAPES) - Código de Financiamento 001.

RESUMO

O colapso da barragem de Fundão em Mariana (MG), em 05 de novembro de 2015, gerou uma avalanche de rejeito que atingiu todo curso do rio Doce e seus principais afluentes, incluindo os rios Gualaxo do Norte e do Carmo. A avalanche teve grande poder de destruição. Soterrou todo distrito de Bento Rodrigues e Paracatu de Baixo. Perdeu energia somente quando alcançou a região da Usina Hidrelétrica Risoleta Neves (UHRN), 136 km a jusante de Fundão. Nesse local, 80% do rejeito de Fundão foi retido pela barragem da usina. A lama que atravessou esse obstáculo alcançou a foz do rio Doce, no Espírito Santo, dias depois. Grande parte das áreas atingidas ainda possui uma disposição de rejeito nas margens e no leito dos principais cursos d'água. Após quatro anos, em episódios de chuva, esse material continua sendo carreado para a calha do rio. Fica, assim, disponível no meio ambiente e representa uma grande ameaça para o ecossistema, biodiversidade e saúde humana. Nessa tese, o objetivo geral da pesquisa foi estabelecer critérios de monitoramento ambiental em múltiplas escalas e compreender a dinâmica dos sistemas fluvial e costeiro atingidos pela lama. Para tanto, foram gerados parâmetros bio-ópticos e indicadores de qualidade da água, extraídos de dados de sensoriamento remoto orbital. Em escala continental, a série histórica de dados e produtos derivados do sensor multiespectral MODIS (satélites Terra e Aqua; pixel de 1km) foi utilizada para obter representações espaço-temporais da pluma de sedimentos do Rio Doce e região costeira. Os indicadores foram utilizados para avaliação das propriedades ópticas aparentes e componentes opticamente ativos da água após o colapso e, subsequentemente, comparados com aqueles abstraídos de um evento natural extremo, ocasionado por um ciclo de precipitação atípica que atingiu a região em 2013. Os resultados indicam que ambos os eventos têm efeitos consideráveis sobre a penetração de luz na coluna de água, mas com intensidade e durações distintas. Em escala de semi-detalhe, uma série temporal de imagens de 30 m de resolução espacial do sensor OLI/Landsat-8, adquiridas pré e pós-colapso da barragem, foram utilizadas para quantificar as áreas afetadas e verificar se o material do rio Doce alcançou a região do Arquipélago de Abrolhos (na costa do Estado da Bahia). Os resultados indicam uma tendência crescente de material particulado em suspensão (SPM) nessas regiões entre 2015 e 2019. Durante o verão, a pluma de sedimentos do rio Doce foi direcionada para o Sul, porém, no inverno, ocorreram mudanças nos padrões de direção do vento. Nesse episódio, a pluma de sedimentos foi invertida para o Norte, alcançando grandes proporções da costa e, possivelmente, atingindo o Arquipélago de Abrolhos. Na região *onshore* atingida pelo colapso, os esforços foram direcionados para avaliação detalhada de três importantes reservatórios do rio Doce. O objetivo foi analisar o avanço da eutrofização da água após o colapso. A metodologia consistiu na parametrização do Material Particulado em Suspensão (SPM), Zona Eufótica (Z_{eu}) e Clorofila-*a* (Chl-*a*) via imagens do sensor OLI/Landsat-8. A série temporal analisada compreende dados de 2013 a 2019. Os resultados mostraram mudanças significativas na concentração de Chl-*a*, após o colapso. O avanço do estado trófico dos reservatórios pode estar associado aos contaminantes espalhados pela lama de rejeito.

Palavras Chave: Sensoriamento remoto; Rio Doce; colapso de barragem de Fundão; arquipélago de Abrolhos; indicadores de qualidade da água.

ABSTRACT

The collapse of the Fundao dam in Mariana, Minas Gerais State, Brazil, on November 5th, 2015, released an avalanche of tailings that reached the entire course of the Doce River and some of its affluents, including the Gualaxo do Norte and Carmo Rivers. The high-energy avalanche covered the Bento Rodrigues and Paracatu de Baixo districts. It lost strength only when it reached the Risoleta Neves Hydroelectric Power Plant (UHRN), some 136 km downstream of the Fundao dam. Approximately 80% of the tailings were retained by the UHRN dam. The rest of the mud that crossed this obstacle reached the mouth of the Doce River, in Espírito Santo a few days later. Currently, most of the affected areas still have tailings on the margins of the main watercourses. Even after four years, in rainy episodes, this material continues to be carried to the river channel. Therefore, it is available in the environment, representing a major threat to the ecosystem, biodiversity and human health. The main goals of this research were to establish criteria for environmental monitoring at multiple scales and to understand the dynamics of the fluvial and coastal systems affected by the mud. To achieve these objectives, bio-optical parameters and water quality indicators from orbital remote sensing data were used. At continental scale, a time series of MODIS multispectral sensor (Terra and Aqua satellites; 1km pixel) data were used to obtain space-time representations of the Doce river sediments plume and coastal regions. Indicators based on these data were computed to assess the apparent optical properties and optically active components of water after the collapse and, subsequently, compared to those abstracted from an extreme natural event, caused by an atypical precipitation cycle that hit the region in 2013. Results show that both events have considerable effects on the light penetration into the water column, however with different intensity and duration. At semi-detail scale, a time series of 30 m spatial resolution OLI /Landsat-8 images were employed. Data comparison between before and after the dam collapse was made to quantify the affected areas and verify if the Doce River sediments reached the Abrolhos Archipelago (Bahia State). Results indicate a growing trend in suspended particulate matter (SPM) in the region from 2015 to 2019. During the summer, the sediment plume of the Doce River was directed to the South; however, in the winter, changes in the wind direction patterns occurred. In this episode, the sediment plume was inverted towards the North, reaching large proportions of the coast and possibly reaching the Abrolhos Archipelago. In the onshore area affected by the collapse, the research focus was a detailed assessment of three important Doce River reservoirs. The objective was to analyze the water eutrophication after the collapse. The methodology includes the parameterization of Particulate Material in Suspension (SPM), Euphotic Zone (Z_{eu}) and Chlorophyll-a (Chl-*a*) from the OLI / Landsat-8 sensor images. The time series comprised data from 2013 to 2019. Results show a significant increase in the Chl-*a* content after the collapse. The advance of the trophic state observed in the reservoirs may be related with the contaminants spread by the tailings mud along the Doce river course.

Keywords: Remote sensing; Doce River; Fundao dam collapse; Abrolhos archipelago; water quality indicators.

LISTA DE FIGURAS

LISTA DE TABELAS

SUMÁRIO

APRESENTAÇÃO

A tese foi estruturada em formato de artigos, seguindo as normas do programa de Pós-graduação em Geociências da Universidade Estadual de Campinas. O capítulo 1 consiste em uma introdução geral de todo conteúdo, onde são pontuadas as hipóteses testadas na pesquisa e também os objetivos, caracterização da área de estudo e síntese dos resultados. No capítulo 2, tem-se a contextualização do tema da tese, que foi amparada na revisão bibliográfica de artigos, relatórios e notícias, assim como na exposição de fotos e imagens de satélite de alta resolução espacial. Na sequência, dos capítulos 3 ao 5, tem-se a apresentação dos artigos. Por último, é apresentada uma breve sessão com as principais conclusões da tese e sugestões para trabalhos futuros.

CAPÍTULO 1

INTRODUÇÃO

Os desastres socioambientais têm aumentando cada vez mais, principalmente devido às mudanças climáticas, aumento populacional, globalização e o consequente aumento da demanda por produtividade. Esses desastres incluem fenômenos meteorológicos, como tempestades, inundações, terremotos, avalanches, tsunamis, erupções vulcânicas, ou episódios de seca, como a desertificação (Garcia et al., 2017). No Brasil, é notável a ocorrência de desastres socioambientais, como secas severas (como aquelas que ocorrem no núcleo de desertificação do nordeste e no norte de Minas Gerais), deslizamento de terra e inundações, que ocorrem em várias regiões do país (Tomasella et al., 2018).

Já os desastres com influencia antropogênica (ou riscos tecnológicos) têm origem em condições tecnológicas ou industriais, procedimentos perigosos, falhas de infraestrutura ou atividades humanas específicas (https://www.undrr.org/terminology/hazard). São exemplos desses desastres, falhas em barragens, colapso de pontes, acidentes industriais, colisões marinhas, derramamento de óleo, deposição de resíduos tóxicos e radioativos (Baum et al., 1983; Lari et al., 2009).

O número de desastres com influência antropogênica envolvendo barragem de rejeito em mineração mostra uma tendência mundial crescente desde 1970. Só na última década, foram registrados pelo menos 50 falhas em barragens em todo o mundo, das quais as nove mais graves estão destacados na Fig. 1. (https://worldminetailingsfailures.org/). Desse recorte, três dos acidentes de maior impacto aconteceram no Brasil: o desastre do rio Pomba em 2007 (Rio de Janeiro, RJ), o colapso da barragem de Fundão em 2015 (Mariana, MG), e o colapso da barragem de Córrego do Feijão em 2019 (Brumadinho, MG).

As barragens de Brumadinho e de Mariana são propriedades da mineradora SAMARCO. Foram construídas com base no método tipo "*Upstream*" - um método de construção mais barato e menos estável (ICOLD, 2001). Nesse tipo de construção, a barragem é formada com o próprio material bombeado da mina. No caso de Brumadinho, estima-se que 12 milhões de m^3 de rejeito foram extravasados da

barragem após o colapso; já em Fundão, cerca de 43 milhões de m^3 de rejeito. A pesquisa aqui apresentada focou no estudo de caso do colapso da barragem de Fundão.

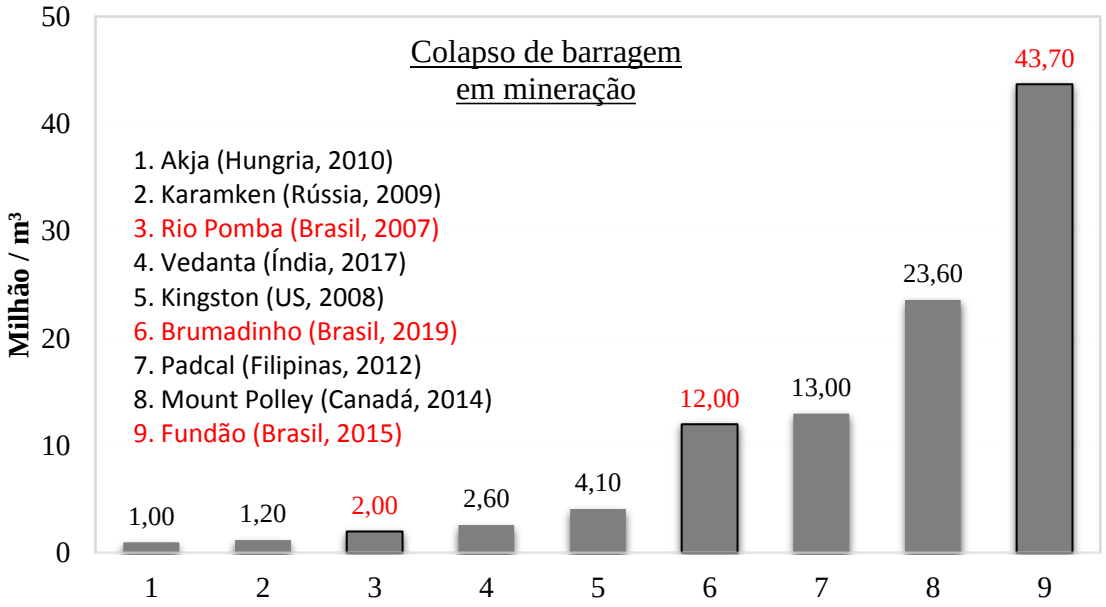

Fig. 1. Panorama das ocorrências de desastres tecnológicos relacionados a barragens de mineração. Fonte: (https://worldminetailingsfailures.org/). Em vermelho estão destacados os desastres em barragens no Brasil.

A barragem de Fundão encontra-se dentro dos limites da bacia do rio Doce, que abrange parte dos Estados de Minas Gerais e Espírito Santo, no Sudeste do Brasil (Fig. 2A). Devido ao seu desenvolvimento histórico de atividades econômicas voltadas para extração mineral, a bacia abriga diversas estruturas para deposição de rejeitos derivados dessa atividade. No Brasil, há registros de acidentes envolvendo pilhas de rejeitos de mineração, porém, nenhum deles atingiu as proporções do evento ocorrido em Fundão, no município de Mariana-MG, em 05 de novembro de 2015 (CRH-ANA, 2015).

Com o rompimento desta barragem, uma mistura de rejeito e água foi liberada, destruindo o distrito de Bento Rodrigues e parte de Paracatu de Baixo, deixando os rios Gualaxo do Norte e Carmo intensamente assoreados (Carmo et al., 2017). Estima-se que cerca de 80% desse material foi retido pela barragem da Usina Hidrelétrica Risoleta Neves (UHRN), a 136 km do local do colapso (Fig. 2B). A porção que ultrapassou essa barreira chegou até a foz do rio Doce, no oceano Atlântico, no dia 21 de novembro de 2015 (CPRM, 2015a; PCGRSS, 2016).

A passagem da onda de lama causou a morte e desaparecimento de pessoas e animais, isolamento e destruição de áreas urbanas, rurais e de preservação permanente (Fernandes et al., 2016). Como consequência, serviços ecossistêmicos foram afetados, refletindo na suspensão do abastecimento público de água, restrição à pesca e turismo, além do comprometimento da geração de energia pelas hidrelétricas atingidas (IBAMA, 2015).

Diante do cenário aqui exposto, é imprescindível o desenvolvimento de pesquisas científicas que forneçam subsídios para o entendimento dos efeitos do colapso da barragem no meio físico, que atingiu grandes proporções de ecossistemas aquáticos, tanto da parte *onshore* da bacia do rio Doce quanto *offshore*. Abordagens de monitoramento ambiental com coleta de amostras pontuais demandam grande investimento de tempo e recursos financeiros. Em áreas muito extensas, como no caso do rio Doce, esse tipo de amostragem não mostra representatividade espacial. Assim, justifica-se o uso de metodologias com dados de sensoriamento remoto, pois as imagens podem ser obtidas por vários satélites de forma gratuita, como por exemplo, as imagens do MODIS/Aqua e do OLI/Landsat-8, utilizadas nessa pesquisa. Esse tipo de dado pode ser acessado por meio de plataformas *on-line*, que oferecem a série histórica de uma gama de produtos.

Modelos parametrizados com dados de sensoriamento remoto, por meio de métodos estatísticos ou técnicas de otimização numérica, são amplamente empregados nos estudos de qualidade da água. Eles podem fornecer importantes indicadores dos parâmetros físicos, químicos ou biológicos do ecossistema. Esses estudos consideram as propriedades ópticas da água para a calibração e parametrização de algoritmos, tais como refletância de sensoriamento remoto (R_{rs}), coeficiente de atenuação difusa da irradiância descendente (K_d), o coeficiente de absorção total (*a)* e o coeficiente de retroespalhamento (b_b) (Alcântara et al, 2013).

Tais modelos têm sido desenvolvidos em diferentes regiões do Brasil e do mundo, com resultados satisfatórios (e.g. Miller et al., 2004; Chen et al., 2006; Lahet e Stramski., 2010; Augusto-Silva et al., 2014; Gangloff et al., 2017; Gomes et al., 2020; Kark et al., 2020; Nechad e Park., 2010; Nechad et al., 2010; Pahlevan et al., 2020; Zhao et al., 2013). Uma das vantagens dessas abordagens é que os algoritmos podem ser ajustados para diferentes ambientes.

Transcorridos mais de quatro anos desde o colapso de Fundão, ainda há quantidade considerável de rejeito nas margens dos afluentes do rio Doce e na região da UHRN (RAMBOLL, 2019). Em estações chuvosas, os metais potencialmente tóxicos associados aos sedimentos finos das margens dos rios podem ser carreados e conduzidos pelos cursos d'agua, ficando disponíveis no meio e podendo alcançar a região costeira (Eg. Segura et al., 2016, Hatje et al., 2017, Gomes et al., 2017, Botino et al., 2017; Queiroz et al., 2018; Weber et al., 2020; Fernandes et al., 2020; Passos et al., 2020).

Além dos danos à biodiversidade e à saúde humana, a presença desses metais nos ecossistemas pode acarretar o avanço da eutrofização da água (Gomes et al., 2020; Fielding et al., 2020; Nwankwegu et al., 2020). Isto posto, um dos focos desta tese de doutorado foi verificar se houve, de fato, o aumento da biomassa do fitoplâncton em áreas do rio Doce atingidas pela lama e se essas possíveis alterações podem estar associadas a mudanças físico-químicas dos ecossistemas atingidos pela lama.

No contexto da área offshore afetada pelo colapso, os esforços compreendidos na pesquisa visaram à compreensão da dinâmica sazonal da pluma de sedimentos do rio Doce. Uma das questões científicas que pretendeu-se responder foi: há diferenças nos padrões bio-ópticos da água da foz do rio Doce num período em que foi registrada a maior enchente da última década e os meses posteriores ao colapso? Em ambas as situações, houve uma grande quantidade de sedimentos transportados da bacia do rio Doce para o mar. As partículas em suspensão podem estar associadas a contaminantes espalhados pela avalanche de lama, expondo toda biodiversidade aquática (Eg. Segura et al., 2016, Hatje et al., 2017, Gomes et al., 2017, Botino et al., 2017; Queiroz et al., 2018; Weber et al., 2020; Fernandes et al., 2020; Passos et al., 2020)

Na região costeira, os sedimentos em suspensão na água podem ser transportados por longas distâncias e são fortemente influenciados pelas marés e direção do vento (Dominguez, 2004; Dominguez et al., 1991; Dominguez et al., 1983). É possível que o material descarregado na foz do rio Doce após o colapso tenha alcançado importantes áreas de conservação marinha, como por exemplo, o Arquipélago de Abrolhos, no sul da Bahia. A demonstração dessa hipótese está também compreendida nesta tese.

1.1. **Objetivos**

O objetivo geral da tese é contribuir para a compreensão de efeitos do colapso da barragem de Fundão sobre reservatórios do rio Doce e, ecossistemas aquáticos oceânicos, atingidos pela lama de rejeito de Fundão.

Os objetivos específicos incluem:

- Comparação dos efeitos da inundação do rio Doce (dezembro de 2013) e do colapso da barragem (novembro de 2015), particularmente no que se refere à análise das propriedades ópticas aparentes e os componentes opticamente ativos da água, na foz do rio Doce;
- Análise espaço-temporal da dinâmica da pluma de sedimentos a partir da foz do Rio Doce até a região costeira e oceânica adjacente, avaliando sua direção e alcance, em conformidade com a variação sazonal pré e pós-colapso;
- Verificação de possíveis alterações nos padrões de material particulado em suspensão na região do Arquipélago de Abrolhos e entorno, após o colapso; discussão da possibilidade de os rejeitos trazidos pelo rio Doce ter alcançado a região;
- Análise espaço-temporal dos parâmetros bio-ópticos e indicadores de qualidade da água de reservatórios do rio Doce, para avaliar o avanço da eutrofização da água após o colapso.

1.2. Área de Estudo

A pesquisa foi desenvolvida em duas frentes de trabalho considerando-se as regiões *offshore* e *onshore* afetadas pelo colapso (Fig. 2).

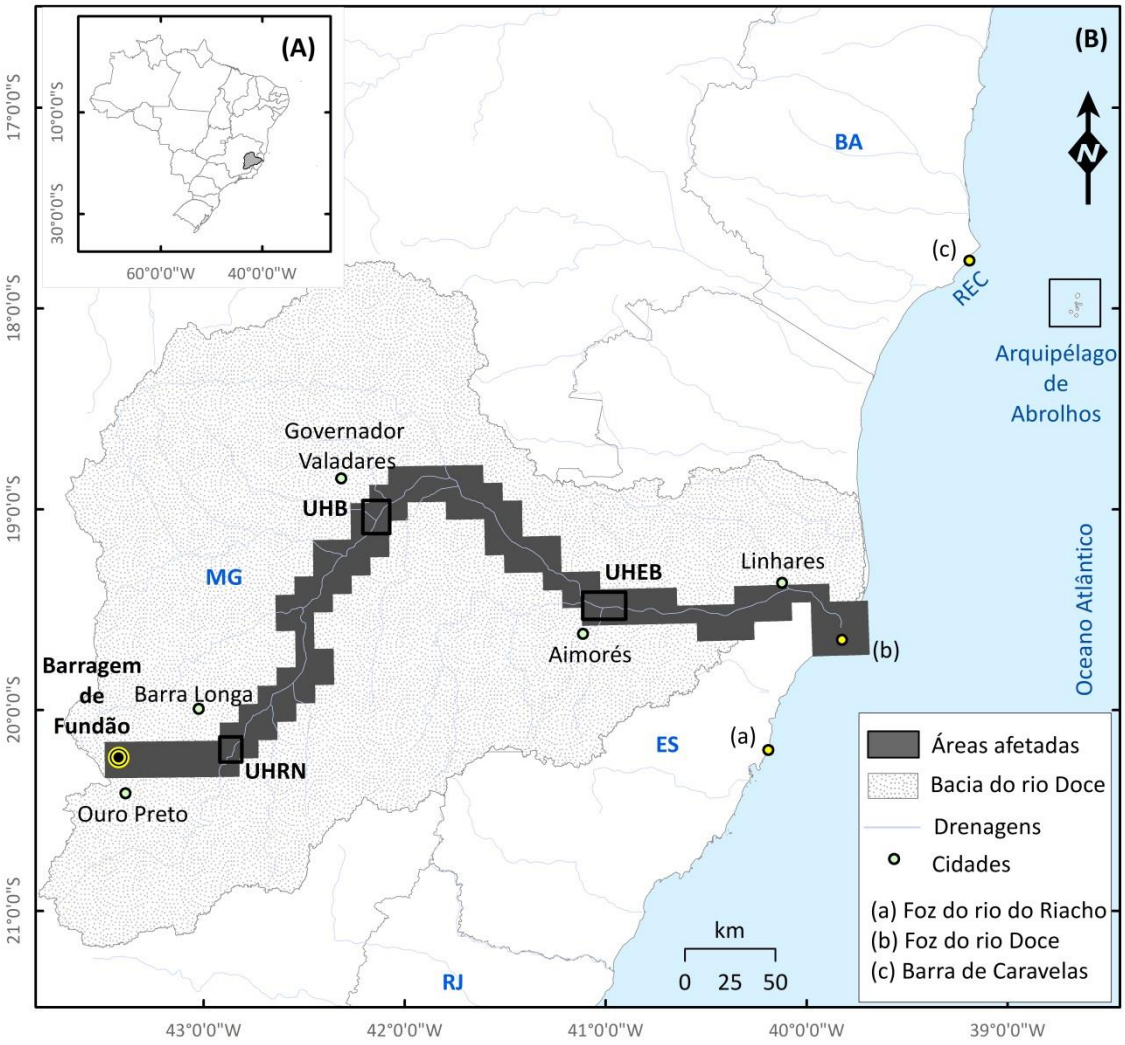

Fig. 2. (A) Localização da bacia hidrográfica do rio Doce no Brasil. (B) Detalhe para a bacia do rio Doce e a extensão de toda a área continental atingida pela lama de rejeito, que vai desde o local da barragem de Fundão, em Mariana, até a foz do rio Doce, no oceano Atlântico. UHRN – Usina Hidroelétrica Risoleta Neves. UHB – Usina Hidroelétrica Baguari. UHEB – Usina Hidroelétrica Eliezer Batista. A região oceânica investigada na pesquisa inclui toda região costeira, desde a foz do rio do Riacho até a foz da Barra de Caravelas, onde está a Reserva extrativista de Cassurubá (REC) e o Arquipélago de Abrolhos. (a) Foz do rio do Riacho; (b) Foz do rio Doce; (c) Barra de Caravelas.

1.2.1. Área atingida: Offshore

A região *offshore* engloba uma extensa área, que vai desde a foz do rio do Doce (no Espírito Santo), até a Barra de Caravelas (na Bahia), e inclui também a Reserva Extrativista de Cassurubá (REC) e o Arquipélago de Abrolhos (Fig. 2B).

A costa do Espírito Santo (ES) está inserida na porção oriental do litoral brasileiro. É uma região caracterizada por chuvas tropicais de verão e estação seca durante o outono e inverno, com uma temperatura média anual de 22° C (Bernardino et al., 2015).

A foz do rio Doce recebe uma expressiva quantidade de material clástico proveniente da bacia. Trata-se de uma região caracterizada por conter o maior e mais importante delta da costa brasileira (com área de 2.500 km²), que tem potencial para carrear sedimentos por longas distâncias (Dominguez, 2004; Dominguez et al., 199; Dominguez et al., 1983). O transporte de sedimentos é influenciado pela ação das marés e do vento, que em grande parte do ano apresentam direções associadas aos ventos alísios (N e NE); porém, eventualmente, podem ter influência dos ventos do Sul, em episódios de frente fria (LACTEC, 2019)

O delta do rio Doce é subdividido por setores (Quaresma et al., 2015). O setor sul é dominado por areia fina e lama. Em eventos de tempestade, os depósitos nas prateleiras internas podem ser remobilizados e transportados para o norte. O setor centro-norte é uma região de influência fluvial que possui predominância de areias (finas e médias) e carbonatos. Nessa área, os processos deposicionais são menos frequentes e é onde ocorre o desvio de sedimentos ressuspensos durante eventos de tempestade. O setor norte possui alto conteúdo de carbonato e é caracterizado por maior taxa de deposição.

A REC está localizada no sul da Bahia, inserida em uma unidade de conservação prioritária que abrange parte da região costeiro-marinha dos municípios de Caravelas, Nova Viçosa e Alcobaça (https://uc.socioambiental.org/pt-br/arp/4778). Essa reserva tem cerca de 100.462,00 ha, sendo constituída por manguezais, formações de restinga, remanescentes de floresta atlântica e ambientes costeiro-marinhos. A REC, junto ao Arquipélago de Abrolhos, tem extrema importância ambiental na região do Atlântico Sul, visto que concentra a maior biodiversidade marinha do Brasil (Nobre et al., 2017).

O Arquipélago de Abrolhos está localizado numa região anômala de plataforma continental, que possui largura de aproximadamente 240 km da linha de costa, sendo uma região relativamente rasa, que não ultrapassa 25 m de profundidade. Existem cinco ilhas vulcânicas na área do Arquipélago: Redonda, Siriba, Sueste, Guarita, e Santa Bárbara (IBAMA, 1991).

A rica diversidade de ambientes costeiros e oceânicos, em conjunto com os fatores geomorfológicos e oceanográficos do Arquipélago de Abrolhos, favorece a

ocorrência de uma elevada biodiversidade na região. O Arquipélago tem destaque pela presença do maior ecossistema de recifes de coral do Atlântico Sul, maior sítio reprodutivo de baleias Jubarte, elevada diversidade e endemismo de peixes recifais e habitat de tartarugas e aves marinhas (Mazzei et al., 2014).

Entre os diversos fatores que propiciam a alta produtividade dessa região destaca-se a mistura de águas costeiras mais profundas com águas quentes provenientes do norte, que são movidas pela corrente do Brasil. Essa corrente é direcionada para o sul, possui uma intensidade maior a partir do Arquipélago dos Abrolhos até a costa do Rio de Janeiro e, progressivamente, fica menos intensa do trópico de Capricórnio para o sul (Werner et al., 2000).

1.2.2. Área atingida: Onshore

A região onshore afetada pelo colapso está dentro das dimensões da bacia do rio Doce, compreendendo uma área aproximada de 640 km de extensão, que integra todo o curso do rio Doce, desde a barragem de Fundão até sua foz, no Espírito Santo. Nessa área, os estudos foram concentrados em reservatórios de três usinas hidroelétricas: Risoleta Neves (UHRN), Baguari (UHB) e Eliezer Batista (UHEB) (Fig. 2B).

- Bacia do rio Doce

A bacia do rio Doce situa-se na região Sudeste do Brasil (Fig. 2A). Possui área de drenagem de, aproximadamente, 86.715 km^2, dos quais 86% pertencem ao Estado de Minas Gerais e o restante ao Espírito Santo. O crescimento econômico centrado na exploração de recursos minerais pressiona o uso e a ocupação do vale do rio Doce, onde existem reservas de minerais metálicos importantes (http://www.cbhdoce.org.br/institucional/a-bacia).

As principais atividades de exploração mineral são aquelas relacionadas à extração de minério de ferro, que somam 31,4% das concessões de lavra, e a extração de rochas ornamentais, que representam 25,1%, destacando-se granitos e gnaisses (CRH-ANA, 2015). As minas de ferro da região operam sob elevado grau de mecanização e equipamentos pesados, sendo empreendimentos de grandes empresas. As duas principais mineradoras que atuam na bacia são a Vale e a Samarco Mineração, as duas maiores produtoras de minério de ferro do país (CRH-ANA, 2015).

O regime pluviométrico da bacia é dividido em um período chuvoso, que vai de outubro a março, e um período de seca, que vai de abril a setembro. O período de chuva é caracterizado por cheias e inundações, em especial ao longo do curso do rio Doce e nos grandes centros urbanos. Esses problemas de inundação são sustentados pelo quadro de grande supressão da cobertura vegetal da bacia. Os remanescentes florestais são restritos às áreas com declives mais acentuados do terreno. Há ainda intensa degradação das áreas de pastagens, que favorece os processos erosivos do solo, formando volumes expressivos de sedimentos que são carreados aos cursos d'água (CRH-ANA, 2015).

A bacia do rio Doce tem um importante potencial hidrelétrico, setor que apresentou a implantação de muitos empreendimentos na última década (http://www.cbhdoce.org.br/institucional/a-bacia). Todavia, esse setor sofreu intensos impactos após o colapso da barragem do Fundão em função do assoreamento dos reservatórios e também da contaminação do meio (SEDRU, 2016).

- Usina Hidrelétrica Risoleta Neves (UHRN)

O Reservatório da UHRN, também conhecida como "Usina de Candonga", está situado mais próximo à cabeceira do rio Doce, a cerca de 136 km a jusante da barragem de Fundão, entre os municípios de Rio Doce e Santa Cruz do Escalvado, Minas Gerais (Fig. 2B). A usina começou a operar em setembro de 2014, com uma área de reservatório de 2,84 km². Antes do colapso, tinha um volume de 54,4 milhões de m³ de água (http://www.candonga.com.br/a-usina/caracteristicas-tecnicas/).

A UHRN foi uma das mais afetadas pelo colapso. Sua barragem foi o primeiro obstáculo encontrado pela onda de lama. Grande quantidade de material proveniente de Fundão ficou retido nessa área. Após a passagem da lama pela UHRN, as consequências em relação ao assoreamento do reservatório se estenderam pelos anos consecutivos (RAMBOLL, 2019). Em momentos de alta precipitação, a água da chuva até hoje carrega aquele material depositado na planície de inundação a montante do rio Doce que, eventualmente, gera alterações nos parâmetros da água em função da ressuspensão de materiais depositados na calha do rio (Hadtje et al., 2017).

Estudos com levantamento batimétrico da UHRN mostraram que, antes do colapso, a vida útil do reservatório seria de 180 anos (LACTEC, 2018). Porém, após o

colapso da barragem, seu funcionamento ficou comprometido. Estima-se que o volume de assoreamento causado pelo rompimento ao reservatório da UHRN é de 10,5 milhões de m³ (https://www.samarco.com/wp-content/uploads/2016/11/Samarco-intensifica-obras-em-Candonga.pdf).

- Usina Hidroelétrica Baguari (UHB)

A UHB está localizada no leito do Rio Doce, em Governador Valadares (Fig.2B), e abrange os municípios mineiros de Periquito, Alpercata, Fernandes Tourinho, Sobrália e Iapu. A usina começou a operar em setembro de 2009 com capacidade para prover energia para 450 mil habitantes. O reservatório possui área inundada na cota máxima de 16 km² e volume de água total de 44 hectômetros/m³, com 22 km de extensão no rio Doce e 5 km no rio Corrente Grande (LACTEC, 2018).

A UHB possui estruturas favoráveis ao fluxo de sedimentos, como soleira do vertedor próxima ao leito, o que permite maior controle do nível de água em todo o ano. Mesmo em momentos de altas vazões, as condições de operação permitem que o reservatório se comporte de maneira similar à condição natural do rio, transferindo os sedimentos diretamente para jusante da barragem (LACTEC, 2018).

- Usina Hidrelétrica Eliezer Batista (EBPP)

A UHEB abrange os municípios de Aimorés, Itueta e Resplendor, em Minas Gerais, e Baixo Gandu, no Espirito Santo (https://aliancaenergia.com.br/br/nossas-usinas/usina-de-aimores/). A usina opera desde maio de 2006, e possui um volume de reservatório de 185,11 hectômetros/m³. Estudos com dados batimétricos mostraram que o aporte de sedimentos e rejeitos advindos do rompimento de Fundão, até dezembro de 2015, foi de aproximadamente 3,35 hectômetros/m³ (LACTEC, 2018).

1.3. Síntese dos Resultados

Para alcançar os objetivos propostos nessa pesquisa, a problemática foi criteriosamente analisada por meio de um estudo multidisciplinar que resultou em três artigos científicos, dois dos quais já foram publicados na revista *Science of the Total Environment* (Fator de Impacto: 6.551) (manuscritos “a” e “b”) e um terceiro foi submetido para a *Environmental Pollution* (Fator de Impacto: 6,792) e encontra-se em avaliação (manuscrito “c”):

(a) Manuscrito intitulado ***"An assessment of natural and technological hazards effects on the solar light field of the Rio Doce River continental shelf"*** (Capítulo 2). Esse estudo foi feito utilizando ferramentas de geotecnologias para avaliar a penetração da luz na água da foz do rio Doce (de 2013 a 2016), tendo como foco dois momentos: a inundação da bacia do rio Doce (que aconteceu em dezembro de 2013) e o colapso da barragem de Fundão (que ocorreu em novembro de 2015). Os resultados mostraram que, em ambos os episódios, aconteceram alterações nos parâmetros bio-ópticos da água, porém, no caso do colapso da barragem de Fundão, os efeitos foram mais duradouros;

(b) O manuscrito intitulado ***"Possible contamination of the Abrolhos reefs by Fundao dam tailings, Brazil – New constraints based on satellite data"*** (Capítulo 3). Esse estudo compreendeu o monitoramento da pluma de sedimentos do rio Doce, com finalidade de indicar possíveis momentos em que o material proveniente da barragem de Fundão atingiu o Arquipélago de Abrolhos e seu entorno. Para tanto, foi realizada uma análise temporal do material particulado em suspensão, obtido com base em algoritmos semi-analíticos e aplicados às imagens do OLI/landsat-8. Foram utilizados também dados meteorológicos de precipitação da chuva e vetores de direção do vento. Após o colapso, houve um aumento do material particulado em suspensão em toda a região costeira. A análise da direção da pluma de sedimentos do rio, em conjunto com os resultados do modelo aplicado, revela que, no inverno, quando ocorrem mudanças nos padrões de direção do vento, do sul para o norte, o material da barragem de Fundão pode ter alcançado o Arquipélago de Abrolhos.

(c) Manuscrito intitulado ***"Satellite Evidence for Pervasive Water Eutrophication in the Doce River Reservoirs following the Fundao Dam Failure, Brazil"*** (Capítulo 4). Esse trabalho envolveu uma avaliação de indicadores de qualidade da água de três importantes reservatórios do rio Doce. O objetivo foi analisar o avanço da eutrofização das áreas estudadas, após o colapso. Para tanto foram utilizados dados do Landsat-8 OLI para estimar a concentração de clorofila, o material particulado em suspensão e a profundidade da zona eufótica. Os resultados mostraram um aumento considerável de clorofila nos reservatórios após o colapso, evidenciando que os poluentes espalhados pela onda de lama da

barragem de Fundão podem ter contribuído para a eutrofização dos reservatórios.

1.4. Referências

Alcântara, E., Nascimento, R., Kampel, M., Stech, J.L., 2013. Uso de propriedades ópticas aparentes e inerentes para a classificação da massa d'água do reservatório hidrelétrico de Itumbiara (GO). Anais XVI Simpósio Brasileiro de sensoriamento remoto – SBSR.

Augusto-Silva, P.B., Ogashawara, I., Barbosa, C.C.F., Carvalho, LA.S., Jorge, .S.F., Fornari, C.I., Stech, J.L., 2016. Analysis of MERIS Reflectance Algorithms for Estimating Chlorophyll-*a* Concentration in a Brazilian Reservoir. *Remote Sensing. 6*, 11689-11707. Doi:10.3390/rs61211689.

Baum, A., Fleming, R., Davidson, A. M. 1983. Natural disaster and technological catastrophe. Environment and behavior, 333-354.

Bernardino, A.F., Netto, S.A., Pagliosa, P.R., Barros, F., Christofoletti, R.A, Rosa Filho, J.S., Colling, A., Lana, P.C., 2015. Predicting ecological changes on benthic estuarine assemblages through decadal climate trends along Brazilian Marine Ecoregions. Estuarine, Coastal and Shelf Science. 166, 74-82.

Bottino, F., Milan, J.A.M., Cunha-Santino, M.B., Bianchini-Jr, I., 2017. Influence of the residue from an iron mining dam in the growth of two macrophyte species. Chemosphere 186, 488-494.

Carmo, F.F., Kamino, L.H.Y., Tobias Júnior, R., Campos, I.C., Carmo, F.F., Silvino, G., Castro, K.J.S.X., Mauro, M.L., Rodrigues, N.U.A., Miranda, Pinto, C.E.F., 2017. Fundão tailings dam failures: the environment tragedy of the largest technological disaster of Brazilian mining in global context. Perspectives in Ecology and Conservation 15, 145–151.

CRH-ANA - Conjuntura dos recursos hídricos no Brasil, Agência Nacional das Águas. Encarte Especial sobre a Bacia do Rio Doce: Rompimento da Barragem em Mariana/MG. Relatório final, 2015.

CPRM – Serviço Geológico do Brasil. Monitoramento especial da bacia do rio Doce: Acompanhamento da onda de cheia. Relatório 1, 2015a.

Chen, S.L., Zhang, G.A., Yang, S.L., Shi, J.Z., 2006. Temporal variations of fine suspended sediment concentration in the Changjiang River Estuary and adjacent coastal waters. China Journal Hydrogeologic, 331 (1-2): 137-145.

Dominguez J.M.L. 2004. The coastal zone of Brazil: an overview. Journal of Coastal Research, SI39:16‑20.

Dominguez J.M.L. & Wanless H.R. 1991. Facies architecture of a falling sealevel, Doce river coast, Brazil. International Association of Sedimentologists Special Publication, 14:259‑281.

Dominguez J.M.L., Bittencourt A.C.S.P., Martin L. 1983. O papel da deriva litorânea de sedimentos arenosos na construção das planícies costeiras associadas a desembocaduras dos rios São Francisco (SE/AL0), Jequitinhonha (BA), Doce (ES) e Paraíba do Sul (RJ). Revista Brasileira de Geociências, 13(4):93‑105.

Fernandes, G.W., Goulart, F.F., Ranierid, B.D., Coelho, M.S., Dalesf, K., Boescheg, N., Bustamanteh, M., Carvalho, F.A., Carvalho, D.C., Dirzob, R., Fernandes, S., Galetti Jr., P.M., Millang, V.E.G., Mielkeg, C., Ramirezk, J.L., Nevesa, A., Rogassg, C., Ribeirol, S.P.,Sariotm, A., Filho, B.S., 2016. Deep into the mud: ecological and

socioeconomicimpacts of the dam breach in Mariana, Brazil. Natureza & Conservação https://doi.org/10.1016/j.ncon.2016.10.003.

Fielding, J., Croudace, I.W., Alan E.S. Kemp, A.E.S., Pearce, R.B., Cotterill, C.J., Langdon, P.,Avery, R., 2020. Tracing lake pollution, eutrophication and partial recovery from the sediments of Windermere, UK, using geochemistry and sediment microfabrics. Science of the Total Environment. 722, 137745.

Gangloffa, A., Verneya, R., Doxaran, D., Ody, A., Estournel, C., 2017. Investigating Rhône River plume (Gulf of Lions, France) dynamics using metrics analysis from the MERIS 300m Ocean Color archive (2002–2012). Continental Shelf Research. 144, 98–111.

Garcia, L.C.; Ribeiro, D.B.; Roque, F.O.; Ochoa-Quintero, J.M.; Laurance, W.F. Brazil's worst mining disaster: corporations must be compelled to pay actual environmental costs. Ecological Applications. 27:5-9. 2017.

Gomes, L.E.O., Correa, L.B., Sá, F., Neto, R.R., Bernadinho, A.F., 2017. The impacts of the Samarco mine tailing spill on the Rio Doce estuary, Eastern Brazil. Marine Pollution Bulletin 120, 28–36.

Gomes, A.C., Alcântara, E., Rodrigues, T., Bernado, N., 2020. Satellite estimates of euphotic zone and Secchi disk depths in a colored dissolved organic matter-dominated inland water. Ecological Indicators. 110, 105848.

Gomes, P., Valente, T., Geraldo, T., Ribeiro, C., 2020. Photosynthetic pigments in acid mine drainage: Seasonal patterns and associations with stressful abiotic characteristics. Chemosphere. 239, 124774.

Hatje, V., Pedreira, R.M.A., Rezende, C.E., Schettini, C.A.F.S., Souza, G.C., Marin, D.C., Hackspacher, P.C., 2017. The environmental impacts of one of the largest tailing dam failures worldwide. Sci. Rep. 7, 10706.

IBAMA, Instituto Brasileiro do Meio Ambiente e dos Recursos Naturais Renováveis., 1991. Plano de Manejo do Parque Nacional Marinho dos Abrolhos. https://www1.icmbio.gov.br/parnaabrolhos/ (Acessado em julho de 2020).

IBAMA, Instituto Brasileiro do Meio Ambiente e dos Recursos Naturais Renováveis., 2015. Impactos ambientais decorrentes do desastre envolvendo o rompimento da barragem de Fundão, em Mariana, Minas Gerais. Laudo Técnico Preliminar. 74p.

ICOLD, International Commission on Large Dams. 2001. Tailings dams: risk of dangerous occurrences, lessons learnt from practical experiences. Paris: ICOLD, 144 p. 2001. (Bulletin, 121).

Karki, S., French, K., McCarthy, V., Hanafin, J., Jennings, E., Delaney, C., Veerkamp, V., Golden, A., McKinstry, A., Ahmed, M., 2020. In-Situ Validation of Water Quality Algorithms and Monitoring of Irish Lakes using Sentinel 2 Imagery. Presentation at European Geophysical Meeting – EGU. 2020-2223.

LACTEC., 2018. Diagnóstico socioambiental dos danos decorrentes do rompimento da barragem de Fundão na bacia do rio Doce. Relatório Pós-Desastre 2: Meios Físico e Biótico. http://www.mpf.mp.br/grandes-casos/caso-samarco/documentos/relatorios-lactec/lactec_relatorio-pos-desastre-grupo-02 (acessado em julho de 2020).

LACTEC., 2019. Diagnóstico socioambiental dos danos decorrentes do rompimento da barragem de Fundão na bacia do rio Doce: Atualização Linha-Base Ambientes

Costeiros. http://www.mpf.mp.br/grandes-casos/caso-samarco/documentos/relatorios-lactec/ (Acessado em julho de 2020).

Lahet, F., Stramski, D. 2010. MODIS imagery of turbid plumes in San Diego coastal waters during rainstorm events. Remote Sensing of Environment, 114 (2010), 332–344.

Lari, S., Frattini, P., Crosta, G.B. 2009. Integration of natural and technological risks in Lombardy, Italy. Natural Hazards and Earth System Sciences, 9:2085-2106.

Mazzei, E.F., Bertoncini, A.A., Pinheiro, H.T., Machado, L.F., Vilar, C.C., Guabiroba, H.C., Costa, T.J.F., Bueno, L.S., Santos, L.N., Francini-Filho, R.B., Hostim-Silva, M., 2017. Newly discovered reefs in the southern Abrolhos Bank, Brazil: anthropogenic impacts and urgent conservation needs. Joyeux Marine Pollution Bulletin 114, 123–133. https://doi.org/10.1016/j.marpolbul.2016.08.059.

Miller, R. L., Mckee, A. B. 2004. Using MODIS Terra 250 m imagery to map concentrations of total suspended matter in coastal waters. Remote Sensing of Environment, 93: 259-266.

Nwankwegu, A.S., Li, Y., Huang, Y., Wei, J., Norgbey, E., Lai, Q., Sarpong, L., Wang, K., Ji, D., Yang, Z., Paerl, H.W., 2020. Nutrient addition bioassay and phytoplankton community structure monitored during autumn in Xiangxi Bay of Three Gorges Reservoir, China. Chemosphere. 247, 125960.

Nechad, B., Ruddick, K.G., Park, Y., 2010. Calibration and validation of a generic multisensor algorithm for mapping of total suspended matter in turbid waters. Remote Sens. Environ. 114, 854–866

Nechad, B., Ruddick, K.G., Park, Y., 2010. Calibration and validation of a generic multisensor algorithm for mapping of total suspended matter in turbid waters. Remote Sens. Environ. 114, 854–866. https://doi.org/10.1016/j.rse.2009.11.022.

Nobre, D. M., Alarconc, D. T., Cintid, A., Schiavettie, A., 2017. Governance of the Cassurubá Extractive Reserve, Bahia State, Brazil: An analysis of strengths and weaknesses to inform policy. 77, 44-5.

Pahlevana, N., Smitha, B., Schalles, J., Binding, C., Cao, Z., Ma, R., Alikas, K., Kangro, K., Gurlin, D., Hà, N., Matsushita, B., Moses, W., Greb, S., Lehmann, M.K., Ondrusek, M., Oppelt, N., Stumpf, R., 2020. Seamless retrievals of chlorophyll-a from Sentinel-2 (MSI) and Sentinel-3 (OLCI) in inland and coastal waters: A machine-learning approach. Remote Sensing of Environment. 240, 111604.

Passos, L.S., Gnocchi, K.G., Pereira, T.M., Coppo, G.C., Cabral, D.S., Gomes, L.C., 2020. Is the Doce River elutriate or its water toxic to Astyanax lacustris (Teleostei: Characidae) three years after the Samarco mining dam collapse?. Science of the Total Environment. 736, 139644.

PCGRSS – Programa de caracterização Geoquímica dos Rejeitos, Solos e Sedimentos, rompimento da barragem de Fundão. 2016. Rel. de monitoramento ambiental, Golder Associates.

Quaresma, V.S., Catabriga, G., Bourguignon, S.N.,Godinho, E., Bastos, A.C., 2015. Modern sedimentary processes along the Doce river adjacent continental shelf. Brazilian Journal of Geology. 45(4), 635-644.

Queiroz, H.M., Nóbrega, G.N., Ferreira, T.O., Almeida, L.S., Romero, T.B., Santaella, S.T., Bernadinho, A.F., Otero, X.L., 2018. The Samarco mine tailing disaster: a

possible time-bomb for heavy metals contamination? Sci. Total Environ. 637–638, 498–506.

RAMBOL., 2019. Relatório de monitoramento consolidado dos programas socioeconômicos e socioambientais para a restauração da bacia do rio Doce. http://www.mpf.mp.br/grandes-casos/caso-samarco/atuacao-do-mpf/pareceres-e-relatorios. Acessado em 16 de agosto de 2020.

SEDRU – Secretaria de Estado de desenvolvimento regional, política e urbana e gestão metropolitana., 2016. Avaliação dos efeitos e desdobramentos do rompimento da Barragem de Fundão em Mariana-MG. Relatório do Grupo da Força-Tarefa, Belo Horizonte..http://www.agenciaminas.mg.gov.br/ckeditor_assets/attachments/770/relatorio_final_ft_03_02_2016_15h5min.pdf. Acessado em 16 de agosto de 2020.

Segura, F.R., Nunes, E.A., Paniz, F.P., Paulelli, A.C.C., Rodrigues, G.B., Braga, G.U.L., Pedreira Filho,W.R., Barbosa Jr., F., Cerchiaro, G., Silva, F.F., Batista, B.L., 2016. Potential risks of the residue fromSamarco'smine damburst (Bento Rodrigues, Brazil). Environ. Pollut. 218, 813–825.

Tomasella, J., Vieira, R. M. S. P., Barbolsa, A. A., Rodriguez, D. A., Santana, M. O., Sestini, S. M. F. 2018. Desertification trends in the Northeast of Brazil over the period 2000–2016. International Journal of Applied Earth Observation and Geoinformation, (73): 197-206, DOI: https://doi.org/10.1016/j.jag.2018.06.012.

Weber, A, A., Sales, C.F., Faria, F.S., Melo, R.M.C., Bazzoli, N., Rizzo, E., 2020. Effects of metal contamination on liver in two fish species from a highly impacted neotropical river: A case study of the Fundão dam, Brazil. Ecotoxicology and Environmental Safety. 190,110165.

Zhao, J., Barnes, B., Melo, N., English, D., Lapointe, B., Karger, F.M., Schaeffer, B., Hu, C., 2013. Assessment of satellite-derived diffuse attenuation coefficients and euphotic depths in south Florida coastal waters. Remote Sens. Environ. 131, 38–50.

CAPÍTULO 2

CONTEXTUALIZAÇÃO DO TEMA

Neste capítulo é fornecida uma visão sobre o histórico da barragem de Fundão, desde o momento de sua construção até seu colapso. O objetivo principal é demonstrar o cenário das áreas atingidas pela lama de rejeito, apresentando os impactos em escala micro e macrorregional, incluindo os danos humanos, materiais e ambientais. Para alcançar o objetivo proposto, foi realizada uma revisão bibliográfica de materiais disponíveis na literatura, como artigos, relatórios técnicos e notícias. Imagens de satélite de alta resolução espacial, em conjunto com registro fotográfico obtido em campo, são utilizadas para expor a situação das áreas atingidas. As imagens dos satélites WorldView 2 e WorldView 3 foram fornecidas pelo Instituto Brasileiro do Meio Ambiente e dos Recursos Naturais Renováveis (IBAMA), que contribuiu também para realização de visitas de campo, que aconteceram entre agosto e setembro de 2016. A revisão histórica de Fundão revela que, desde o início de sua operação, a barragem veio apresentando indícios de falhas estruturais, que não receberam a devida atenção e reparos. Problemas relacionados a drenagem do sistema foram recorrentes ao longo dos anos. O aumento da carga de material depositado em um dos condutos avariado criou um cenário ideal para seu colapso, onde a ruptura foi desencadeada após um abalo sísmico de baixa magnitude. Mesmo depois de mais de quatro anos da tragédia, os danos aos ecossistemas ainda estão presentes nas regiões *offshore* e *onshore*. Nesses locais, a fauna e a flora apresentam registros da contaminação por metais potencialmente tóxicos trazidos pela lama. Os padrões de qualidade da água do rio e do mar sofreram alterações substanciais. Muitos municípios precisaram de captações alternativas de água. Ainda que em algumas regiões a água do rio Doce possa parecer limpa em determinadas épocas do ano, há uma crescente preocupação relacionada aos períodos chuvosos. Nessa época, o rejeito depositado nas margens do rio é carreado e transportado ao longo da calha principal e o material depositado no fundo do rio pode também ser ressuspenso.

2.1. Histórico da barragem de Fundão

A barragem de Fundão faz parte do complexo Germano (Fig. 1). O beneficiamento de minério de ferro resulta em dois tipos distintos de rejeitos: (i) o rejeito arenoso, composto de areia e partículas com granulometria de silte; e (ii) a lama de granulação fina e argilosa. Ambos eram produzidos e transportados em forma de polpa como fluxos separados. O rejeito arenoso, durante a deposição, forma uma praia levemente inclinada com uma geometria que possibilita com que a água seja drenada de forma rápida. Já no rejeito lamoso (de baixa permeabilidade), as partículas de argila em

suspensão vão se assentando na água de forma mais lenta (Morgenstern et al., 2016). O método de construção do complexo Germano é do tipo “Upstream” ou “a montante”, onde o rejeito é aproveitado para a base de contenção. Nesse método, uma das maiores vulnerabilidades é a resistência à liquefação do material arenoso, que depende principalmente da projeção adequada das estruturas de drenagem (ICOLD, 2001).

Os depósitos de rejeitos existentes em Germano foram se aproximando de sua capacidade máxima em 2005 e, com isso, a barragem de Fundão foi projetada. O planejamento de Fundão foi feito para receber 70% de areia e 30% de lama, do total recebido de todas as plantas. Esses rejeitos ficariam separados fisicamente, com a areia sendo depositadas atrás do Dique 1 e a lama atrás do Dique 2 (Fig. 1). No entanto, após a finalização dos diques, a estrutura começou a apresentar defeitos na base do dreno de fundo, em 2009. Para tentar solucionar o problema, um projeto que permitia uma saturação mais disseminada foi adotado, sem sucesso, pois foi o momento que se iniciou o processo de liquefação da areia (Morgenstern et al., 2016).

Problemas relacionados à lama e gestão de água foram frequentes entre 2011 e 2012. A água chegou a alcançar até 60 m da crista da barragem. A lama sedimentou em locais inadequados, intensificando os problemas de drenagem do sistema. Nesse episódio, um dos condutos de concreto da barragem foi considerado ineficiente para suportar a carga adicional do rejeito. As operações da mina não foram paralisadas para a estabilização do conduto. Por sua vez, medidas ineficientes foram tomadas, onde o aterro foi direcionado sobre a lama previamente depositada, favorecendo as condições da liquefação de rejeito arenoso (Morgenstern et al., 2016).

O local destinado ao controle de saturação atingiu sua capacidade máxima entre 2013 e 2014. A mistura indevida dos rejeitos em conjunto ao constante aumento da carga favoreceu a compressão da lama, sua extrusão lateral e a liquefação do rejeito arenoso superposto. Dessa forma, as condições de estabilidade da barragem já eram críticas e a ruptura iminente. Antes do colapso em 2015 aconteceram tremores de baixa magnitude na região (Agurto-Detzel et al., 2016; Morgenstern et al., 2016). Tais abalos aliados a instabilidade da barragem contribuíram para sua ruptura, que ocorreu associado ao deslizamento fluido provocado por liquefação.

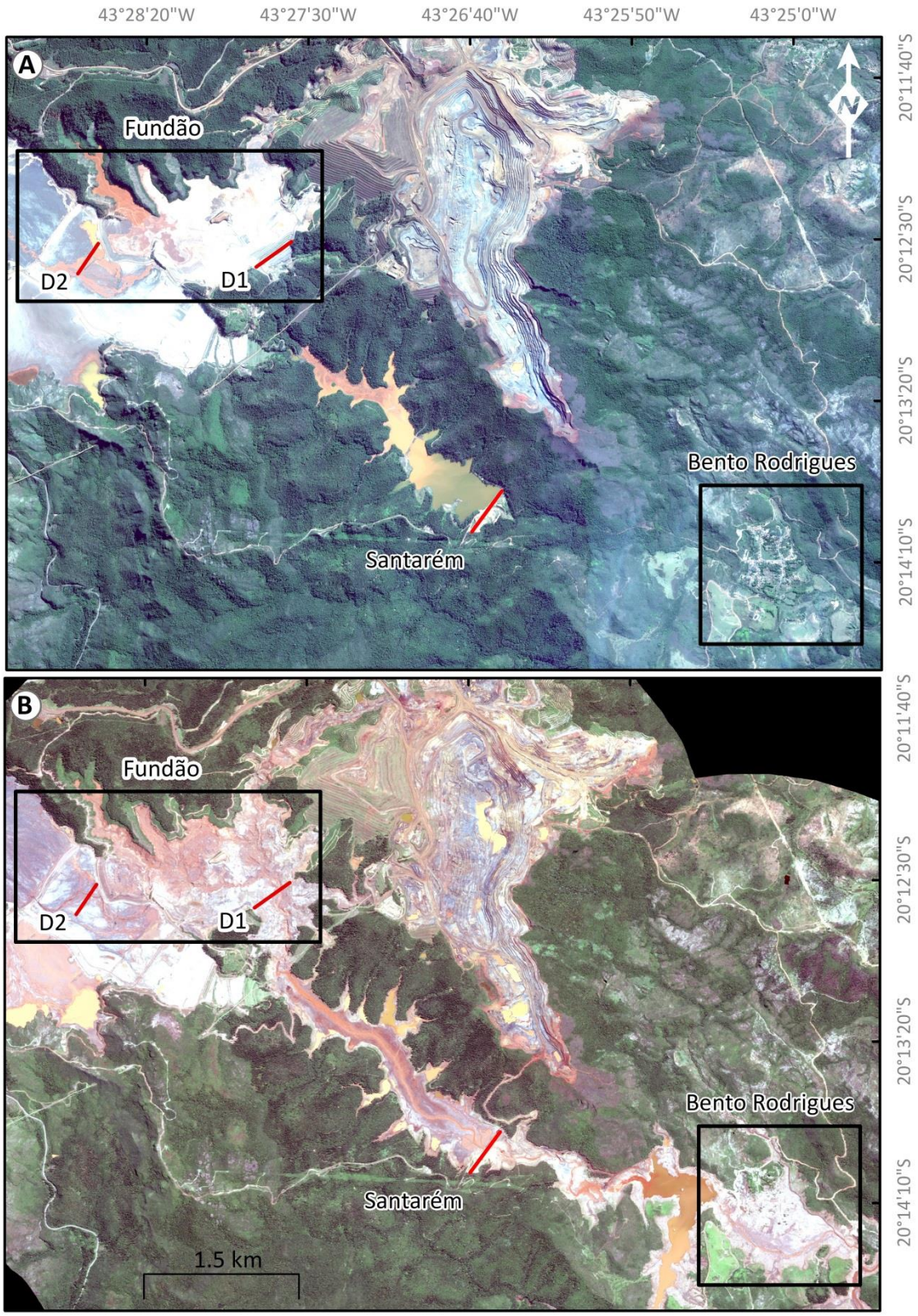

Fig. 1. Barragem de Fundão, antes e depois do colapso (A) 21 de julho de 2015. (B) 20 de fevereiro de 2016. D1 e D2 – Diques da barragem. Ênfase para o distrito de Bento Rodrigues, que foi totalmente destruído.

2.2. Cenário Pós-colapso

Estima-se que cerca de 43 milhões de m³ de rejeito foram liberados após o colapso da barragem, formando uma avalanche que destruiu o distrito de Bento Rodrigues (Figs. 1 e 5) e soterrou parte de Paracatu de Baixo, além dos rios Gualaxo do Norte e Carmo, afluentes do rio Doce (Anexo 1, 2, 3 e 4; Carmo et al 2017). De acordo com Carmo et al (2017), alvos diretamente impactados pela avalanche de lama incluem: a barragem de Santarém, construções, vegetação arbórea, pastagem, curso d'água, hidrelétrica Risoleta Neves e solos. Na Fig. 2 tem-se uma estimativa em hectare correspondente a esses alvos.

A lama de rejeito percorreu mais de 650 km até a foz do rio Doce, em Linhares, no litoral do Espírito Santo, porém grande volume desse material foi retido pela barragem da Usina Hidrelétrica Risoleta Neves - UHRN (Fig. 3). O trecho entre Fundão e a usina foi o mais devastado. A força da avalanche escavou as margens dos rios e teve grande potencial de destruição (ANA, 2016).

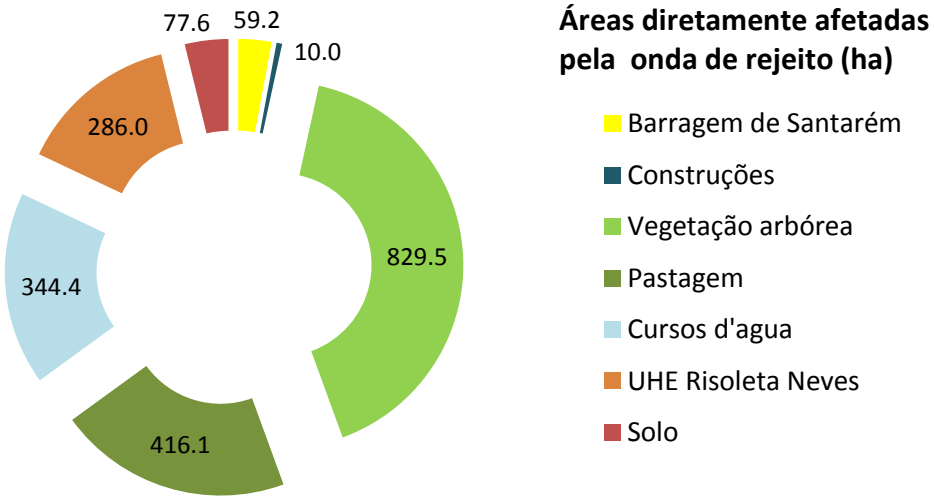

Fig. 2. Áreas diretamente impactadas pela avalanche de lama (modificado de Carmo et al., 2017).

2.2.1. Reparação dos danos

Em resposta ao desastre, a Fundação Renova, uma organização sem fins lucrativos, foi contratada mediante o compromisso jurídico chamado Termo de Transação e Ajustamento de Conduta (TTAC), assinado pela Samarco, BHP Billiton e Vale. A Renova é a responsável pela mobilização para reparo dos danos causados pelo

rompimento da barragem de Fundão. O escopo da atuação compreende 42 programas (Tabela 1) que se desdobram em projetos socioeconômicos e socioambientais (www.fundacaorenova.org/a-fundacao/). O monitoramento do progresso e da efetividade dos programas implementados no âmbito do TTAC é feito pela empresa RAMBOLL, em conjunto com Ministério Público Federal (RAMBOLL, 2020a).

Tabela 1. Programas propostos no TTAC para a reparação dos danos do colapso da barragem de Fundão. Fonte: RAMBOL (2020a)

Programa	**Objetivo**
Programa 1	Levantamento e cadastro dos atingidos
Programa 2	Programa de Indenização Mediada (PIM)
Programa 3	Proteção e recuperação da qualidade de vida dos povos indígenas
Programa 4	Proteção e recuperação da qualidade de vida de outros povos e comunidades tradicionais
Programa 5	Proteção Social
Programa 6	Comunicação, participação, diálogo e controle social
Programa 7	Assistência aos animais
Programa 8	Reconstrução, recuperação e realocação de Bento Rodrigues, Paracatu de Baixo e Gesteira
Programa 9	Recuperação do reservatório da Usina Hidrelétrica (UHE) Risoleta Neves
Programa 10	Recuperação das demais comunidades e infraestruturas atingidas entre Fundão e Candonga
Programa 11	Recuperação de escolas e reintegração da comunidade escolar
Programa 12	Preservação da memória histórica, artística e cultural
Programa 13	Apoio ao turismo, cultura esportes e lazer
Programa 14	Apoio à saúde física e mental dos atingidos
Programa 15	Promoção à inovação
Programa 16	Retomada das atividades aquícolas e pesqueiras
Programa 17 e 40	Retomada das atividades agropecuárias e fomento ao CAR e PRA
Programa 18	Desenvolvimento e diversificação econômica
Programa 19	Recuperação de micro e pequenos negócios
Programa 20	Estímulo à contratação local
Programa 21	Auxílio financeiro emergencial
Programa 22 e 41	Gerenciamento dos programas socioeconômicos e socioambientais
Programa 23 e 24	Manejo de rejeitos
Programa 25	Recuperação da área ambiental -1
Programa 26	Recuperação de áreas de preservação permanente (APP)
Programa 27	Recuperação de nascentes
Programa 28	Conservação da biodiversidade aquática

Programa 29	Fortalecimento das estruturas de triagem e reintrodução da fauna silvestre
Programa 30	Conservação da fauna e flora terrestre
Programa 31	Coleta e tratamento de esgoto e destinação de resíduos sólidos
Programa 32	Melhoria dos sistemas de abastecimento de água
Programa 33	Educação para a revitalização da Bacia do Rio Doce
Programa 34	Preparação às emergências ambientais
Programa 35	Informação para a população
Programa 36	Comunicação nacional e internacional
Programa 38	Investigação e monitoramento da Bacia do Rio Doce, áreas estuarina, costeira e marinha atingidas
Programa 39	Consolidação de unidades de conservação
Programa 42	Ressarcimento dos gastos públicos extraordinários

2.2.2. Danos em escala micro e macrorregional

Para melhor visualização do cenário pós-colapso, nesse capítulo, foi adotada a subdivisão das áreas atingidas de acordo com SEDRU (2016). Os autores demonstraram os impactos em escala micro e macrorregional, em que são discutidos os danos humanos, materiais e ambientais. A escala microrregional inclui a região de Bento Rodrigues até a UHRN. A escala macrorregional abrange toda área atingida pela lama, de Fundão até a foz do rio Doce (Fig. 3).

Nesse capítulo, serão enfatizados principalmente os danos ambientais, que abrangem a qualidade e disponibilidade da água e solo, e danos causados à biodiversidade. Os danos humanos são aqueles que impactam a saúde e segurança pública, educação, lazer e organização social. Os danos materiais incluem os impactos à economia e a infraestrutura (Fig. 4; SEDRU, 2016).

Visitas de campo, em parceria com o IBAMA, foram realizadas entre agosto e setembro de 2016, nas dependências de Bento Rodrigues, Paracatu de Baixo e na UHRN, no trecho que compreende a escala microrregional. Alguns pontos visitados em campo, assim como a localização das fotos expostas nesse capítulo, estão indicados na Fig. 3A e B. Já na Fig. 3C, é mostrado o perfil longitudinal A-B, que possibilita uma visão panorâmica da área atingida, bem como permite situar cada trecho de acordo com a distância do local do colapso, principais municípios e as usinas Hidrelétricas no curso do rio Doce.

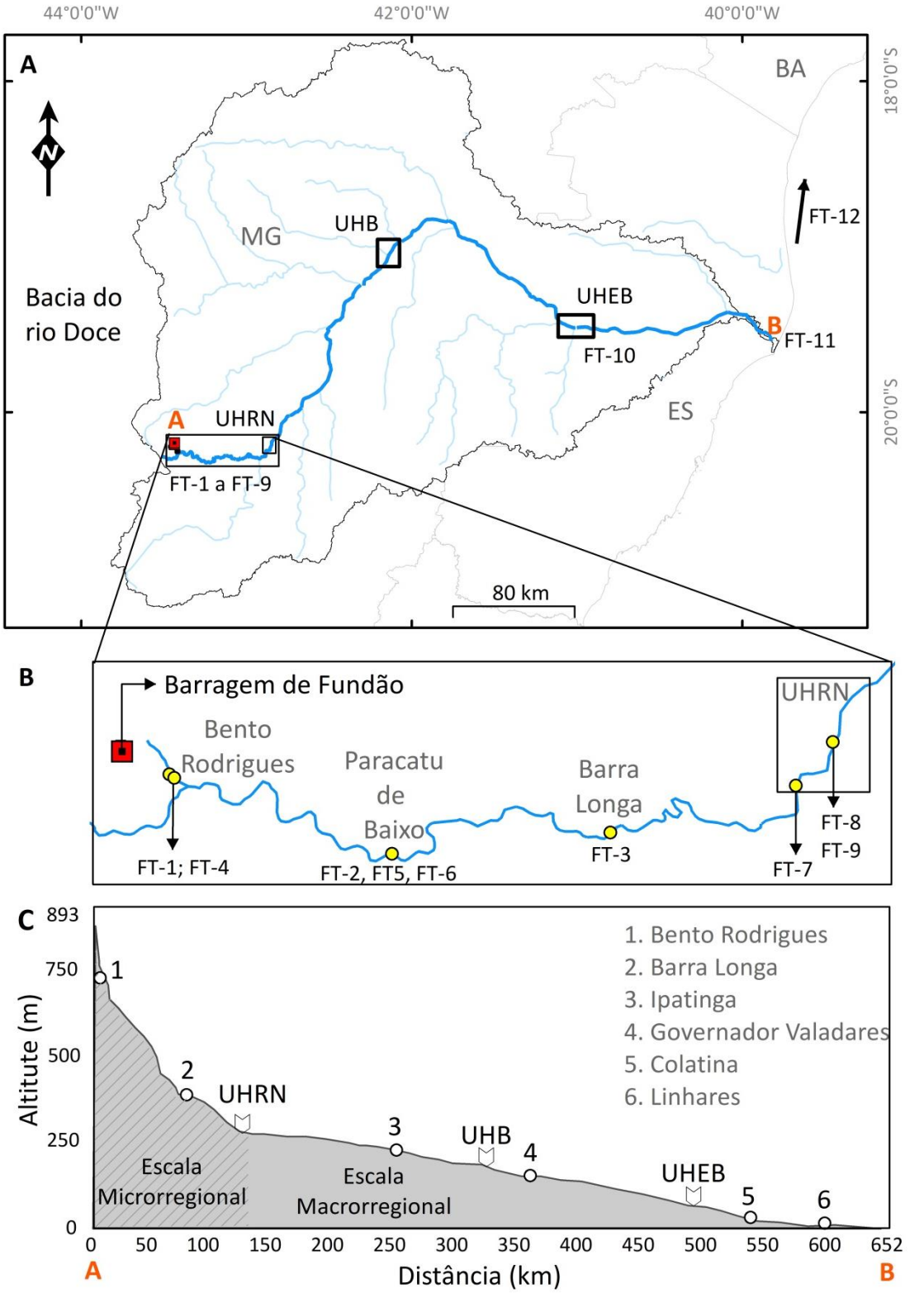

Fig. 3. (A) Limite da Bacia do rio Doce com indicação do perfil AB (escala macrorregional) dos sítios fotografados (FT-1 a FT-12) e usinas hidrelétricas. (B) Detalhes na escala microrregional. (C) Perfil Longitudinal modificado de ANA (2016), incluindo as duas escalas estudadas, principais cidades e usinas hidrelétricas. UHRN – Usina Hidrelétrica Risoleta Neves. UHB – Usina Hidrelétrica Baguari. UHEB – Usina Hidrelétrica Baguari.

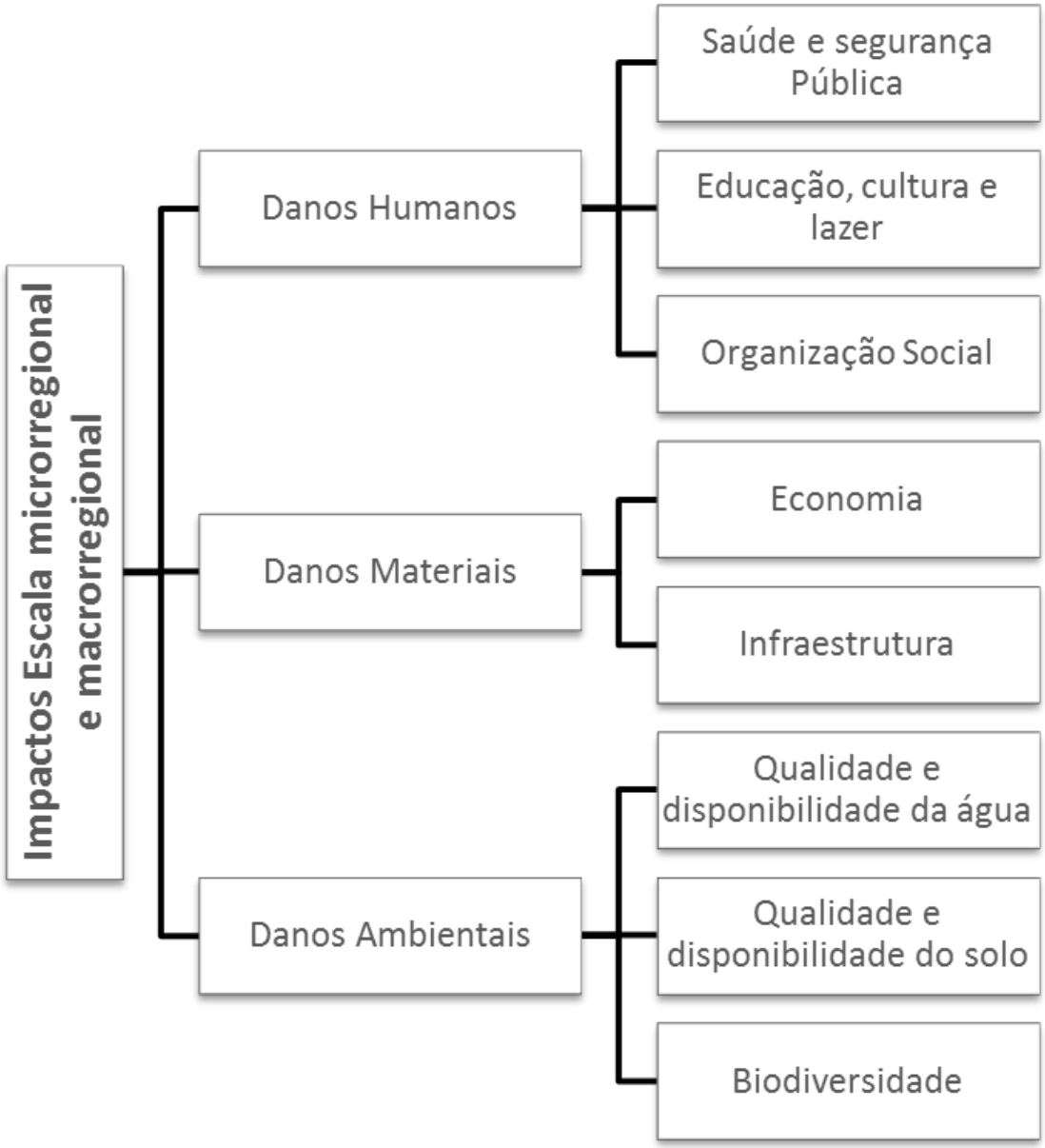

Fig.4. Danos socioeconômicos e socioambientais causados pelo colapso da barragem de Fundão. Adaptado de SEDRU (2016).

- Danos humanos e materiais

A avalanche de lama colocou em risco a integridade e segurança das pessoas, causando danos irreversíveis, incluindo 19 vítimas fatais, além de 256 feridos. Na Fig. 5, tem-se a imagem de alta resolução espacial da região de Bento Rodrigues e o registro fotográfico das ruínas, meses depois da tragédia.

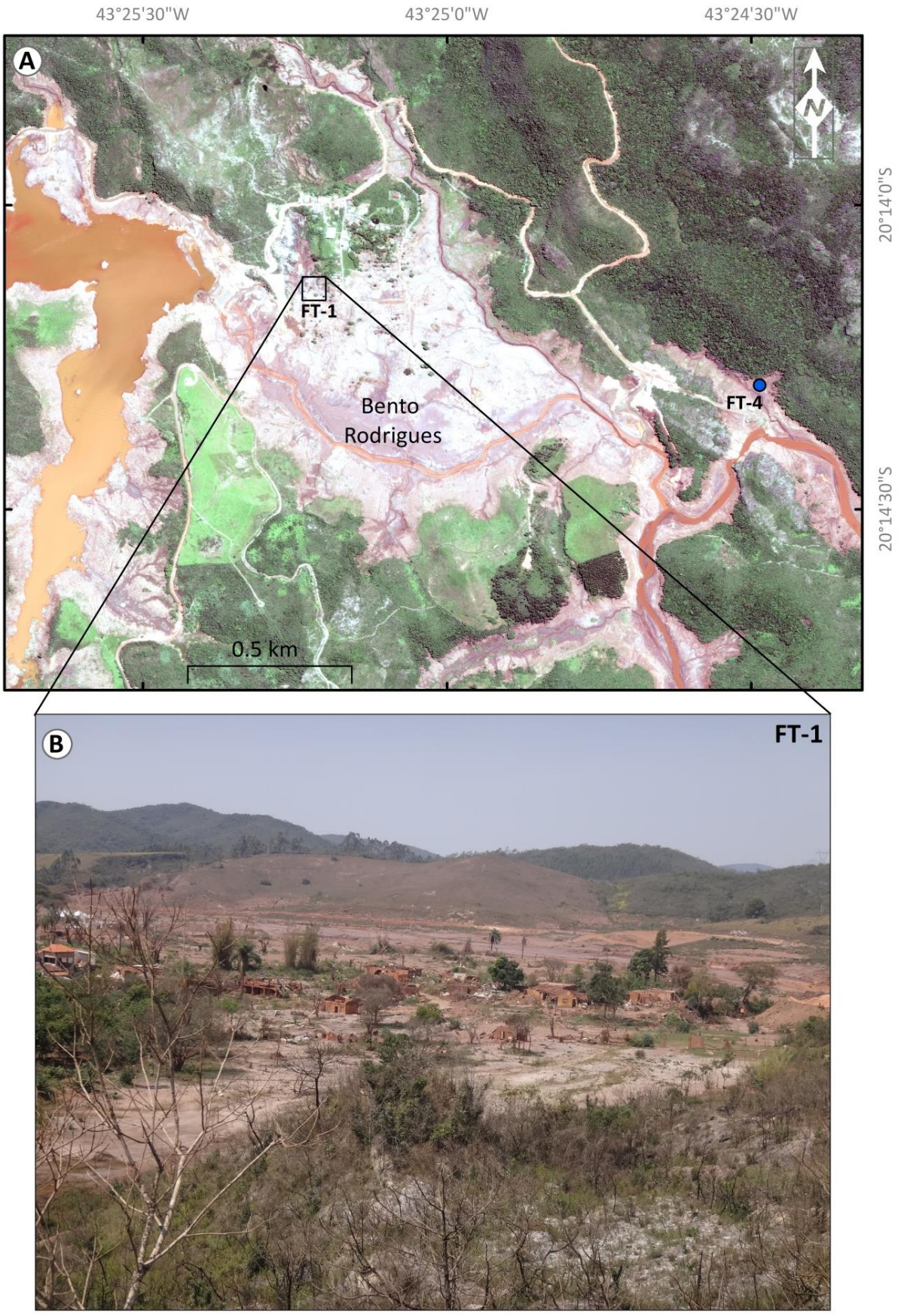

Fig. 5. (A) Composição colorida cor real obtida com dados do sensor orbital WorldView-2 (RGB123) mostrando o distrito de Bento Rodrigues três meses após o colapso. (B) Foto FT-1: ruinas de Bento Rodrigues, obtida no dia 14 de setembro de 2016 (Fonte: acervo pessoal).

Os impactos no setor de educação, cultura e lazer aconteceram pela destruição de habitats indígenas, perda de fotografias e registro histórico familiar, destruição de igrejas, casas de orações, centros espíritas, escolas e praças (Fig. 7; SEDRU, 2016; RAMBOL, 2017).

A realocação do distrito de Bento Rodrigues, Paracatu de Baixo e Gesteira exemplifica o maior dano humano sobre organização social (SEDRU, 2016). Neste cenário, cerca de 644 pessoas foram desabrigadas, 716 desalojadas, e três etnias indigenas atingidas (Fig. 6). Após a destruição dessas comunidades, as pessoas foram instaladas em abrigos temporários para aguardar a contemplação de residências propostas em projetos de reassentamento definitivo (Programa 8, do TACC, tabela1), que, após quatro anos desde o colapso, não foram entregues aos atingidos (Rambol, 2020).

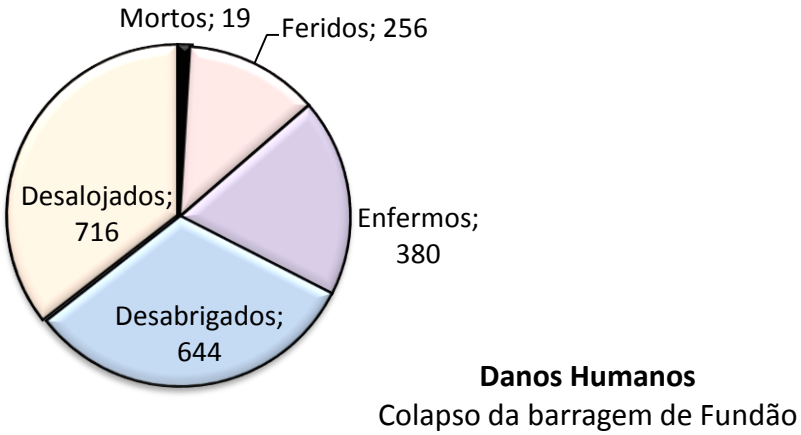

Fig 6. Danos humanos causados pelo colapso da Barragem de Fundão, dados extraídos de SEDRU (2016).

Na escala macrorregional, os danos humanos são voltados principalmente para a disponibilidade de água, devido à disseminação de doenças que tem como causa a água imprópria para o consumo ou escassez desse recurso (SEDRU, 2016). Mesmo que análises de toxicidade realizadas por diferentes órgãos públicos e empresas privadas indiquem que a água do rio Doce não oferece riscos a saúde, existe um sentimento de insegurança da população em fazer o uso da mesma (SEDRU, 2016). De acordo com RAMBOL (2017), dois anos depois do colapso da barragem, o abastecimento de água potável ainda não estava completamente resolvido, ou estava sendo oferecido de maneira insatisfatória em grande parte dos municípios atingidos.

Entre os prejuízos públicos e privados em escala microrregional, destaca-se a paralisação da Samarco e da UHRN, que somam mais de 226,5 milhões de reais. Já em escala macrorregional, esses danos estão relacionados principalmente com o uso e disponibilidade de água e abastecimento elétrico, que gerou perdas em setores diversos dos municípios da calha do Rio Doce, como agropecuária, comércio, indústria e atividades relacionadas à pesca e turismo (SEDRU, 2016).

Fig.7. (A) FT-2 (setembro, 2016): Residência em zona rural destruída pela avalanche de lama na região de Paracatu de baixoFonte: Acervo pessoal. (B) FT-3: Exemplo de dano ao patrimônio cultural: capela de Barra Longa. Fonte: Sánchez et al. (2019).

- Danos Ambientais

Os danos ambientais desencadeados pelo colapso da barragem incluem impactos aos ecossistemas e à biodiversidade. Pesquisas desenvolvidas nas regiões atingidas, tanto no rio Doce quanto na região costeira, indicam que os efeitos da contaminação pela lama devem persistir nos ecossistemas por um longo período. Os resultados dessas pesquisas são sintetizados nessa sessão.

As análises físico-químicas da água do rio Doce e seus afluentes, Gualaxo do Norte e do Carmo, revelaram que, após o colapso, foram recorrentes valores mais elevados dos parâmetros de qualidade de água, de modo geral. No rio Doce, destacam-se alterações significativas para oxigênio dissolvido, turbidez, pH, alumínio, arsênio, ferro, manganês e zinco (LACTEC, 2018). Já para o rio do Carmo, todos os parâmetros físico-químicos da água mostraram medidas extrapolando os valores da série histórica após o colapso.

A assembleia mineralógica primária do rejeito coletado na região de Bento Rodrigues, 30 dias após o colapso, é constituída essencialmente de hematita e magnetita. Os minerais secundários incluem goethita e greenalita. A identificação dessa associação de minerais em ambientes costeiros pode ser usada como importante marcador do rejeito (Orlando et al., 2020). Os autores mostraram que em 2019 a concentração desses minerais no mar foi relativamente mais alta que em 2012.

Análises químicas da água, sedimentos e material particulado em suspensão, de amostras coletadas no rio e no mar, apontam o enriquecimento em metais potencialmente tóxicos no ambiente após o colapso (Hatje et al 2017; Gomes et al 2017; Quadra et al., 2019; Weber et al., 2020). As partículas finas carreadas pela lama foram incorporadas aos sedimentos arenosos do rio. Houve um aumento significativo de cádmio, arsênio, chumbo e níquel, denotando valores acima dos limites permitidos pela CONAMA (Weber et al.,2020; Duarte et al., 2020). O cádmio está relacionado ao rejeito de minério de ferro de Fundão. O aumento de arsênio é devido à remobilização de sedimentos das margens dos rios (Duarte et al 2020).

Além do impacto direto sobre a qualidade da água, a avalanche de lama causou a remoção de mata ciliar, estresses na vegetação e desencadeou intensa sedimentação de rejeito sobre as margens do rio, principalmente em escala

microrregional (Figs. 8 e 9). Nesse trecho, áreas de preservação permanentes foram arrasadas e restaram apenas os bambuzais que se curvaram ou quebraram sem sofrer arranque total (IBAMA, 2015; Viana e Costa, 2016; Schaefer et al., 2016). Omachi et al (2018) estimaram, via sensoriamento remoto, que a perda de área florestal devido ao colapso foi de 457,6 ha, ocorrendo principalmente ao longo dos primeiros 74 km da Barragem do Fundão.

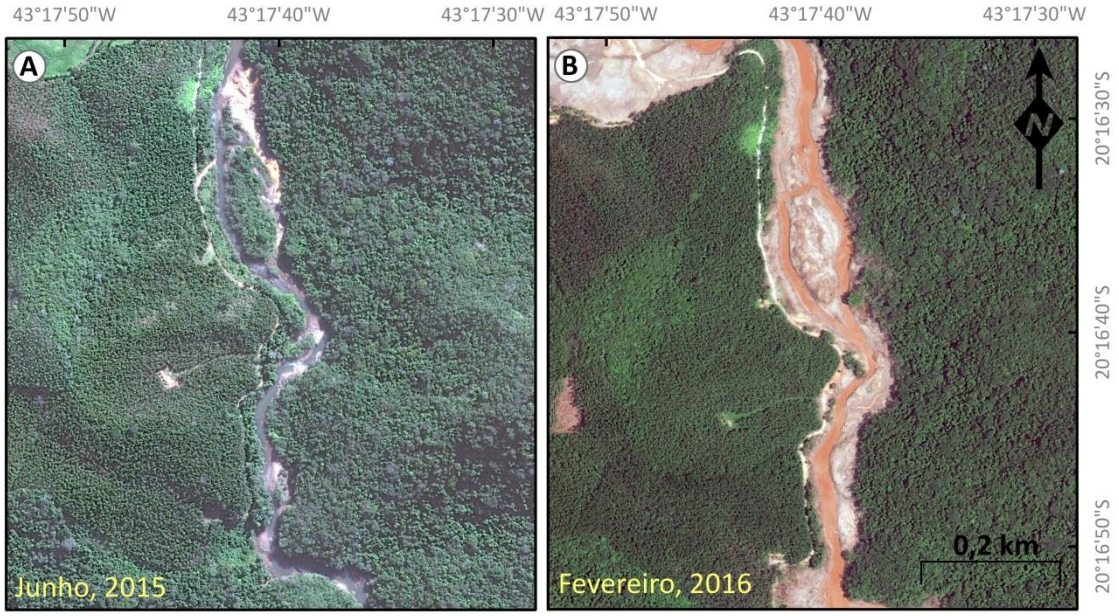

Fig.8. Composição colorida cor real obtida com dados do sensor orbital WorldView-3 (RGB123) de um trecho do rio Doce, entre Bento Rodrigues e Paracatú de Baixo, mostrando uma área de preservação ambiental que sofreu a devastação de toda mata ciliar após o colapso. (A) Junho de 2015. (B) Fevereiro de 2016.

Nesse cenário, a erosão e o assoreamento dos cursos d'água foram favorecidos. O soterramento concomitante do solo, banco de semente e plantas mais jovens ou de menor porte, comprometeu severamente a sucessão vegetal. O solo resultante passou a ter baixa atividade microbiana (Viana e Costa, 2016; Schaefer et al., 2016; Segura et al 2016). Nos locais atingidos, os solos passaram a ter menor capacidade de troca catiônica, menores teores de nutrientes disponíveis às plantas (cálcio, magnésio, potássio), pH elevado, teor de carbono mais baixo e teor de sódio mais elevado (EMBRAPA, 2015; LACTEC, 2018).

Do ponto de vista da recuperação ambiental, um dos maiores desafios é remediar os danos físicos do solo, uma vez que houve um aumento considerável na sua densidade ao longo de todo o trecho ribeirinho. Após quatro meses do desastre, já foi possível verificar o assentamento e o selamento da camada superficial do perfil

pedológico, onde se observou a formação de uma crosta de areia fina/silte praticamente impermeável (Schaefer et al., 2016)

Nas Figs. 9B e C. têm-se um dos trechos do rio do Gualaxo do Norte, em Paracatu de Baixo, mostrando ravinas e sulcos erosivos em desenvolvimento. Nesse local, a avalanche de lama removeu todo o horizonte A do solo, que é mais rico em matéria orgânica. A deposição do rejeito resultou na compactação do solo e eliminação da vegetação. A remoção do horizonte A é mais um agravante para a recuperação ambiental.

O assoreamento dos cursos d'agua aconteceu principalmente em escala microrregional. A UHRN foi um dos locais que mostrou maior acúmulo de rejeito ao longo do reservatório e na sua barragem, com estimativa de volume assoreado de 10,5 milhões de m³ (https://www.samarco.com/wp-content/uploads/2016/11/Samarco-intensifica-obras-em-Candonga.pdf).

Na imagem de satélite de alta resolução espacial é possível visualizar o rejeito nas margens do reservatório (Fig. 10A). As fotos obtidas no campo mostram a grande quantidade de rejeito nas margens do rio Doce (Fig. 10B; Anexo 4).

Fig.9. Áreas atingidas pela lama mostrando os danos ao solo e à vegetação. (A) Região de Bento Rodrigues, onde a avalanche arrancou grande volume de árvores. (B e C) Margens do rio Gualaxo do Norte, na região de Paracatu de Baixo. Ressalta-se o solo compactado com ausência de vegetação e matéria orgânica, além de locais caracterizados por ravinas e sulcos erosivos. Fotos FT-4 a FT-6 obtidas no dia 14 de setembro de 2016 (Fonte: Acervo pessoal).

O funcionamento da UHRN ficou comprometido devido aos danos nas estruturas do vertedor, que operou com apenas uma das três comportas durante vários dias, deixando a usina em situação crítica. O volume de material na área de barragem gerou risco de rompimento (ANA, 2016).

Para a reparação dos danos, a Renova apresentou o projeto de limpeza do reservatório da UHRN (Programa 9 do TTAC, tabela 1), que tem como prioridade a remoção de 1,3 milhões de metros cúbicos de rejeito em uma área prioritária de 400 m do reservatório, próximo à barragem (Fig. 10A e 11A e B).

O plano de limpeza apresentado pela Renova compreende uma série de etapas. Primeiro, o material, que é constituído por 80% de água e 20% de rejeito, é dragado do reservatório e bombeado para as ensecadeiras, onde permanece para a decantação do rejeito. A seguir, o efluente segue para pequenos diques para ser drenado e, antes de ser devolvido ao rio, recebe tratamento nas bacias construídas. Por fim, o rejeito das ensecadeiras é transferido para zonas de empilhamento (SAMARCO, 2016). Destaca-se que a dragagem é feita quando as comportas da barragem estão fechadas. Após essa etapa, todo o processo segue na fazenda Floresta, localizada a 3 km da usina (Fig. 10A).

O projeto começou a ser executado em julho de 2016. O prazo para a conclusão da etapa prioritária foi estipulado pelo TTAC inicialmente para dezembro de 2016, e posteriormente foi repactuado para julho de 2018, não sendo cumprido nas duas vezes (RAMBOLL, 2019). O atraso das obras aconteceu devido a diversos motivos, entre eles destaca-se que um dos diques localizados na Fazenda Floresta apresentou uma ruptura no maciço de solo onde seria apoiada uma de suas ombreiras, resultando na paralisação dessa obra em maio de 2018 (RAMBOLL, 2019). Em uma nota publicada em julho de 2019, a Fundação Renova, informou que a limpeza na área prioritária será concluída apenas em 2020 (https://www.fundacaorenova.org/noticia/renova-esclarece-obras-no-reservatorio-da-usina-hidreletrica-risoleta-neves-candonga/).

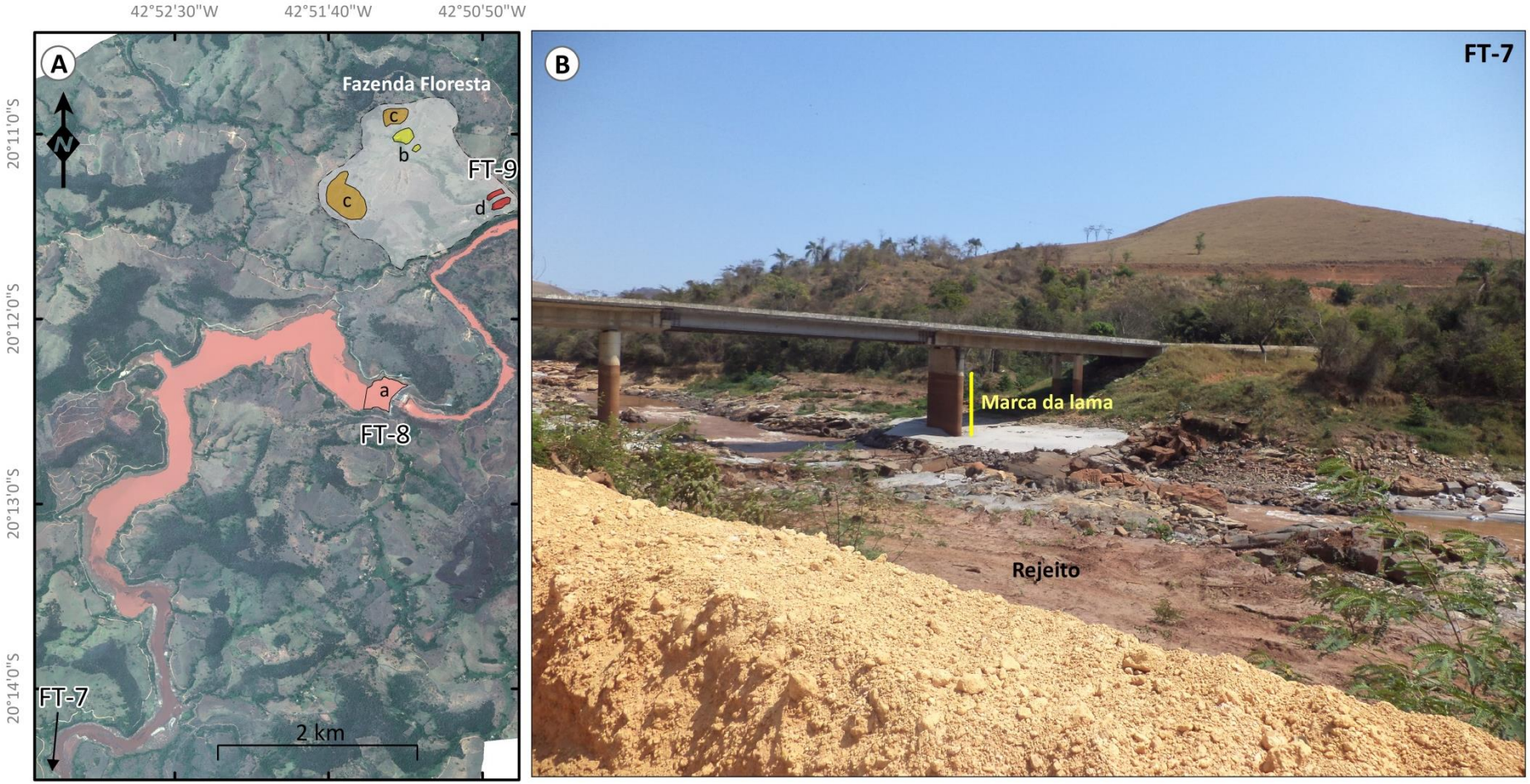

Fig. 10. (A) Região do reservatório da UHRN e a fazenda Floresta, vistas pela imagem de alta resolução espacial do sensor WorldView-2, numa composição colorida cor real (RGB-123), do dia 8 de abril de 2016. Na imagem nota-se que o reservatório transbordou e tem aspecto lamoso. *a – local de dragagem do rejeito, na área prioritária de 400 m (FT-8 da Fig. 11); b – ensecadeiras e sumps; c – local destinado ao empilhamento do rejeito; d – bacias construídas para o tratamento de efluente (FT-9 da Fig. 11). (B) Ponte da BR-120 sobre o rio Doce, que permite o acesso a UHRN. Detalhe para o rejeito depositado na planície de inundação do rio e a marca da lama na base da ponte. Foto FT-7 obtida em 18 de setembro de 2016 (Fonte: Acervo pessoal).

Fig.11. (A) Barragem da UHRN, mostrando a área considerada prioritária para retirada de rejeito. (B) Vista para um dos diques construídos na Fazenda Floresta, que compreende parte do processo de remoção do rejeito do reservatório. Fotos FT-8 e FT-9 obtidas em 18 de setembro de 2016 (Fonte: Acervo pessoal).

Já em escala macrorregional, as usinas a jusante da UHRN não experimentaram assoreamento do curso d'agua e de nenhum dos reservatórios. Porém, com a passagem da lama de rejeito, a quantidade de material em suspensão e a turbidez excederam as médias históricas observadas durante as estações chuvosas. Transcorridos

quatro anos desde o desastre, parâmetros de qualidade da água anômalos ainda são revelados em diferentes trechos do rio Doce (RAMBOLL, 2020). Nas Figs. 12A e B tem-se a região da UHEB visualizada por uma imagem de satélite de alta resolução espacial e por uma foto obtida em um voo dias após o desastre. As imagens destacam o aspecto lamoso da água.

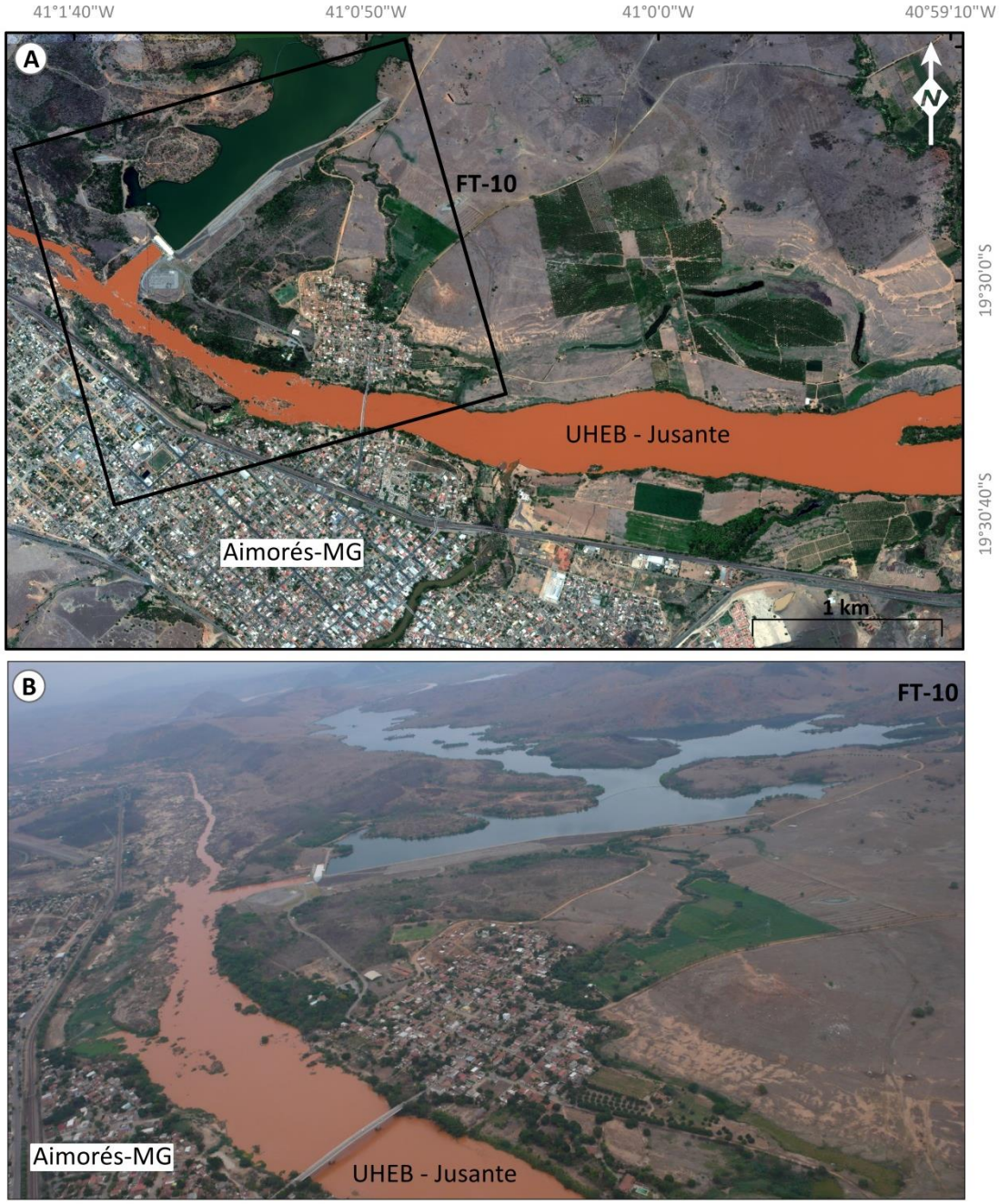

Fig. 12. (A) Composição colorida cor real obtida com dados do sensor orbital WorldView-2 (RGB123) da região do reservatório da UHEB, em 29 de novembro de 2015. Na imagem percebe-se que o médio curso do reservatório ainda não tinha sido atingida pela lama. É nítido o contraste da cor da água dessa região com a parte central do rio, de aparência turva. (B) Foto FT-9 obtida a partir de helicóptero por agentes do IBAMA, em novembro de 2015 (Fonte: Cláudio Dubas).

Apesar dos valores anômalos observados nos parâmetros de qualidade da água do rio Doce, LACTEC (2018) sugere uma tendência ao retorno da linha de base dos parâmetros avaliados até março de 2017. Todavia, IGAM (2018) destaca que, no período chuvoso, compreendido entre os meses de outubro a dezembro de 2017, a turbidez e os sólidos em suspensão, em diferentes trechos do rio, apresentaram valores acima da média histórica e fora do limite permitido para os usos destinados. Nesses trechos, houve variação anormal para os teores de ferro dissolvido, além de alumínio, manganês, chumbo, cobre e níquel.

A recuperação da qualidade da água é um dos temas inclusos nos programas do TACC considerados prioritários, que determinou medidas de captações alternativas de água para vários municípios atingidos (RAMBOLL, 2020). No entanto, nesses programas, os projetos relacionados ao tratamento de água não estão demonstrando resultados eficientes. Por exemplo, em Barra Longa, a estação de tratamento de água encontra-se paralisada desde 2018. Com isso, a população está recebendo esse recurso sem nenhum tipo de tratamento, mesmo com laudos indicando que a qualidade da água não atende os critérios de potabilidade exigidos pelo Ministério da Saúde (RAMBOLL, 2020).

Os danos diretos ou indiretos causados pelos contaminantes do rejeito vão além do comprometimento da saúde das pessoas que fazem uso da água do rio. Eles podem também afetar todo o ecossistema e a biodiversidade aquática. Experimentos controlados para avaliação do crescimento de macrófitas foram realizados por Botino et al (2020). Os autores simularam um ambiente contendo lama de rejeito de ferro e; mostraram que, nessas condições, a produtividade das plantas foi afetada em longo prazo, resultando no comprometimento do desenvolvimento da biomassa.

Efeitos citogenotóxicos, como alterações em DNA, foram observados em espécies coletadas a centenas de quilômetros a jusante do desastre (Segura et al., 2016; Quadra et al., 2019). Partículas contaminadas suspensas na água funcionam como uma fonte de oligoelementos, possibilitando que os seres que habitam o ecossistema do rio Doce estejam expostos a esses poluentes (Quadra et al., 2019).

Na foz do rio Doce, a rápida sedimentação após o colapso impactou as assembleias de macrofaunas estuarinas por meio de taxa de perda de superfície, dentro

de três dias de exposição ao rejeito (Gomes et al., 2017). Já os efeitos de longo prazo, como a bioacumulação de Fe e Mn no fígado e nas brânquias de peixes, foram observados em animais coletados no rio e também na região costeira, três anos após o colapso (Passos et al., 2020; Weber et al., 2020; Bonecker et al., 2019). Tais efeitos causaram danos hepáticos nos peixes, além de induzir a expressão de proteínas e enzimas relacionadas à contaminação por metais (Weber et al., 2020).

A pluma de sedimentos espalhou-se também por centenas de quilômetros adjacentes à costa (Fig. 13), englobando uma área que abrange desde o Rio de Janeiro até a Barra de Caravelas, na Bahia, pondo em risco importantes áreas de preservação marinha, como por exemplo, a Reserva extrativista de Cassurubá e o Arquipélago de Abrolhos (Marta-Almeida et al., 2016; Gomes et al., 2017; Evangelista e Valeriano, 2017; Rudorff et al., 2018; Magris et al., 2019; Valeriano et al., 2019; Quadra et al., 2019, Francini-filho et al., 2019).

Após a chegada da lama na foz, a pluma de sedimentos foi monitorada por dois meses através de simulações matemáticas. O modelo mostrou forte influência do vento na dispersão da pluma de sedimentos do rio Doce, afetando uma imensa região mais ao sul, incluindo áreas marinhas protegidas (Marta Almeida et al 2016). Análises por isótopos radiogênicos de Sr e Nd de amostras de sedimentos, coletadas entre agosto e novembro de 2016, sugerem mistura de material do Arquipélago de Abrolhos com aqueles liberados na Foz do Rio Doce após o rompimento da barragem (Evangelista e Valeriano, 2017). Os autores apontam que o período de coleta das amostras foi caracterizado pela advecção de frentes frias de inverno, que aumentam a componente sul-norte dos ventos de superfície.

Essas inversões da direção da pluma de sedimentos foram um dos temas estudados nessa tese de doutorado, utilizando-se dados de vetores de vento e estimativa de material particulado em suspensão obtida via sensoriamento remoto para indicar possíveis momentos em que o material da foz do rio Doce pode ter alcançado o Arquipélago de Abrolhos. Estudos paralelos desenvolvidos também por métodos de sensoriamento remoto demonstraram que os sedimentos do rio Doce alcançaram a porção sul do Banco de Abrolhos em junho de 2016 (Francelini Filho et al (2019). Os autores validaram a informação com análises da água, composição isotópica e microbiana das amostras, bem como a composição bentônica de recifes.

Na região costeira, um mapeamento de larvas de peixes foi realizado entre janeiro e abril de 2016 (Bonecker et al 2019). Grande parte das espécies coletadas continham sedimentos avermelhados aderidos ao corpo, além de tratos digestivos danificados. Os autores destacaram que houve ainda um aumento de metais pesados no sistema das larvas, se comparados às amostras coletadas antes do desastre. Fernandes et al (2020) avaliaram as respostas de curto prazo da comunidade zooplanctônica ao enriquecimento do metal após os rejeitos atingirem a região costeira. Os autores demonstram impacto agudo nessas comunidades, onde foi reportado o desaparecimento de espécies dentro de três dias após o aumento de turbidez da água da foz.

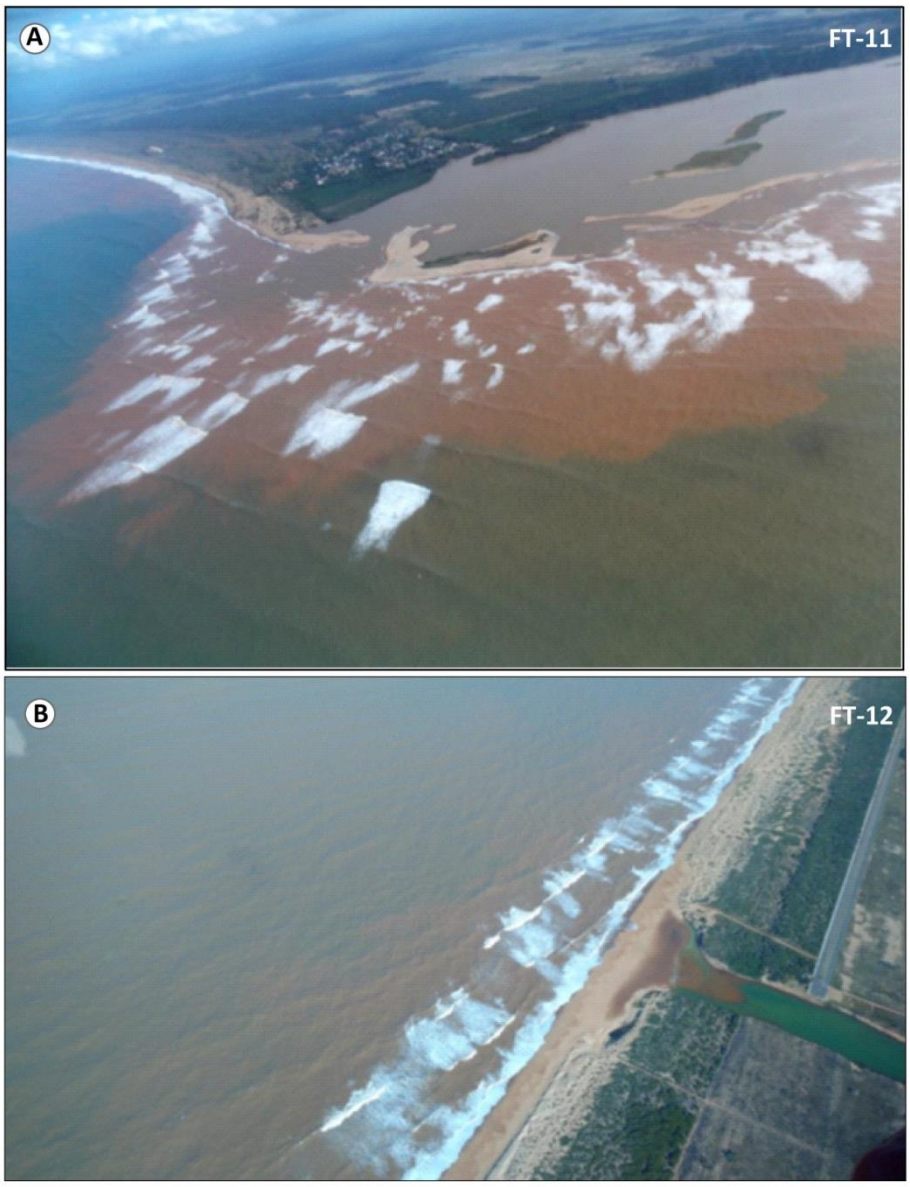

Fig. 13. Dispersão dos sedimentos do rio Doce na região costeira após o colapso. (A) Foto da foz do rio Doce em Linhares-ES, em maio de 2017. (B) Foto do Pontal do Ipiranga, ao norte da desembocadura do rio Doce, em setembro de 2017. Fonte: ICMBio (2017).

2.3. Referências

Agurto-Detzel, H., Bianchi, M., Assumpção, M., Schimmel, M., Collaço, B., Ciardelli, C., Barbosa, J.R., Calhau, J., 2016. The tailings dam failure of 5 November 2015 in SE Brazil and its preceding seismic sequence, Geophysical Research Letter. 43, 4929-4936. http://dx.doi.org/10.1002/2016GL069257.

ANA – Agência Nacional de Águas., 2016. Encarte Especial sobre a Bacia do Rio Doce, Rompimento da Barragem em Mariana/MG. https://www.ana.gov.br/noticias-antigas/encarte-da-ana-reaone-informaassaues-sobre-rio.2019-03-15.9924387769. Acessado em 16 de agosto de 2020.

Bonecker, A.C.T., Castro, M.S., Costa, P.G., Bianchini, A., Bonecker, S.L.C., 2017. Larval fish assemblages of the coastal area affected by the tailings of the collapsed dam in southeast Brazil. Regional Studies in Marine Science. 32, 100848. https://doi.org/10.1016/j.rsma.2019.100848.

Bottino, F., Milan, J.A.M., Cunha-Santino, M.B., Bianchini-Jr, I., 2017. Influence of the residue from an iron mining dam in the growth of two macrophyte species. Chemosphere 186, 488-494.

Carmo, F.F., Kamino, L.H.Y., Tobias Júnior, R., Campos, I.C., Carmo, F.F., Silvino, G., Castro, K.J.S.X., Mauro, M.L., Rodrigues, N.U.A., Miranda, Pinto, C.E.F., 2017. Fundão tailings dam failures: the environment tragedy of the largest technological disaster of Brazilian mining in global context. Perspectives in Ecology and Conservation 15, 145–151. http://dx.doi.org/10.1016/j.pecon.2017.06.002.

Duarte, E.B., Neves, M.A., Oliveira, F.B., Martins, M.E., Oliveira, C.H.R., Burak, D.L., Orlando, M.T.D.A., Rangel, C.V.G.T., 2020. Trace metals in Rio Doce sediments before and after the collapse of the Fundão iron ore tailing dam, Southeastern Brazil. Chemosphere. 262, 127879.

EMBRAPA - Empresa Brasileira de Pesquisa Agropecuária, Ministério da Agricultura, Pecuária e Abastecimento., 2015. Tragédia em Mariana: produção agropecuária em áreas atingidas está comprometida. https://www.embrapa.br/busca-de-noticias/-/noticia/8410974/tragedia-em-mariana-producao-agropecuaria-em-areas-atingidas-esta-comprometida (Acessado em 17 de agosto de 2020).

Evangelista, H., Valeriano, C., 2017. Sumário das análises de isótopos radiogênicos de Sr e Nd em sedimentos da foz do rio Doce-ES e do Parque Nacional dos Abrolhos-BA (Antes e depois do rompimento da barragem de rejeitos da Samarco em Mariana-MG. Relatório. Laboratório de radioecologia e Mudanças Globais. Disponível em: http://www.consultaesic.cgu.gov.br/busca/dados/Lists/Pedido/Attachments/612349/RESPOSTA_PEDIDO_02680002082201705%20-%20sumario_de_analises_UERJ_21Set2017.pdf (Acessado em julho de 2020).

Fernandes, L.F.L., Paiva, T.R., Longhini, C. M., Pereira, J. B., Ghisolfi, R.D., Lázaro, G.C.S., Demoner, L.E., Laino, P.S., Conceição, L.R., Sá, F., Neto, R.R., Dias-Jr, C., Lemos, K.N., Quaresma, V.S., Oliveira, K.S., Grilo, C.F., Rocha, G.M., 2020. Marine zooplankton dynamics after a major mining dam rupture in the Doce River, southeastern Brazil: Rapid response to a changing environment. Science of the Total Environment. 736, 139621.

Francini-Filho, R.B., Cordeiro, M.C., Omachi, C.Y., Rocha, A.M., Bahiense, L., Garcia, G.D., Tschoeke, D., Almeida, M.G., Rangel, T.P., Oliveira, B.C.V.,

Almeida, D.Q.R., Menezes, R., Mazzei, E.F., Joyeux, J.C., Rezende, C.E., Thompson, C.C., Thompson, F.L., 2019. Remote sensing, isotopic composition and metagenomics analyses revealed Doce River ore plume reached the southern Abrolhos Bank Reefs. Science of the Total Environment. 697, 134038.

Gomes, L.E.O., Correa, L.B., Sá, F., Neto, R.R., Bernadinho, A.F., 2017. The impacts of the Samarco mine tailing spill on the Rio Doce estuary, Eastern Brazil. Marine Pollution Bulletin 120, 28–36.

Hatje, V., Pedreira, R.M.A., Rezende, C.E., Schettini, C.A.F.S., Souza, G.C., Marin, D.C., Hackspacher, P.C., 2017. The environmental impacts of one of the largest tailing dam failures worldwide. Sci. Rep. 7, 10706.

IBAMA - Instituto Brasileiro do Meio Ambiente e dos Recursos Naturais Renováveis., 2015. Laudo Técnico Preliminar dos Impactos ambientais decorrentes do desastre envolvendo o rompimento da barragem de Fundão, em Mariana, Minas Gerais. 38 p.

ICMBio – Instituto Chico Mendes de Conservação da Biodiversidade., 2017. Monitoramento da Pluma de Sedimentos Proveniente da Barragem de Fundão. Nota Técnica nº 23/2017/TAMAR. 44p.

ICOLD, International Commission on Large Dams. 2001. Tailings dams: risk of dangerous occurrences, lessons learnt from practical experiences. Paris: ICOLD, 144 p. 2001. Bulletin, 121.

IGAM - Instituto Mineiro de Gestão das Águas Gerência de Monitoramento de Qualidade das Águas., 2018. Acompanhamento da Qualidade das Águas do Rio Doce Após o Rompimento da Barragem da Samarco no distrito de Bento Rodrigues – Mariana/MG. Relatório técnico. 27 p.

LACTEC., 2018. Diagnóstico socioambiental dos danos decorrentes do rompimento da barragem de Fundão na bacia do rio Doce. Relatório Pós-Desastre 2: Meios Físico e Biótico. http://www.mpf.mp.br/grandes-casos/caso-samarco/documentos/relatorios-lactec/lactec_relatorio-pos-desastre-grupo-02 (acessado em julho de 2020).

Magris, R.A., Marta-Almeida, M.,Monteiro, J.A.F., Ban, N.C., 2019. A modelling approach to assess the impact of landmining onmarine biodiversity: assessment in coastal catchments experiencing catastrophic events (SWBrazil). Sci. Total Environ. 659, 828–840. https://doi.org/10.1016/j.scitotenv.2018.12.238.

Marta-Almeida, M.M., Mendes, R., Amorim, F.N., Cirano, M., Dias, J.M., 2016. Fundao Dam collapse: oceanic dispersion of River Doce after the greatest Brazilian environmental accident. Mar. Pollut. Bull. 112, 359–364.

Morgenstern, N.R., Vick, S.G., Viotti, C.B., Watts, B.D., 2016. Comitê de Especialistas para Análise da Ruptura da Barragem de Rejeitos de Fundão. Relatório sobre as Causas Imediatas da Ruptura da Barragem de Fundão. 83p.

Orlando, M.T.A., Galvão, E.S., Cavichini, A.S.A., Rangel, C.V.G.T., Orlando, C.G.P., Grilo, C.F., Soares, J., Oliveira, K.S.S.O., Sá, F., Junior, A.S., Bastos, AC., Quaresma, V.S., 2020. Tracing iron ore tailings in the marine environment: An investigation of the Fundão dam failure. Chemosphere. 257, 127184. https://doi.org/10.1016/j.chemosphere.2020.127184.

Passos, L.S., Gnocchi, K.G., Pereira, T.M., Coppo, G.C., Cabral, D.S., Gomes, L.C., 2020. Is the Doce River elutriate or its water toxic to Astyanax lacustris (Teleostei:

Characidae) three years after the Samarco mining dam collapse?. Science of the Total Environment. 736, 139644.

Quadra, G.R., Roland, F., Barros, N., Malm, O., Lino, A.S., Azevedo, G.M., Thomaz, J.R., Vieira, L.F.A., Fontes, M.M.P., Almeida, R.M., Mendonça, R.F., Cardoso, S.J., Guida, Y.S., Campos, J.M.S., 2019. Far-reaching cytogenotoxic effects of mine waste from the Fundão dam disaster in Brazil. Chemosphere. 215, 753-757.

RAMBOL., 2017. Avaliação do programa de reparação integral da bacia do rio Doce. http://www.mpf.mp.br/grandes-casos/caso-samarco/atuacao-do-mpf/pareceres-e-relatorios. Acessado em 16 de agosto de 2020.

RAMBOL., 2019. Relatório de monitoramento consolidado dos programas socioeconômicos e socioambientais para a restauração da bacia do rio Doce. http://www.mpf.mp.br/grandes-casos/caso-samarco/atuacao-do-mpf/pareceres-e-relatorios. Acessado em 16 de agosto de 2020.

RAMBOL, 2020a. Relatório de Monitoramento Mensal – Mês 039 – Março/2020. http://www.mpf.mp.br/grandes-casos/caso-samarco/atuacao-do-mpf/pareceres-e-relatorios (Acessado em 16 de agosto de 2020).

RAMBOL, 2020b. Parecer técnico - eixo prioritário n° 3: Sistema de abastecimento de água de gesteira (Barra Longa). http://www.mpf.mp.br/grandes-casos/caso-samarco/atuacao-do-mpf/pareceres-e-relatorios (Acessado em 16 de agosto de 2020).

Rudorff, N., Rudorff, C.M., Kampel, M., Ortiz, G., 2018. Remote sensing monitoring of the impact of a major mining wastewater disaster on the turbidity of the Doce river plume off the eastern Brazilian coast. ISPRS J. Photogramm. Remote Sens. https://doi.org/10.1016/j.isprsjprs.2018.02.013.

Schaefer, C.E.G.R., Santos, E.E., Fernandes-Filho, E.I., Assis, I.R., 2016. Paisagens de Lama: Os Tecnossolos para recuperação ambiental de áreas afetadas pelo desastre da barragem do Fundão, em Mariana. Boletim Informativo - SBSC. 18-23.

SEDRU – Secretaria de Estado de desenvolvimento regional, política e urbana e gestão metropolitana., 2016. Avaliação dos efeitos e desdobramentos do rompimento da Barragem de Fundão em Mariana-MG. Relatório do Grupo da Força-Tarefa, Belo Horizonte..http://www.agenciaminas.mg.gov.br/ckeditor_assets/attachments/770/relatorio_final_ft_03_02_2016_15h5min.pdf. Acessado em 16 de agosto de 2020.

Segura, F.R., Nunes, E.A., Paniz, F.P., Paulelli, A.C.C., Rodrigues, G.B., Braga, G.U.L., Pedreira Filho,W.R., Barbosa Jr., F., Cerchiaro, G., Silva, F.F., Batista, B.L., 2016. Potential risks of the residue fromSamarco'smine damburst (Bento Rodrigues, Brazil). Environmental Pollution. 218, 813–825.

Valeriano, C.M., Neumann, R., Alkimim, A.R., Evangelista, H., Heilbron, M., Neto, C.C.A., Souza, G.P., 2019. Sm–Nd and Sr isotope fingerprinting of iron mining tailing deposits spilled from the failed SAMARCO Fundão dam 2015 accident at Mariana, SE-Brazil. Applied Geochemistry. 106, 34–44.

Viana, J.H.M., Costa, A.M., A Ciência do Solo como instrumento para a recuperação das áreas afetadas pelo desastre de Mariana e dos solos na Bacia do Rio Doce. Boletim Informativo - SBSC. 24-27.

Weber, A, A., Sales, C.F., Faria, F.S., Melo, R.M.C., Bazzoli, N., Rizzo, E., 2020. Effects of metal contamination on liver in two fish species from a highly impacted neotropical river: A case study of the Fundão dam, Brazil. Ecotoxicology and Environmental Safety. 190,110165.

CAPÍTULO 3

An assessment of natural and manmade hazard effects on the underwater light field of the Doce River continental shelf

K.T.O. Coimbra, E. Alcântara, C.R. Souza Filho.

Published in the *Science of The Total Environment*. Volume 685, 1 October 2019, Pages 1087-1096. https://doi.org/10.1016/j.scitotenv.2019.06.127

Natural and manmade disasters have occurred more frequently due mainly to climate change and human pressure for productivity. One of the world's vastest disasters in the mining industry occurred due to the collapse of the Fundao dam, Brazil, which discharged about 43 million m^3 of iron tailings at the Doce River basin. Extreme natural events also affect this region and provoke substantial mass movement and substantial floods in the Doce River basin, and flow of anomalous volumes of sediments in its mouth. The extent of tailings and the sediment flow in these events were approached in previous research. However, their effects on the penetration of sunlight into the water column in the coastal region are unknown. Here, we evaluate the effects of an extreme natural event and a manmade disaster on the light regime of the water column at the Doce River mouth, using remote sensing data. In both events, the spatial and temporal distribution of suspended particulate matter (SPM), diffuse light attenuation coefficient (K_d490) and Euphotic Zone (Z_{eu}) were analyzed. During the natural event, light penetration into the water column was strongly attenuated (K_d490: 0.35 m^{-1}; SPM: 8.81 g/m^3) but re-established after 1 month due to sediment deposition. In the case of the dam collapse, the attenuation of light penetration was also intense along the event (K_d490: 0.34 m^{-1}; SPM: 13.87 g/m^3); however, sediment deposition occurred sooner. Resuspension of sediments due to wind action was recurrent after 8 months of the dam collapse, in contrast to the natural event, where re-suspension was not perceptible in satellite images. The results indicate that both events have considerable effects on the penetration of light in the water column, but with different intensity and length.

3.1. Introduction

Climate and environmental changes, population growth, globalization, and demand for higher productivity make human beings increasingly exposed to natural and manmade disasters. These events are comparable in many ways and can cause social, economic and environmental damage at different scales (Garcia et al., 2017). Extreme natural events include climatic and meteorological phenomena that can be sudden, such as storms, floods, hurricanes, avalanches, earthquakes, tsunamis, and volcanic eruptions, or episodic, such as heat waves and droughts.

Manmade disasters are sudden events caused by failures involving technology and manipulation of the natural environment, such as dam failure, collapse of bridges, industrial accidents, marine collisions, toxic and radioactive waste dumping (Baum et al., 1983; Lari et al., 2009). Extreme natural events have been increasingly common in Brazil, among which are heat waves, severe droughts, heavy rainfall with consequent floods and landslides.

Among manmade disasters, the most recent and serious documented in Brazil occurred on November 5th, 2015, with the rupture of Fundao dam (Marta-Almeida et al., 2016) in the Doce River basin. This basin covers part of the States of Minas Gerais and Espirito Santo, in southeastern Brazil (Fig. 1A).

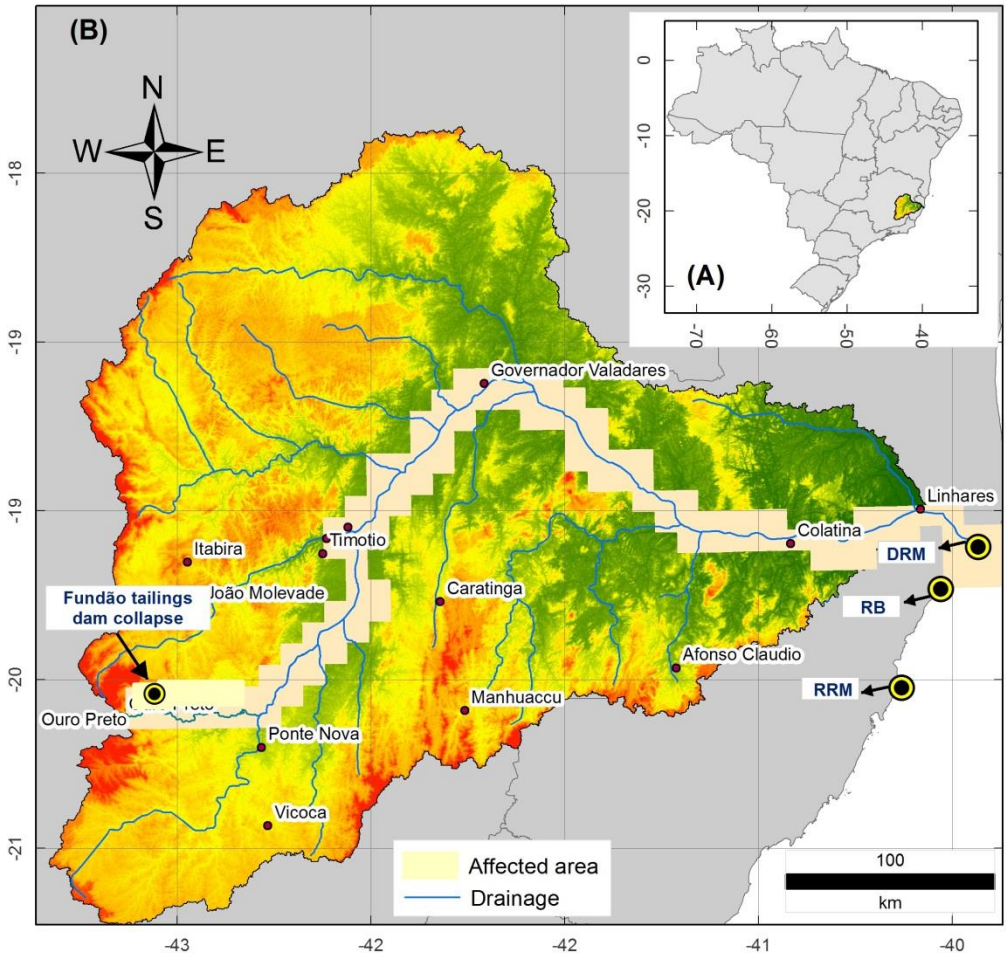

Fig.1. (A) Doce River basin in Brazil. (B) Site of the collapse of the Fundao tailing dam indicated by black arrow. DRM= Doce river mouth; RRM= Riacho River mouth. RB= Regência Beach.

According to Fernandes et al. (2016), the abrupt disruption of the Fundao dam discharged between 55 and 62 million m^3 of tailings in the Doce River basin, destroyed the Bento Rodrigues district, and reached the Atlantic Ocean (approximately 600 km from the site of rupture), by November 22, 2015 (Figs. 1B, 2A, B, C and D).

In the same basin, it is common to occur above average rainfall at certain times of the year, which occasionally cause flooding of rivers and floods in cities located close to the river banks. One of these anomalous flood events occurred in 2013 and was recorded by the flood alert system of the Brazilian Geological Survey (CPRM, 2014). Fig. 2E shows the suspended particulate matter discharged simultaneously at the Doce and Riacho Rivers mouths, under this high precipitation (523 mm/month) condition observed in 2013.

Marta-Almeida et al. (2016) analyzed the dispersion of the freshwater plume at the Doce River mouth after 2 months of the disaster based on a hydrodynamic model and satellite images. The authors showed that water from the river may have spread hundreds of miles after the accident and highlighted the importance of wind action in this process.

Gomes et al. (2017) carried out sediment sampling to investigate short term impacts on benthic communities and accumulation of metallic traces in post-disaster estuarine sediments. High concentrations of trace metals were detected. According to the authors, the rapid sedimentation after the accident also affected the macroalgal estuarine communities by increasing the mortality rate.

Hatje et al. (2017) collected sediment and water samples along the affected area in the Doce River basin 75 days after the accident and observed that during sediment transport there was a tendency for all trace elements dissolved to increase, except Mn.

Fernandes et al. (2016) evaluated the ecological and socioeconomic impacts of this catastrophe. They verified that about 1 million people in 41 municipalities were hampered due to reduced local access to fishing resources, drinking water, production sites crop, hydroelectric power generation and raw materials. The authors indicate that the soil stability of the basin in the affected regions was compromised, and these sites were susceptible to new disturbances, including landslides and mass movements.

Understanding the causes and effects of disasters, either natural or manmade, is a major scientific challenge due to the lack of information about the previous state of the environment. The use of remote sensing images in disaster monitoring has become increasingly common due to the expansion of geospatial technologies and the availability of daily images (Joyce et al., 2009).

The monitoring of water color in coastal environments has been successfully carried out through the development of bio-optical algorithms applied to satellite images (Le et al., 2016). The Moderate Resolution Imaging Spectroradiometer - MODIS/Aqua sensor has been used frequently because of its temporal, spatial, radiometric and spectral characteristics, as well as easily accessible ocean color products (e.g., Miller and Mckee, 2004; Chen et al., 2006; Lahet and Stramski,2010).

Bio-optical parameters of water are often used to assess the quality of ocean water, as their color is the result of a complex mixture of dissolved or particulate materials having various optical properties, called apparent and inherent, which interact with light differently according to their concentration and nature (Babin et al., 2003).

Previous studies have dealt variously with the consequences of the disruption of the Mariana dam. However, there was no comparative study of the effect of that disaster with the other triggered by excessive precipitation in 2013 on solar light penetration in the water column at the mouth of the Doce River. In both events, a large volume of sediments was carried to the main channel of the river, reaching its mouth and the Atlantic Ocean. The Mariana disaster caused the transport of material from the tailings with different granulometry and composition (dominantly dense, sandy sediments, composed of quartz and hematite) in comparison to that transported by surface runoff in the basin generated by precipitation (clay and silt sediments, with lower density) (Silva et al., 2016). The composition and granulometry of the suspended sediment control the absorption and scattering of light as it penetrates the surface of the water (Chang and Whitmire, 2009).

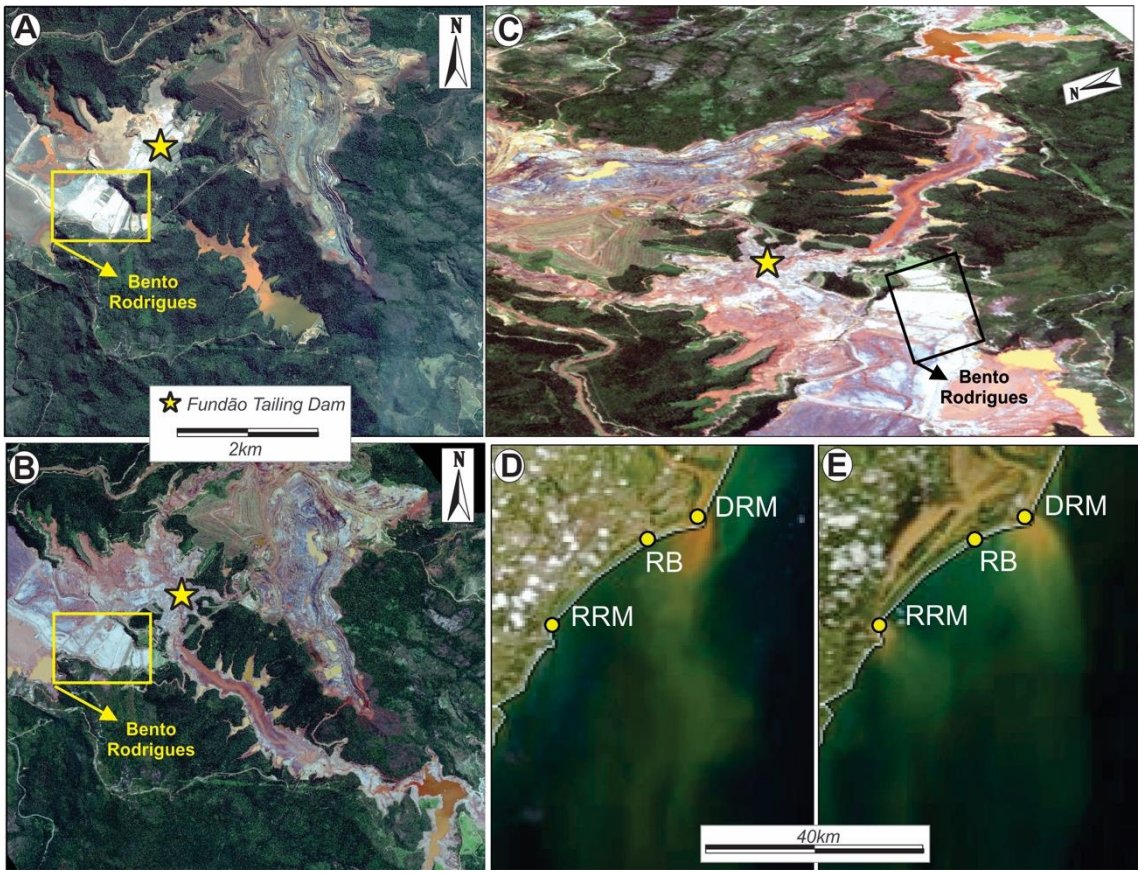

Fig.2. Worldview-2 true color compositions of the Fundao dam(located in the starmark) three months before the collapse (A) and after the collapse (B, C). The squares indicate the Bento Rodrigues district. (D) and (E) correspond to true color composite images from MODIS/Aqua data, respectively showing the dispersion of suspended particulate matter as a result of the collapse of the Fundao tailings dam (December 2015) (D) and under the extreme rainfall event (December 2013) (E). DRM= Doce River mouth. RB = Regência Beach. RRM = Riacho River mouth.

In this context, the hypothesis to be tested in this work considers that the extreme precipitation will have a short-term effect, similar to that caused by the rupture of the dam. However, the sediments produced by the rupture, due to its composition, should have prolonged consequences to the environment.

To test the hypothesis, the aim of this work was to evaluate and compare the effects of the aforementioned events on the penetration of sunlight into the water column of the Doce River mouth. This evaluation was carried out using satellite data between 2011 and 2016.

The necessary steps to reach the proposed aim include: (i) gathering of a time series of precipitation and wind speed for the study area; (ii) applying a bio-optical algorithm to estimate the concentration of suspended particulate matter (SPM) and the

depth of the euphotic zone (Z_{eu}); (iii) obtaining the vertical diffuse attenuation coefficient for downwelling irradiance (K_d) from satellite data; (iv) an evaluation of the extent of the sediment plume in both events and (e) a comparison of the impact of both events on the light attenuation.

3.2. Materials and methods

3.2.1. Rainfall and wind speed

Monthly average areal rainfall and wind speed data from 2011 to 2016 were downloaded from NASA's Geospatial Interactive Online Visualization and analysis Infrastructure (Giovanni) (https://giovanni.gsfc.nasa.gov/giovanni/). The average values were obtained using the Doce River basin outline. The Tropical Rainfall Measuring Mission (TRMM), product 3B43, provided rainfall data (Curtarelli et al., 2014). The rainfall data from TRMM were validated for the Brazilian territory by Franchito et al. (2009). The results showed that TRMM PR seasonal rainfall is well correlated with ANEEL (Brazilian Electricity Regulatory Agency) data over most of Brazil (particularly for the southeastern region).

Wind speed data were obtained via the Modern-Era Retrospective Analysis for Research and Applications, version 2 (MERRA-2). MERRA-2 is a NASA atmospheric reanalysis for the satellite era using the Goddard Earth Observing System Model, Version 5 (GEOS-5), with its Atmospheric Data Assimilation System (ADAS), version 5.12.4 (Rienecker et al., 2011). The wind speed data from MERRA-2 were validated by Gelaro et al. (2017). They found that the mean difference (1980–2015; mm day−1) between the (corrected) MERRA-2 precipitation seen by the land surface and the model-generated precipitation within the MERRA-2 system ranged from 2 to 8 mm day−1 for our study area. Here, it is important to highlight that the feature of interest for our analysis of wind and rainfall data is the variability and not exact values.

3.2.2. Satellite images

A monthly time series of MODIS/Aqua images from 2011 to 2016 were downloaded from the Ocean Biology Processing Group – OBPG website (https://oceancolor.gsfc.nasa.gov/) at level 3 processing (spatial resolution of 4 km). We downloaded the monthly product in remote sensing reflectance (R_{rs}, sr^{-1}). The monthly

images contain the best possible observations and were selected based on high coverage, absence of clouds (or cloud shadow), low viewing angle and aerosol loading.

The R_{rs} product has been tested and validated in coastal waters in different sites (e.g., Carswell et al., 2017; Goyens et al., 2013). The spectral R_{rs} is the ratio between the water-leaving radiance (L_w, w m^{-2} sr^{-1} nm^{-1}) and the downwelling irradiance (E_d, w m^{-2} nm^{-1}). According to Gordon and Wang (1994), the derived L_w is normalized to remove remaining effects of solar orientation and atmospheric attenuation of the downwelling radiation to produce normalized water leaving radiance (nL_w). The R_{rs} is then obtained by simply dividing L_w by the mean extraterrestrial solar irradiance, $F_0(\lambda)$, as follows:

$$R_{rs} = \frac{L_w\,(\lambda)}{F_0 \text{ x } f_s \text{ x } \cos(\theta_s) \text{ x } td_s} x\ f_b(\lambda)\ x\ f_\lambda \quad (1)$$

where F_0 is the extraterrestrial solar irradiance (Thuillier et al., 2003), f_s is the adjustment of F_0 for variation in Earth-Sun distance, f_b is the bidirectional reflectance correction, and f_λ is the correction for out-of-band response.

We also used images from the Operational Land Imager (OLI) onboard Landsat-8 (OLI/L8) satellite in surface reflectance (SR, dimensionless), with 30 m of spatial resolution. SR is a product derived from processing the data through the LASRC (Landsat 8 Surface Reflectance Code) algorithm. The OLI/L8 images from 2013 to 2016 were downloaded from USGS Earth Explorer (https://earthexplorer.usgs.gov). Different authors (e.g. Bernardo et al., 2017; Pahlevan et al., 2017) have validated this product. The general rule to select the OLI/L8 images was to have at least one image representative of each month of the searched years.

Due to the intense cloud cover in some months of the time series, only 25 cloud free images were used. The OLI/L8 surface reflectance was converted to remote sensing reflectance dividing surface reflectance images by π (Moses et al., 2012). OLI/L8 images were only used to map the SPM because their spatial resolution can provide more detail about the distribution and horizontal gradient.

In this case, it is expected that the SPM values obtained by MODIS and OLI/L8 will be different because the spatial resolution can influence the pixel

reflectance value, as showed by Dorji and Fearns (2017). Also, we need to consider that MODIS products comprise monthly compositions, whereas OLI/L8 products are yielded from single scenes.

3.2.3. Diffuse attenuation coefficient (K_d, m^{-1})

The water column light availability determines the euphotic zone and can limit the type and vertical distribution of algal species. The light attenuation is traditionally quantified as the attenuation coefficient of downwelling irradiance at 490 nm (K_d490). K_d is an important optical property because is related to penetration and availability of light and heat transfer in aquatic systems, being considered as a proxy for water quality classification. K_d can be defined as the exponential decay of downwelling irradiance (E_d, $W \cdot m^{-2}$) with depth (z). In this work, we utilized K_d490 derived from MODIS images (Werdell, 2005) as:

$$K_d490 = 0.1853\ x\ \left(\frac{nL_{w4}\ 490}{nL_{w4}\ 555}\right)^{-1.349} \quad (2)$$

where nL_w (490) and nL_w (555) are normalized water-leaving radiances at 490 and 555 nm.

3.2.4. Euphotic zone (Z_{eu})

Z_{eu} is defined as the depth where photosynthetic available radiation (PAR) corresponds to 1% of its surface value (Kirk, 1994). Z_{eu} is a measure of water clarity, which is an indicator for primary production, heat and gas transfer between the water surface and the atmosphere, specially greenhouse gases, such as CO_2 (Shang et al., 2011). Changes in Z_{eu} can reveal environmental patterns associated with climate changes, such as changes in phytoplankton and associated environmental parameters or changes in type and size of particles entering the aquatic system. Here, we used the algorithm developed by Zhao et al. (2013) and validated by many authors (e.g. Lee et al., 2013) to estimate Z_{eu}:

$$Z_{eu} = 0.28 + \left(\frac{395.92\ x\ 0.0092}{0.0092 + K_d490}\right) \quad (3)$$

Where Z_{eu} is the euphotic zone depth (m) and K_d490 is the downwelling attenuation coefficient (m^{-1}), which was obtained by Eq. (2).

3.2.5. Suspended particulate matter (SPM)

SPM is composed of organic and terrestrial particles and their concentration and variability affect the biological community by blocking the sunlight penetration into the water column. The SPM concentration was estimated using MODIS and OLI/L8 images based on the algorithm proposed and validated by Nechad et al. (2010) and tested in different environments with relative success (e.g. Gangloff et al., 2017; Cao et al., 2017). The algorithm is a multisensor model, which means the model is applicable to any sensor (Eq. (4)).

$$SPM = \left(\frac{A^p \, x \, \rho w}{1 - \rho w / C^p}\right) + B^p \quad (4)$$

Where ρw corresponds to the water leaving reflectance (ρw = Rrs × π) at a certain wavelength. A^p, C^p and B^p are coefficients dependent on the chosen wavelength. As advised by Nechad et al. (2010), for satellite data applications, B^p is set to zero because the satellite sensor and processing will probably have different measurement errors from the calibration data. For MODIS, at 667 nm, A^p = 374.11 and C^p = 17.36; for OLI/L8, at 654 nm, A^p= 289.29 and C^p = 16.86.

3.3. Results

3.3.1. Time series

The time series of rainfall, wind speed, Kd490, SPM and Zeu from 2011 to 2016 are shown in Fig. 3. Two events were highlighted in this figure: the first, corresponding to the natural event caused by extreme precipitation, which was responsible for the flood of the Doce River in December of 2013 (E1-2013) and, the second, representing the manmade disaster of the Fundao dam collapse in November 2015 (E2-2015).

In addition, there are three periods highlighted in Fig. 3: P1, from January 2011 to the occurrence of E1-2013; P2, the period between event E1-2013 and E2-2015; and P3, between event E2-2015 and December 2016. In these periods it is possible to observe a significant difference in the bio-optical properties of the water between the events.

The time series of monthly rainfall of the Doce River basin shows a clear division between dry and rainy periods (Fig. 3A). In 2011, the dry period occurred between May and September. In this interval, the mean rainfall was 10.3 mm/month. In 2012 and 2016, the dry period occurred between February and October, with an average rainfall of 49 and 58 mm/month, respectively. In 2013, the dry period began in April and remained until October, with an average rainfall of 40 mm/month. In 2014, it was from April to September, with an average of 34 mm/month. In 2014 and 2015, the monthly precipitation did not exceed 200 mm/month, in contrast to 2011, 2012 and 2016, when precipitation reached up to 300 mm/month. Discrepant precipitation occurred in December 2013, with values reaching up to 523 mm/month. The wind speed showed a clear pattern with higher values between August and October (5-6 m/s) and lower values for the other months (3.8-5 m/s; Fig.3B).

The time series of K_d490, SPM and Z_{eu} extracted from the "S" pixel in the MODIS images, located near the DRM, are shown in Fig. 3. The K_d490 (Fig. 3C) has a well-defined pattern with a tendency to increase in the timeline. The values of K_d490 were relatively higher for E1-2013 (= 0.35 m^{-1}) than for E2-2015 (= 0.34 m^{-1}). Comparing the three periods of the historical series it is possible to note that the higher values of K_d490 appear in the P3 (values up to 0.42 m^{-1}).

The SPM data (Fig. 3D) follow practically the same pattern as K_d490. However, the values of SPM in the E2-2015 (= 11.60 g/m^3) were higher than E1-2013 (= 8.81 g/m^3). The highest SPM values also occurred in P3 with concentration up to 13.87 g/m^3. Consequently, Z_{eu} had an inverse pattern to that presented by K_d490 and SPM, with the extreme values observed in P1 (average of 24.30 m) and slightest values for P2 and P3 (average of 21.74 m and 15.07 m, respectively). This tendency is expected because Z_{eu} is directly affected by the amount of suspended material that can scatter the light, preventing its penetration into the water column.

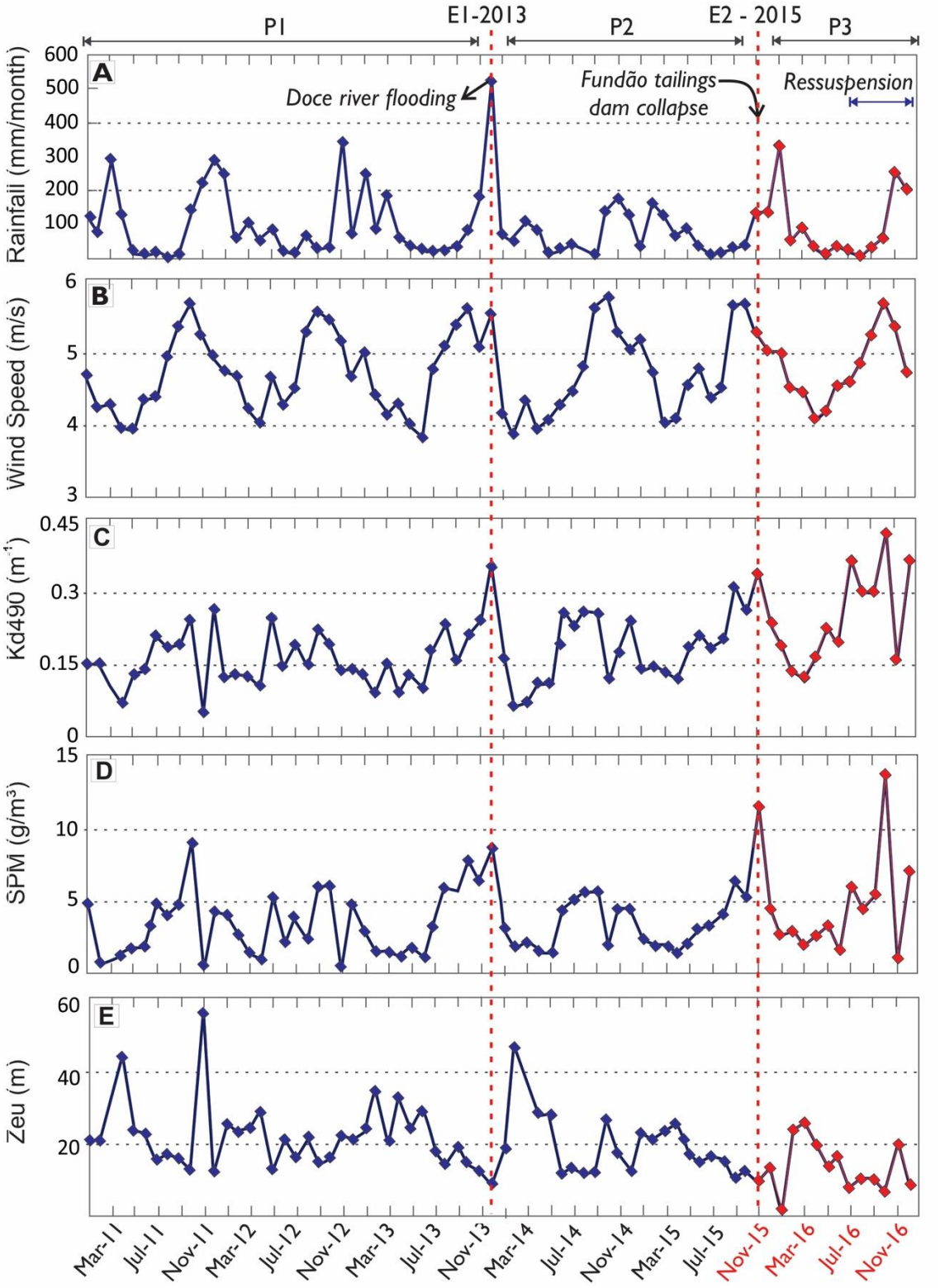

Fig.3. Historical series of the meteorological data of the Doce River basin from 2011 to 2016: (A) Rainfall, (B) wind speed. Bio-optical parameters at the sampling point *S at Doce River mouth: (C) K_d490 (D) SPM (E) Z_{eu}. In E1-2013, the highest rainfall value of all historical series (523 mm/month) is recorded. Note that high values of the bio-optical parameters of water, like K_d490 and SPM and low values of Z_{eu}, occur both in E1-2013 and in E2-2015.

3.3.2. Spatial-temporal analysis of K_d490, SPM and Z_{eu}

Fig. 4 shows the dispersion maps of K_d490, SPM and Z_{eu} for the Doce River plume according to the data analyzed for the months of December of 2011 to 2016. The month of December was chosen for the analysis because it is representative of the events E1-2013 and E2-2015 that was highlighted in Fig. 3.

The maps in Fig. 4 reveal that the SPM dispersion was more pronounced in 2013 (E1) and 2015 (E2) than in other years. The anomalous rainfall of the Doce River basin, which caused the flooding of both the Doce River and the Riacho River, characterizes the E1-2013 event; under these conditions, considerable volumes of sediments were discharged into DRM and RRM and, consequently, SPM reaches up to 19 g/m^3.

In 2015, the sediment plume also reached broad proportions along the coastline, but the greatest SPM values (19 g/m^3) occur only between DRM and RB. It is known that in 2015, the rainfall did not exceed 135 mm/month, and the large volume of sediments released in DRM is linked to the material coming from the dam. In December 2011, 2012 and 2014, the monthly rainfall was 288 mm, 68.13 mm, 125 mm, respectively; in these years, SPM concentrations up to 17 g/m^3 were mapped in the coastal region between DRM and RB. In 2016, which marks P3 (post-collapse of the dam), rainfall was 204 mm/month. In this case, the sediment plume was smaller if compared to 2015; however, the SPM values close to DRM and RRM were higher.

In December of 2011, the sediment plume was up to 15 km to NE and 50 km to SW from DRM. In this situation, high values of K_d490 (~ 0.4 m^{-1}) and low values of Z_{eu} (8.8 m) were verified at approximately 12 km to SW from DRM. Moving away from DRM, the values of K_d490 decrease and remain lower than 0.3 m^{-1}; consequently, the values of Z_{eu} increase (>12 m).

In December 2012, the plume arrived about 7 km to NE and 40 km to SW of DRM. The K_d490 values up to 0.4 m^{-1} and Z_{eu} ~ 8 m were restricted to RB. In December 2014, the plume dispersion was 15 km to NE and 40 km to SW of DRM. The highest values of K_d490 were around 0.4 m^{-1} and the lowest values of Z_{eu} around 9 m, which occur punctually in the RB region. In December 2013, the largest plume area was mapped, which reached 20 km to NE and 76 km to SW of DRM.

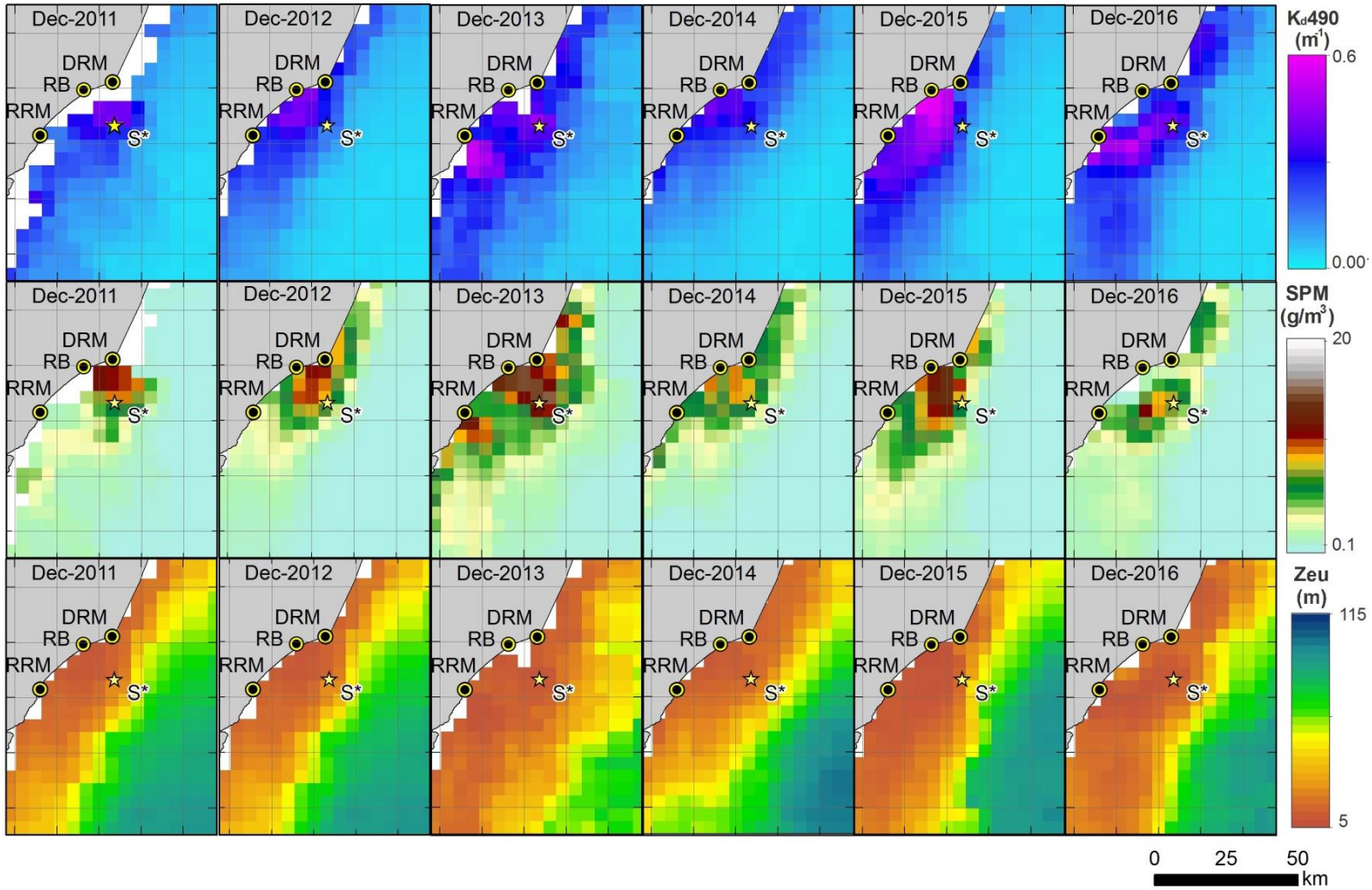

Fig.4. Spatial distribution of K_d490, SPM and Z_{eu} for December between 2011 and 2016. S* in the maps indicates where the time series displayed in Fig. 3 were sampled. RB = Regência beach. DRM = Doce River Mouth. RRM= Riacho River Mouth.

Fig. 4 shows three regions with high K_d490 and low Z_{eu} values (with reference to DRM): (i) ~ 15 km to NE, with K_d490 ~ 0.35 m^{-1} and Z_{eu} ~ 10 m; (ii) ~ 8 km to SW, with K_d490 ~ 0.47 m^{-1} and Z_{eu} ~ 7.8 m; (iii) ~ 30 km to SW, in RRM, with K_d490 ~ 0.53 m^{-1} and Z_{eu} ~ 7.2 m. Regarding 2015, the K_d490 around 0.57 m^{-1} and Z_{eu} 6.51 m are located in the RB, and the plume has reached 70 km to SW of DRM. In December 2016, the plume reached 25 km to NE and 60 km to SW of DRM.

The A-B profile positioned to compare the SPM dispersion during the two analyzed events is shown in Fig. 5. The profiles (with values extraction in every 7 km) have NE-SW direction with approximately 49 km distance from DRM. The profile is along the RB (P1 to P3) and the RRM regions (P5). It is noticed that both events show a gradual decay tendency between P2 and P8. In E1-2013 (Fig. 5A), SPM peaks were observed in P2 (SPM > 10 g/m^3) and P5 (SPM > 7 g/m^3). In E2-2015 (Fig. 5B), the SPM peaks occur between P2 and P3 (SPM > 10 g/m^3) from which the values tend to decrease (SPM < 6 g/m^3).

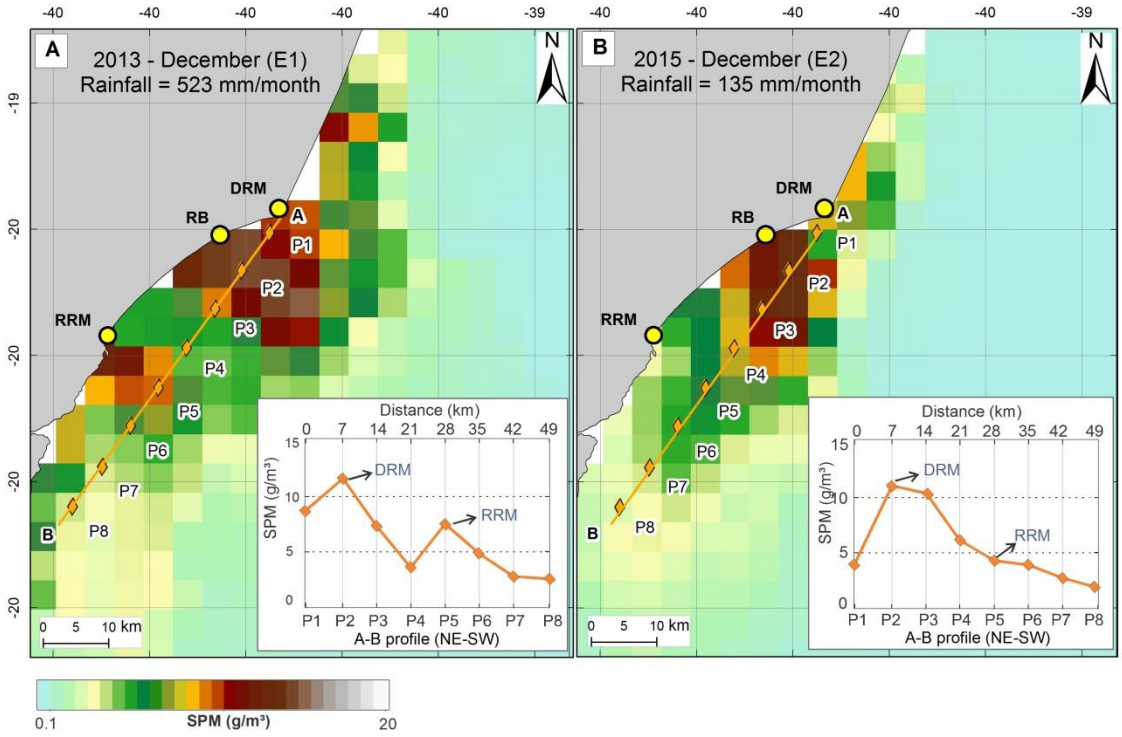

Fig.5. Sediment dispersion profile in DRM and RRM in E1-2013 and E2-2015. (A) Profile highlighting SPM peaks in P2 and P5,which are areas influenced by the discharge of sediments in DRM and RRM, respectively, under conditions of high rainfall precipitation (E1-2013). (B) Profile showing decreasing dispersion pattern from P2 to P8. High values reach up to 14 km of DRM. Note that in RRM the values are relatively lower compared to 2013.

Table 1 shows the estimate (in km) of sediment plume coverage based on the visual comparison of PMS spatial distribution maps of all months between 2011 and 2016. The sampling distance for mapping the plume was up to 36 km from DRM to NE and 76 km to SE. The direction of the Doce River sediment plume is predominant to SW, but sometimes, under specific conditions, such as change of wind direction and ocean currents, it is also observed trending in the NE direction.

Table 1. Temporal analysis of the Doce River plume dispersion. The profiles were leased from DRM up to 70kmto SW and 35 km to NE. The bold numbers represent the inversion of sediment plume to the North.

	2011		2012		2013		2014		2015		2016	
	NE	SW	NE	SW	NE	SW	NE	SW	NE	SW	NE	SW
Jan	27	52	24	65	36	20	33	65	22	45	8	65
Feb	10	55	20	58	25	30	10	28	10	29	10	69
Mar	8	46	32	22	30	27	4	29	31	27	30	56
Apr	30	58	28	35	36	38	33	34	30	47	25	50
May	33	40	36	50	36	30	35	21	35	63	35	43
Jun	36	59	36	37	36	18	35	69	35	45	36	35
Jul	34	60	35	45	34	40	34	70	34	60	32	67
Aug	35	61	35	69	36	71	34	74	36	67	30	59
Sep	36	55	38	56	28	74	23	71	35	54	32	76
Oct	35	70	36	67	31	66	31	42	30	70	30	73
Nov	36	32	33	22	31	59	35	40	30	71	35	70
Dec	15	50	22	54	20	73	20	43	15	72	30	74

The plume direction to NE occurred in November of 2011 (NE = 36 km, SW = 32 km); in March (NE = 32 km, SW = 22 km), June (NE = 36 km, SW = 37 km) and November (NE = 33 km, SW = 22 km) of 2012; in January (NE = 36 km, SW = 20 km), March (NE = 30 km, SW = 27 km), May (NE = 36 km, SW = 30 km) and June (NE = 36 km, SW = 18 km) of 2013; in May of 2014 (NE = 35 km, SW = 21 km); in March of 2015 (NE = 31 km, SW = 27 km). For all months of 2016 the sediment plume was to SW direction. The statistical summary of the plume dispersion can be accessed in Table 2. The minimum plume dispersion (km) was observed for June (0.47 ± 13.07 SW) and the maximum for September (38.00 ± 5.13 NE and 38.00 ± 11.01 SW). The highest standard deviation was observed for June (±13.07 SW).

Table 2. Descriptive statistics for the plume dispersion (km), where: Min, is the minimum distance; Max, the maximum distance; Ave, is the average; and Stdev, the standard deviation.

	NE				SW			
	Min	Max	Ave	Stdev	Min	Max	Ave	Stdev
Jan	8.00	36,00	25.00	9.01	8.00	36.00	18.00	10.56
Feb	10.00	25,00	14.16	6.06	6.06	25.00	12.53	6.04
Mar	4.00	32,00	22.50	11.74	4.00	32.00	21.87	10.60
Apr	25.00	36,00	30.33	3.49	3.49	36.00	24.97	10.30
May	33.00	36,00	35.00	1.00	1.00	36.00	29.16	12.62
Jun	35.00	36,00	35.66	0.47	0.47	36.00	29.69	13.07
Jul	32.00	35,00	33.83	0.89	0.89	35.00	27.95	12.14
Aug	30.00	36,00	34.33	2.05	2.05	36.00	28.06	11.89
Sep	23.00	38,00	32.00	5.13	5.13	38.00	27.52	11.01
Oct	30.00	36,00	32.16	2.40	2.40	36.00	26.76	11.09
Nov	30.00	36,00	33.33	2.21	2.21	36.00	27.75	11.64
Dec	15.00	36,00	20.33	5.05	5.05	30.00	19.23	8.85

3.3.3. Estimation of SPM from OLI/L8 images

To observe the SPM spatiotemporal distribution in more detail, Eq. (4) was applied to OLI/L8 images from 2013 to 2016 (Fig. 6). It is possible to observe that between July and December the river plume dispersion was dominantly oriented towards NE, whereas the leading direction during the other months was to the SW. The SPM concentration obtained from OLI/L8 images ranged between 0.05 and 103 g/m^3, with maximum concentration up to 5 times higher than those SPM concentrations derived from MODIS/Aqua images.

The spatial resolution of MODIS is ~133 times lower than that of OLI/L8 images. The MODIS product is yielded from composite data collected over 30 days, whereas the OLI/Landsat-8 product is based on a single image, collected at a single date and time. These factors explain the difference in SPM concentrations derived from data acquired by these sensors.

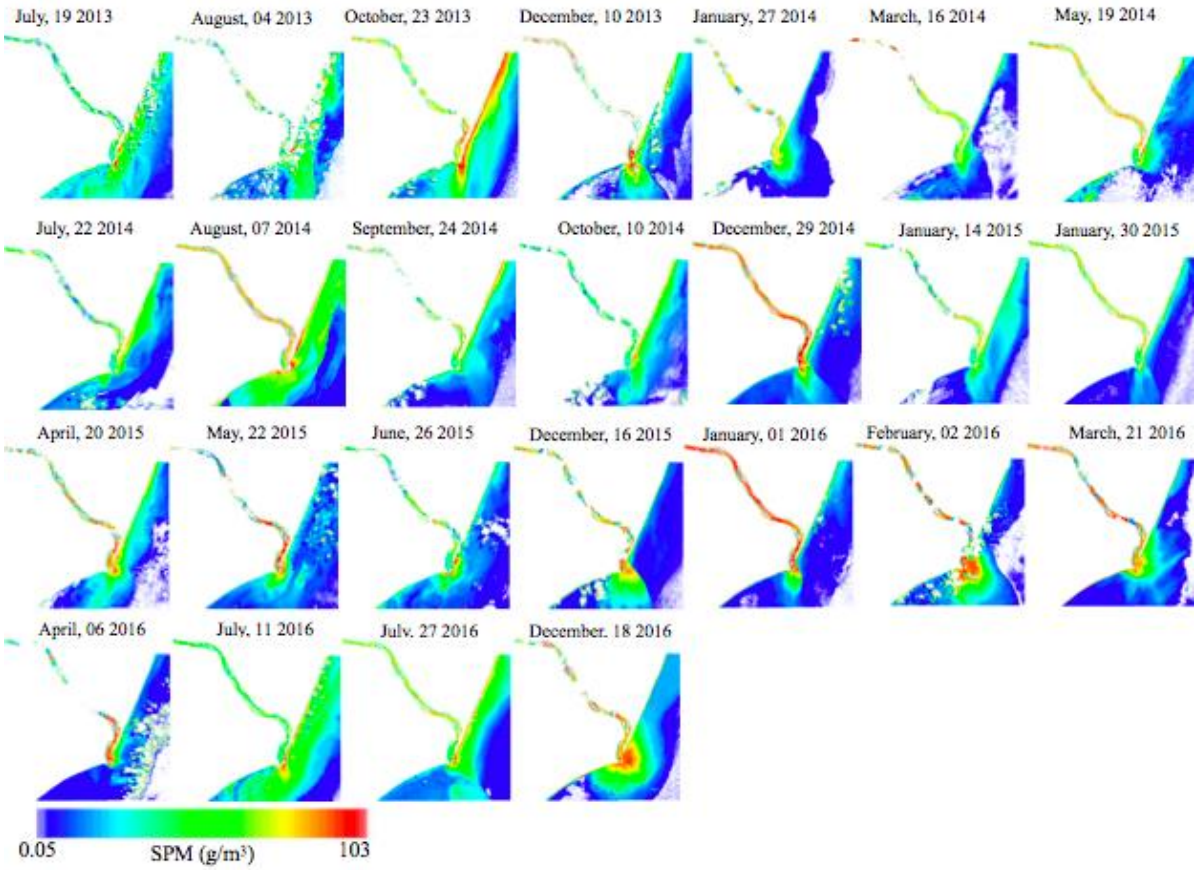

Fig 6. SPM distribution based on OLI/L8 images from 2013 to 2016. DRM and RRM, respectively, under conditions of high rainfall precipitation (E1-2013). (B) Profile showing decreasing dispersion pattern from P2 to P8. High values reach up to 14 km of DRM. Note that in RRM the values are relatively lower compared to 2013.

December 2014 and 2016 showed high SPM concentrations in the Doce River, with dispersion of the plume through the DRM. The image of December 2013 displays dense clouds near the DRM, which hindered the proper estimation of SPM concentration.

The SPM maps allowed us to observe that the bulk of SPM was deposited in RB right after the DRM. To compare the time series of SPM from MODIS images, we sampled the SPM map from OLI/L8 in the same pixel location to build an OLI/L8-based time series (Fig. 7). From January to November 2013, the SPM concentration increased as a result of increased rainfall, except in July 2013, when the rainfall was low. The SPM concentration did not rise immediately after the flooding; instead, the concentration climbed up smoothly, as observed in the SPM map of January 2014 (see Fig. 6).

After that, the SPM concentrations fell and reached a minimum of 1.36 g/m^3 in May 2014. From June 2014 to October 2015, although with low rainfall, the SPM concentration exceeded 30 g/m^3. After the Fundao dam collapse, the SPM concentration reached the highest value (= 73.23 g/m^3); then, the concentration decreased down to 6.02 g/m^3 in April 2016. From July to December 2016, an increase of SPM concentration was observed, which was caused by the wind action on the water surface.

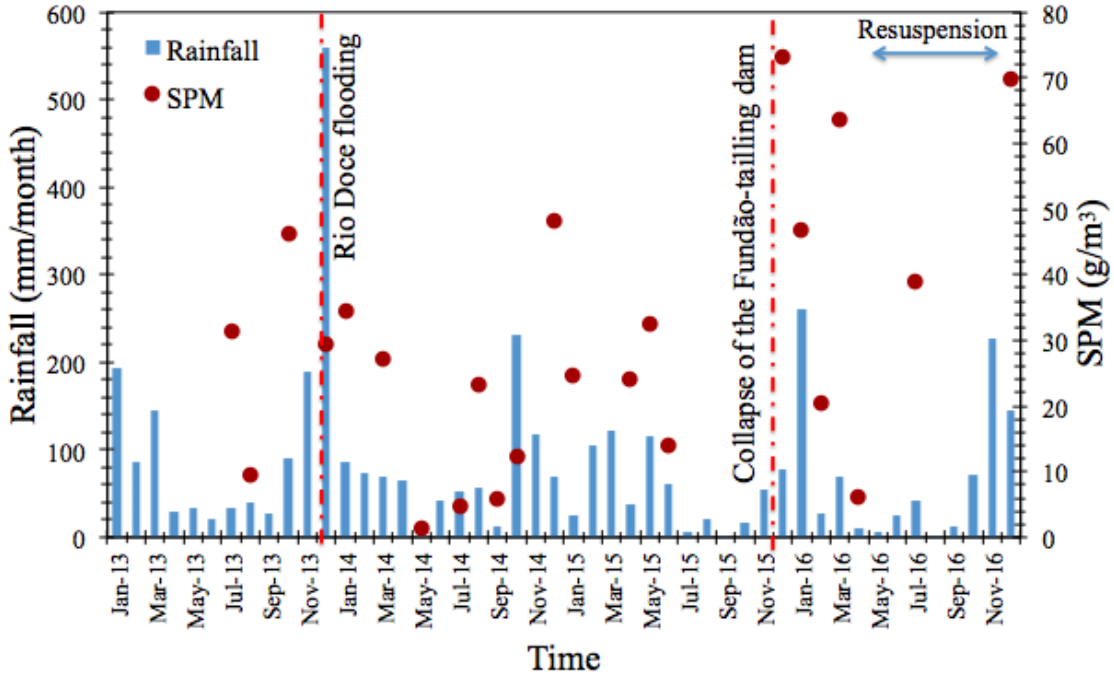

Fig.7. Temporal variability of SPM concentration based on OLI/L8 images and rainfall data. Highlighted events: the flooding (E1-2013) and the collapse of dam (E2-2015).

3.4. Discussion

A quite clear relationship between the time series of bio-optical parameters and the rainfall and wind speed was observed. The highest rainfall value was observed during the E1-2013 event; as a result, high SPM concentrations and K_d490 were also observed due to the excessive amount of sediments discharged in both DRM and RRM. On the other hand, despite the low rainfall rates during the E2-2015 event, the high concentrations of SPM and K_d490 values were observed 21 days after the dam collapse.

According to Cloern et al. (2014), sediment-associated turbidity restricts Z_{eu}, limiting the penetration of photosynthetic sunlight into the water column and decreasing nutrient uptake into phytoplankton biomass. The annual particle transport

(e.g., re-suspension, redistribution, and deposition) varies seasonally in coastal waters, which are driven primarily by wind speed and direction (Booth et al., 2000).

This may justify the occurrence of a characteristic pattern identified in the time series produced here, which consists of high values of K_d490 and SPM between September and November, even under conditions of relatively low rainfall. Thus, these values can be related to the stress of the wind on the surface of the water that transforms the potential energy into mechanics, generating internal waves and turbulence, causing re-suspension of the deposited sediments.

Quaresma et al. (2015) showed that the south of the DRM is composed of mud, with recent deposition of lacustrine material. The mixture of the mud and sand dominates the central area. In turn, the north is dominated by sand mixed with carbonate. The sediment composition in combination with wind speed and direction explains the spatial distribution of SPM, K_d490 and Z_{eu}. The sediment flows from the river to the coastal zone and the wind, on the other hand, controls the direction of the surface sediment and increases the SPM concentration through re-suspension.

Alcântara et al. (2010) estimated the relationship between the minimum wind speed and the fetch of its performance as a function of the depth of a lake in the Amazon region, suggesting that for a fetch of 10.3 km and a depth of 2.32 m, a wind with velocity greater than or equal to 1.14 m/s is able to cause the re-suspension of sediments.

In the coastal zone, the fetch may be even larger, however, resuspension should occur only at low depths (> 5 m), which are subject to high tidal energy and drift from the material from coastal erosion (Dagg et al., 2004). In Fig. 5 it is possible to notice that resuspension occurs only in the shallower regions, that is, closer to DRM, RRM and RB.

Hatje et al. (2017) compared suspended sediments flow in the plumes of the Doce River with the sediment plume coming from the mouths of rivers of other watersheds, similar in size to the Doce River basin, such as the basins of northeastern Brazil, the coast of Argentina and Uruguay. The authors concluded that the sediment flow of the Doce River is relatively higher than these basins, probably due to the intense contribution of the mining activities of the Doce River basin.

The occurrence of heavy rains may have caused the erosion of the tailings deposited in the Doce River plain and main tributaries after the dam collapse. Possibly this material was eroded and transported to the main channel of the river, thus supporting the high concentrations of SPM in the river and DRM (Hatje et al., 2017). This can be observed in the graphs and spatial distribution maps of SPM, mainly for period P3 of the time series analyzed in this paper. The spatial comparison of the plume between 2013 and 2015 (Fig. 5) illustrates the relationship between sediment flow and rainfall events. Note that in E1-2013 the plume was more extensive than in E2-2015, probably because in E1-2013 there was the contribution of other smaller basins, such as the Riacho River basin.

In the case of E2-2015, the plume received sediments exclusively from the discharge of the material from the collapse of the dam, since at that time the precipitation was relatively low. The mud that was discharged at the mouth of the fresh river deposited quickly, due to its composition. According to Silva et al. (2016), this material has a rather high density and low porosity. In addition, Gomes et al. (2017) detected that the sites impacted by E2-2015 at the DRM showed concentrations of metallic traces in sediments comparable to other basins and highly impacted urban estuaries.

3.5. Conclusion

The quantitative analysis of bio-optical parameters of the water showed anomalous values of K_d490, SPM and Z_{eu} in the suspended sediment plumes generated during events E1-2013 and E2-2015.

In E1-2013, under conditions of high precipitation, in addition to sediment discharge in the DRM, other river basins contributed to the accumulation of suspended sediments in the plume, as observed in the RRM. In contrast, under low rainfall conditions (E2-2015), this influence was not observed in the images. In both events, the large sediment discharge immediately affected the bio-optical parameters of the water, and the sediments were deposited between the first and third months.

In the case of E1-2013, the situation gradually normalized in the following months, maintaining the historical average. This situation differs from E2-2015, where

the mud was deposited quickly, but eight months later, the sediment was re-suspended due to wind action, increasing the values of SPM and K_d490 and reducing Z_{eu}.

Considering these observations, it was possible to prove the hypothesis that the flood of the Doce River, as well as the collapse, affected water quality and the underwater light field in the coastal region. However, the manmade event produced a higher impact, especially in the DRM, where the particles remained in suspension for a much longer time.

A long-term monitoring program should be developed in order to detect possible effects in the marine environment due to sporadic sediment resuspension because of wind and/or rainfall events. Also, there is a need to collect more data in order verify if this mud wave reached the Abrolhos bank ecosystem.

3.6. References

Alcântara, E., Novo, E., Stech, J., Lorenzzetti, J., Barbosa, C., Assireu, A., Souza, A., 2010. A contribution to understanding the turbidity behaviour in an Amazon floodplain. Hydrol. Earth Syst. Sci. 14, 351–364.

Babin,M., Stramski, M., Ferrari, G.M., Claustre, H., Bricaud, A., Obolensky, G., Hoepffner, N., 2003. Variations in the light absorption coefficients of phytoplankton, nonalgal particles, and dissolved organic matter in coastal waters around Europe. J. Geophys. Res. 108, 3211.

Baum, A., Fleming, R., Davidson, A.M., 1983. Natural disaster and manmade catastrophe. Environ. Behav. 15, 333–354.

Bernardo, N., Watanabe, F., Rodrigues, T., Alcântara, E., 2017. Atmospheric correction issues for retrieving total suspended matter concentrations in inland waters using OLI/Landsat-8 image. Adv. Space Res. 59, 2335–2348.

Booth, J.G., Miller, R.L., McKee, B.A., Leathers, R.A., 2000. Wind-induced bottom sediment resuspension in a microtidal coastal environment. Cont. Shelf Res. 20, 785–806.

Cao, Z., Dua, H., Feng, L., Ma, R., Xue, K., 2017. Climate and human induced changes in suspended particulate matter over Lake Hongze on short and long timescales. Remote Sens. Environ. 192, 98–113.

Carswell, T., Costa, M., Young, E., Komick, N., Gower, J., Sweeting, R., 2017. Evaluation of MODIS-Aqua Atmospheric Correction and Chlorophyll Products of Western North American Coastal Waters Based on 13 Years of Data. Remote Sens. 9, 1063.

Chang, G., Whitmire, A.L., 2009. Effects of bulk particle characteristics on backscattering and optical closure. Opt. Express 17, 2131–2142.

Chen, S.L., Zhang, G.A., Yang, S.L., Shi, J.Z., 2006. Temporal variations of fine suspended sediment concentration in the Changjiang River Estuary and adjacent coastal waters, China. J. Hydrol. 331, 137–145.

Cloern, J.E., Foster, S.Q., Kleckner, A.E., 2014. Phytoplankton primary production in the world's estuarine-coastal ecosystems. Biogeosciences 11, 2477–2501.

CPRM – Serviço Geológico do Brasil, 2014. Sistema de alerta de enchentes da bacia do rio Doce. Relatório Técnico do Período Crítico de Dezembro de 2013.

Curtarelli, M., Rennó, C.D., Alcântara, E., 2014. Evaluation of the Tropical Rainfall Measuring Mission 3B43 product over an inland area in Brazil and the effects of satellite boost on rainfall estimates. J. Appl. Remote. Sens. 8 (083589-083589-14).

Dagg, M., Benner, R., Lohrenz, S., Lawrence, D., 2004. Transformation of dissolved and particulate materials on continental shelves influenced by large rivers: plume processes. Cont. Shelf Res. (ISSN: 0278-4343) 24 (7–8), 833–858. https://doi.org/10.1016/j.csr.2004.02.003.

Dorji, P., Fearns, P., 2017. Impact of the spatial resolution of satellite remote sensing sensors in the quantification of total suspended sediment concentration: a case study in turbid waters of Northern Western Australia. PLoS One 12, e0175042.

Fernandes, F.W., Goulart, F.F., Raniere, B.D., Coelho, M.S., Dales, K., Boesche, N., Bustamante, M., Carvalho, F.A., Carvalho, D.C., Dirzo, R., Fernandes, S., Galetti Jr., P.M., Millan, V.E.G., Mielke, C., Ramirez, A.N., Rogass, C., Ribeiro, S.P., Scariot, A., Soares Filho, B., 2016. Deep into the mud: ecological and socioeconomic impacts of the dam breach in Mariana, Brazil. Natureza Conservação Braz. J. Nat. Conserv. 14, 35–45.

Franchito, S.H., Rao, V.B., Vasques, A.C., Santo, C.M.E., Conforte, J.C., 2009. Validation of TRMM precipitation radar monthly rainfall estimates over Brazil. J. Geophys. Res. Atmos. 114, D02105.

Gangloff, A., Verney, R., Doxaran, D., Ody, A., Estournel, C., 2017. Investigating Rhône River plume (Gulf of Lions, France) dynamics using metrics analysis from the MERIS 300m Ocean Color archive (2002−2012). Cont. Shelf Res. 144, 98–111.

Garcia, L.C., Ribeiro, D.B., Roque, F.O., Ochoa-Quintero, J.M., Laurance, W.F., 2017. Brazil's worst mining disaster: corporations must be compelled to pay actual environmental costs. Ecol. Appl. 27, 5–9.

Gelaro, et al., 2017. The modern-era retrospective analysis for research and applications, version 2 (MERRA-2). J. Clim. 30, 5419–5454. Gomes, L.E.O., Correa, L.B., Sá, F., Neto, R.R., Bernadinho, A.F., 2017. The impacts of the Samarco mine tailing spill on the Rio Doce estuary, Eastern Brazil. Mar. Pollut. Bull. 120, 28–36.

Gordon, H.R., Wang,W., 1994. Influence of oceanic whitecaps on atmospheric correction of SeaWiFS. Appl. Opt. 33, 7754–7763.

Goyens, C., Jamet, C., Ruddick, K.G., 2013. Spectral relationships for atmospheric correction. II. ImprovingNASA's standard and MUMM near infra-red modeling schemes. Opt. Express 21 (18), 21176–21187.

Hatje, V., Pedreira, R.M.A., Rezende, C.E., Schettini, C.A.F.S., Souza, G.C., Marin, D.C., Hackspacher, P.C., 2017. The environmental impacts of one of the largest tailing dam failures worldwide. Sci. Rep. 7, 10706.

Joyce, K.E., Belliss, S.E., Samsonov, S.V., McNeill, S.J., Glassey, P.J., 2009. A reviewof the status of satellite remote sensing and image processing techniques for mapping natural hazards and disasters. Prog. Phys. Geogr. 33, 183–207.

Kirk, J.T.O., 1994. Light and Photosynthesis in Aquatic Ecosystems. Cambridge University Press, New York.

Lahet, F., Stramski, D., 2010. MODIS imagery of turbid plumes in San Diego coastal waters during rainstorm events. Remote Sens. Environ. 114, 332–344.

Lari, S., Frattini, P., Crosta, G.B., 2009. Integration of natural and manmade risks in Lombardy, Italy. Nat. Hazards Earth Syst. Sci. 9, 2085–2106.

Le, C., Lehrter, J.C., Schaeffer, B.A., Hu, C., Murrell, M.C., Hagy, J.D., Greene, R.M., Beck, M., 2016. Bio-optical water quality dynamics observed from MERIS in Pensacola Bay, Florida. Estuar. Coast. Shelf Sci. 173, 26–38.

Lee, Z.P, Hu, C., Shang, S., Du, K., Lewis,M., Arnone, R., Brewin, R., 2013. Penetration of UV visible solar radiation in the global oceans: insights from ocean color remote sensing. J. Geophys. Res. Oceans 118 (9), 4241–4255.

Marta-Almeida, M.M., Mendes, R., Amorim, F.N., Cirano, M., Dias, J.M., 2016. Fundao Dam collapse: oceanic dispersion of River Doce after the greatest Brazilian environmental accident. Mar. Pollut. Bull. 112, 359–364.

Miller, R.L., Mckee, A.B., 2004. Using MODIS Terra 250 m imagery to map concentrations of total suspended matter in coastal waters. Remote Sens. Environ. 93, 259–266.

Moses,W.J., Gitelson, A.A., Perk, R.L., Gurlin, D., Rundquist, D.C., Leavitt, B.C., Barrow, T.M., Brakhage, P., 2012. Estimation of chlorophyll-a in turbid productive waters using airborne hyperspectral data. Water Res. 46, 993–1004.

Nechad, B., Ruddick, K.G., Park, Y., 2010. Calibration and validation of a generic multisensor algorithm for mapping of total suspended matter in turbid waters. Remote Sens. Environ. 114, 854–866.

Pahlevan, N., et al., 2017. Landsat 8 remote sensing reflectance (Rrs) products: evaluations, intercomparisons, and enhancements. Remote Sens. Environ. 190, 289–301.

Quaresma, V.S., Catabriga, G., Bourguignon, S.N., Godinho, E., Bastos, A.C., 2015. Modern sedimentary processes along the Doce river adjacente continental shelf. Braz. J. Geol. 45, 635–644.

Rienecker, M.M., et al., 2011. MERRA - NASA's modern-era retrospective analysis for research and applications. J. Clim. 24, 3624–3648.

Shang, S., Lee, Z., Wei, G., 2011. Characterization of MODIS-derived euphotic zone depth: results for the China Sea. Remote Sens. Environ. 115, 180–186.

Silva, A.C., Cavalcante, L.C.D., Fabris, J.D., Júnior, R.F., Barral, U.M., Farnezi, M.M.M., Viana, A.J., Ardisson, J.D., Outon, L.E.F., Lara, L.R.S., Sumpf, H.O., Barbosa, J.B.S., Silva, L.C., 2016. Chemical, mineralogical and physical characteristics of a material accumulated on the river margin from mud flowing from the collapse of the iron ore tailings dam in Bento Rodrigues, Minas Gerais, Brazil. Rev. Espinhaço 5, 44–53.

Thuillier, G., Hersé, M., Labs, D., Foujols, T., Peetermans, W., Gillotay, D., Simon, P.C., Mandel, H., 2003. The solar spectral irradiance from 200 to 2400 nm as measured by the SOLSPEC spectrometer from the ATLAS and EURECA missions. Sol. Phys. 214, 1–22. https://doi.org/10.1023/A:1024048429145.

Werdell, P.J., 2005. Ocean Color K490 algorithm evaluation. Available at. http://oceancolor.gsfc.nasa.gov/REPROCESSING/SeaWiFS/R5.1/k490_update.html, Accessed date: 2 May 2017.

Zhao, J., Barnes, B., Melo, N., English, D., Lapointe, B., Karger, F.M., Schaeffer, B., Hu, C., 2013. Assessment of satellite-derived diffuse attenuation coefficients and euphotic depths in south Florida coastal waters. Remote Sens. Environ. 131, 38–50.

CAPÍTULO 4

Possible contamination of the Abrolhos reefs by Fundao dam tailings, Brazil – New constraints based on satellite data

K.T.O. Coimbra, E. Alcântara, C.R. Souza Filho

Published in the *Science of The Total Environment*. Volume 733, 1 September 2020, 138101. https://doi.org/10.1016/j.scitotenv.2020.138101

The Fundao dam, located in Mariana city, Minas Gerais State, southeastern Brazil, collapsed in November 2015, causing the discharge of over 50 million m^3 of iron ore tailings in the Doce river basin. The mud generated by the disaster was composed of fine particulates (silt and clay), which are more sensitive to wind dispersion. Based on laboratory analyses and hydrodynamic modeling, early research postulates the hypothesis that the mud discharged in the ocean traveled 10.000 km up north and may have reached the Abrolhos coral reefs. This research aims to investigate further this hypothesis based on broad-scale remotely sensed data. Satellite images were used to estimate the suspended particulate matter (SPM) in the coastal zone before, during, and after the dam collapse. Results indicate that higher concentrations of SPM appeared during and post-collapse and were restricted to the coastal zone and its shallower regions, including beaches. However, we demonstrate that under exceptional circumstances the wind blew to the north, carrying fine particulate material and potentially-toxic metals derived from the iron ore tailings towards the northeastern Brazilian coastline and possibly the reefs of the Abrolhos Bank.

4.1. Introduction

The collapse of the Fundao dam, located in Mariana city (Minas Gerais State, Brazil), in November 2015 is considered the most notorious socioenvironmental disaster in Brazil and one of the most extensive related to mining activities in the world. Approximately 50 million m^3 of iron ore tailings were discharged along the Doce river banks, causing considerable social and environmental damage. Days after the collapse, material from the dam emerged from the Doce river mouth into the Atlantic Ocean, 600 km from the mine site (Hatje et al., 2017).

Recent studies suggested that this material may have reached the Abrolhos Archipelago region, off the coast of the Bahia State, in northeast Brazil, exposing the coral reefs to heavy metals (Evangelista and Valeriano, 2017). Mazzei et al. (2017) discussed the urgent need to understand and map the ecological function of the

Abrolhos coral reefs and to evaluate whether there are impacts related to the Mariana disaster.

Evangelista and Valeriano (2017) conducted isotopic studies ($^{87}Sr/^{86}Sr$ and $^{143}Nd/^{144}Nd$) of sediment before and after the dam collapse. The authors analyzed surface sediments extracted from the mouth of the Doce river, the Barra de Caravelas coastline, and the Abrolhos Archipelago. The results suggest that sediments discharged from the mouth of the Doce river have mixed with the Abrolhos suspended particulate matter since the collapse of the Fundao dam.

Magris et al. (2019) conducted a simulation of impacts on major ecosystems and protected marine areas, including the coast from Rio de Janeiro to Barra de Caravelas, in Bahia State. The authors evaluated four components: hydrological modeling, hydrodynamic modeling, ecosystem mapping, and biological sensitivity. The model was implemented for the 2015-2016 period, after the arrival of the Fundao tailings at the mouth of the Doce river, and for the 2017-2029 period. The study indicates that the impact intensity on the ecosystems most exposed to disturbances may decrease with time, but the total affected area could increase.

Gomes et al. (2017) collected estuarine sediment samples after the dam collapse to investigate the impacts on benthic communities and the accumulation of metal traces at the Doce river mouth, detecting high concentrations of heavy metals. According to the authors, the fast sedimentation and suspended particle composition after the accident affected the equilibrium of estuarine macro-algae communities.

This rapid sedimentation was also noted by Coimbra et al. (2019), based on analysis of MODIS-Aqua and Landsat-8 OLI images. The authors demonstrated that after the arrival of the tailing sludge in the ocean, the sediments settled after approximately one month. However, after eight months a resuspension process occurred, which consequently changed the vertical diffuse attenuation coefficient (K_d490), the suspended particulate material (SPM) contents, and the depth of the euphotic zone (Z_{eu}).

After the dam collapse, the sediments from the Doce river spread for hundreds of kilometers in the coastal zone, mainly due to the wind action. This dispersion was observed by Marta-Almeida et al. (2016) using hydrodynamic modeling

and by Rudorff et al. (2018) using satellite imagery. A critical issue about the mud dispersion is the chemical composition of this material, which can be associated with potentially toxic metals. Laboratory analyses of sediment and water samples collected in the affected area into the Doce river basin, 75 days after the dam rupture, indicated an increase of dissolved trace elements; Fe, As, Hg and Mn surpassed sediment quality guidelines (Hatje et al., 2017).

The exact extent to which the Fundao dam material traveled in the offshore region affected by the disaster is still unknown. Some authors believe these sediments may have dissipated into very distant areas reaching the Abrolhos Archipelago (Rudorff et al., 2018; Evangelista and Valeriano, 2017; and Magris et al., 2019). Others (e.g., Evangelista et al., 2016) found no evidence to support this notion in their studies.

Magris et al. (2019) showed that the mud might have reached the Abrolhos reefs, using hydrodynamic modeling; however, their work lacks temporal analysis of mud dispersion. Besides, any hydrodynamic simulation model is subject to error, primarily due to incorrect or insufficient data input. The validation of mathematical modeling results is typically limited by low-density sampling and the results obtained from the equations utilized in the model cannot be verified.

Multiple studies have demonstrated that the tailing contamination affected the Doce river and its mouth (Miranda and Marques, 2016; Segura et al., 2016; Silva et al., 2016; Carmo et al., 2017; Garcia et al., 2017; Guerra et al., 2017; Gomes et al., 2017; Hatje et al., 2017; Fernandes et al., 2016; Omachi et al., 2018; Queiroz et al., 2018; Rudorff et al., 2018; Sánchez et al., 2018; Coimbra et al., 2019; Magris et al., 2019; Valeriano et al., 2019). Nevertheless, no research to date has brought sufficient evidence to prove that the tailings reached the Abrolhos coral reefs. Remotely sensed imagery, with enough temporal, spatial and spectral resolution, could contribute to assessing if the mud reached Abrolhos.

This research aims to evaluate the possible contamination of the Abrolhos reefs by the tailings released during the Fundao dam collapse. The specific objectives of this study are (i) to map the spatiotemporal distribution of SPM, (ii) to understand the rainfall pattern in major river basins in the area affected by the disaster and its effect on SPM concentration, (iii) to analyse the wind direction pattern in the studied area and its

impact on the spreading of the Doce river sediment plume, and (iv) to carry out a comparison between the water spectral response near the Doce river mouth and the Abrolhos reefs.

4.1.1. Study area

The offshore region affected by the dam collapse was assessed in three specific areas (Fig. 1B).

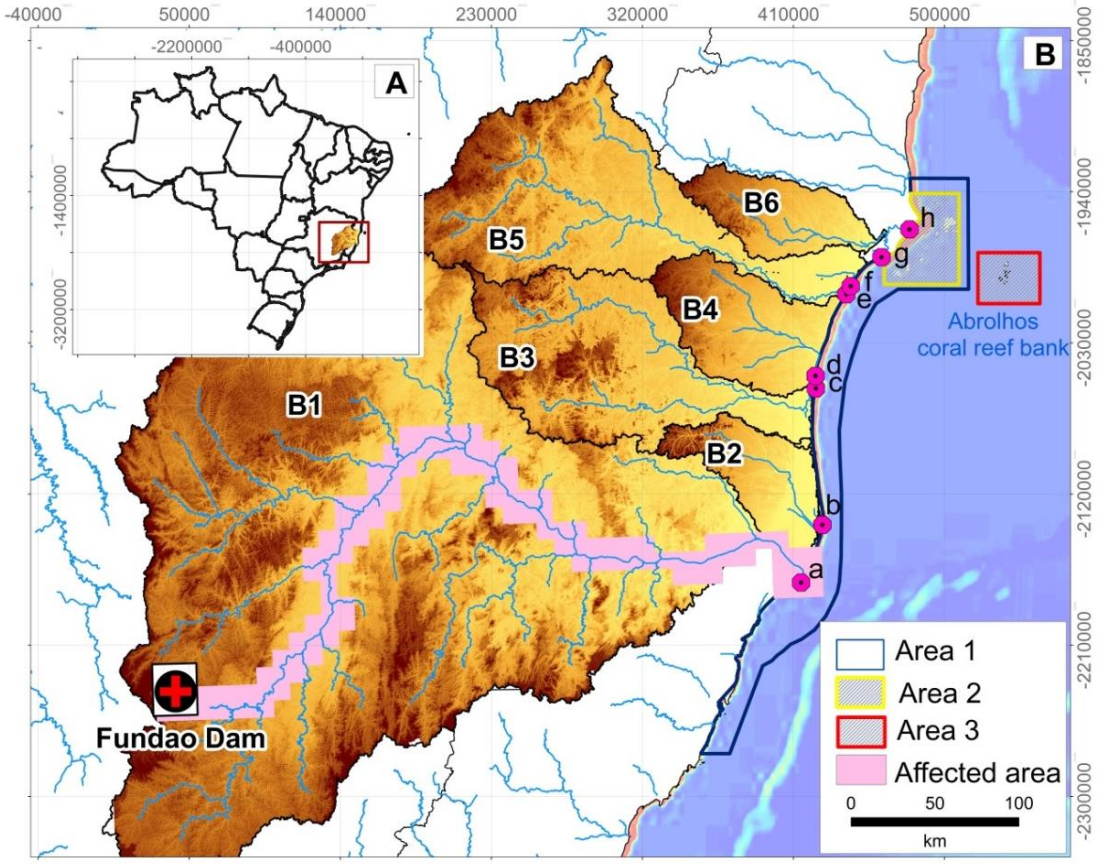

Fig.1. (A) Location of the study area. (B) Areas of interest subdivided from 1 to 3. B1 to B6 correspond to six Nova Viçosa and Caravelas river catchments that were delimited based on Shuttle Radar Topography Mission (SRTM) data. Rainfall data were obtained for the total perimeter of these Nova Viçosa and Caravelas river catchments. Mouth of major rivers are indicated by letters: (a) Doce river, (b) Barra Nova river, (c) São Mateus river, (d) Itaúnas river, (e) Riacho Doce river, (f) Mucurí river, (g) Nova Viçosa river, and (h) Caravelas river.

Area 1 encompasses a large portion of the South Atlantic basin, from the Doce river mouth in the State of Espírito Santo to Barra de Caravelas on the Bahia State coast, spanning approximately 10.200 km2 (Fig. 2A). Area 2 corresponds to a 200 km2 section, located in the northern portion of area 1 (Fig. 2C), comprising the Caravelas river mouth and the Cassurubá Extractive Reserve (CER). Area 3 is outside of Area 1

and is situated 53 km east of Barra de Caravelas, encompassing 20 km2 of the Abrolhos Archipelago, which includes five volcanic islands, named Santa Bárbara, Guarita, Redonda, Siriba, and Sudeste (Fig. 2D).

The CER has an area of 100.767 ha. It consists of mangroves, sandbank formations, remnants of Atlantic forests, and coastal-marine environments (Fig. 2). The CER near the Abrolhos Archipelago has great environmental importance to the South Atlantic region because the highest abundance of marine biodiversity in Brazil is concentrated there. The area is also situated in a region that is a priority for conservation (Nobre et al., 2017).

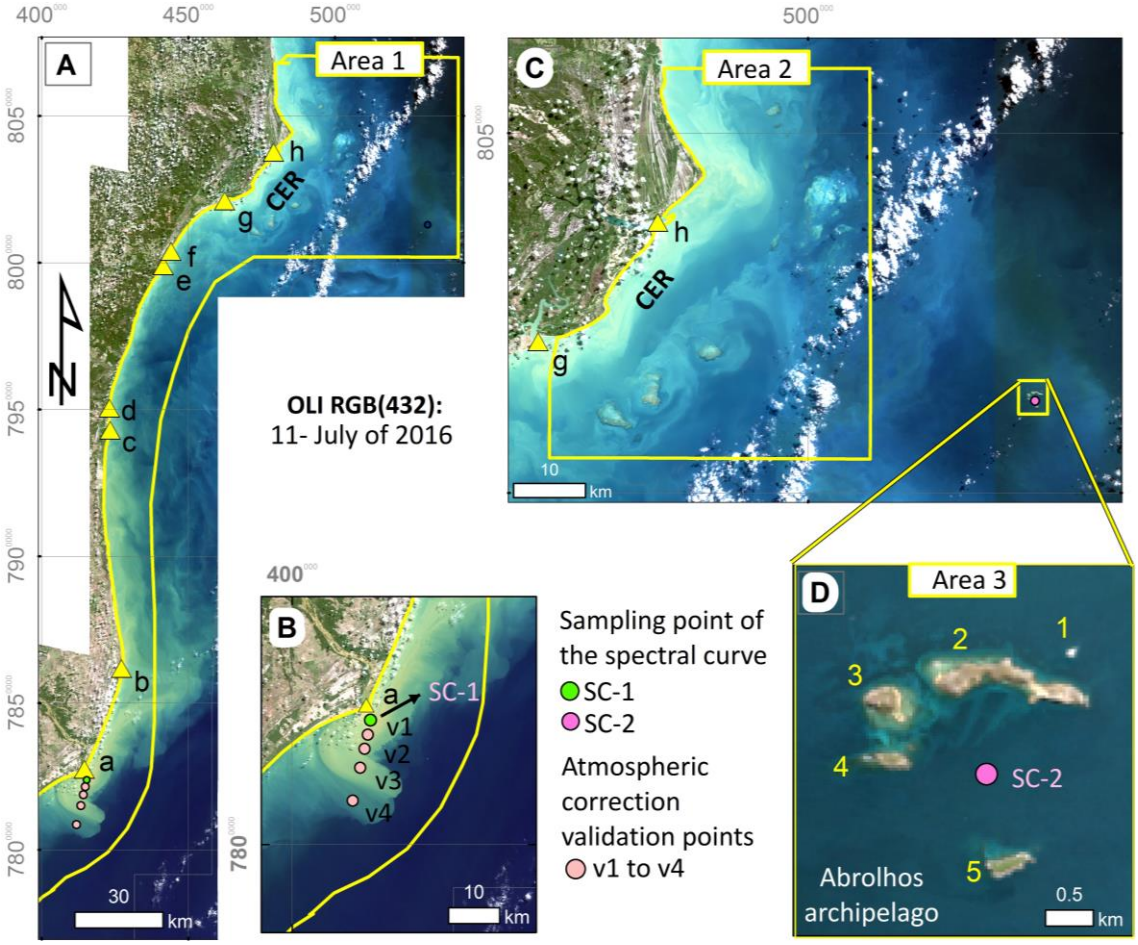

Fig. 2. OLI RGB images (432) from July 11th 2016, when the plume coming from the Doce river was directed towards north, reaching Areas 2 and 3. A) Area 1, containing the offshore region affected by the dam collapse, from the mouth of the Doce river to the Caravelas bar. Mouth of major rivers: (a) Doce river, (b) Barra Nova river, (c) São Mateus river, (d) Itaúnas river, (e) Riacho Doce river, (f) Mucurí river, (g) Nova Viçosa river, and (h) Caravelas river. B) v1 to v4 are the locations of pixels used for validating the atmospheric correction (Fig. 3). C) Area 2 encompasses the region of the Cassurubá Extractive Reserve (CER). D) Area 3 comprises the Abrolhos Archipelago. SC-1 and SC-2 indicate the position of pixels sampled for analysis (Fig. 5C) of spectral signatures at the mouth of the Doce river and the Abrolhos coral reef regions, respectively.

The coral reefs of the Abrolhos (Fig. 2C e D) exhibit a high degree of endemism and are the most biologically rich in Brazil and the South Atlantic (Werner et al., 2000). Mazzei et al. (2017) highlighted the potential for discovery of new species and the need for preservation. The high productivity of this region is due to several factors with the mixing of deep coastal water with warm water coming from the north, moved by the Brazilian current. This current moves southwards with increased intensity in the study area (Werner et al., 2000).

4.2. Materials and methods

4.2.1. Monthly average rainfall

The mean monthly rainfall data were obtained from the Tropical Rainfall Measuring Mission (TRMM) product 3B43 (Curtarelli et al., 2014) hosted by NASA-GIOVANNI platform: Geospatial Interactive Online Visualization and Analysis Infrastructure (https://giovanni.gsfc.nasa.gov/giovanni/). The mean rainfall time series from 2014 to 2019 was extracted employing the six catchments contour, B1 to B6 (Fig. 1).

Rainfall data were used to disclose the rainfall pattern in the study area and to understand how rainfall contributes to the concentration of SPM (Fig. 4).

4.2.2. Daily wind data

Wind vector data were extracted from the Wind METEOP near-real time products for January and July 2016 (Fig. 7). For acquiring these data, we used the Environmental Data Connector (EDC) extension, which connects ArcGIS to the Thredds/OPeNDAP. The Wind METEOP products display measurements of wind direction and wind speed above the sea surface. They are processing level 2 products with a 12.5 km horizontal resolution. The measurements are obtained by processing scatterometer data from the ASCAT instrument in the Metop-A satellite of EUMETSAT (http://www.osi-saf.org/?q=content/metopascat-coastal-winds).

The National Oceanic and Atmospheric Administration (NOAA) Coast Watch distributes these data at https://catalog.data.gov/organization/noaa-gov.wind data are fundamental for understanding the SPM dispersion on the water surface and are

used primarily here to identify conditions affecting the Doce river sediment plume dispersion towards the Abrolhos reefs.

4.2.3. Processing of the OLI/Landsat-8 images

Level 1 images, from 2015 to 2019, from the Operational Land Imager (OLI) aboard the Landsat-8 satellite (referred to as OLI herein) were obtained from the Earth Explorer platform of the United States Geological Survey (https://earthexplorer.usgs.gov). Level 1 images are geometrically-corrected and radiometrically-calibrated and provided with 15–30 m horizontal resolution.

The atmospheric correction of OLI data was performed using ACOLITE. This processor groups atmospheric correction algorithms for application to Landsat (5/7/8) and Sentinel-2 (A/B) data. The atmospheric correction uses the "dark spectrum fitting" approach, but it can be adjusted to use "exponential extrapolation" (Vanhellemont and Ruddick, 2014, 2015). We obtained surface reflectance as output data from ACOLITE, which were further utilized to retrieve the SPM.

The corrected products had clouds removed with masks produced using the 2200 nm OLI band. It was not possible to obtain images for all months in the time series due to the persistent presence of clouds. In total, 21 images were used for estimating the SPM.

The atmospheric correction accuracy was evaluated by comparing the OLI images, corrected by ACOLITE, against the MODIS-Aqua images for surface reflectance, product MYD09GA-V6 (referred to as MODIS herein). The daily datum of surface reflectance from MODIS, with a 500 m spatial resolution, was obtained online through the Earth Explorer platform (https://earthexplorer.usgs.gov/). MODIS offers an estimate of surface reflectance for bands 1 to 7, which are compensated for atmospheric gases, aerosols and Rayleigh scattering (https://oceandata.sci.gsfc.nasa.gov/).

MODIS and ACOLITE-derived OLI surface reflectance were compared to assess the quality of the atmospheric correction procedure. The following bands were used in the evaluation: 442 nm (Blue), 561 nm (Green), 654 nm (Red), and 864 nm (Near Infrared [NIR]) from images of January 1, 2016. The mean percentage error (ε) for these bands was calculated according to Lee et al. (2007) (Eq. (1)).

$$\varepsilon = \frac{\sum_{i=1}^{n} \left| \frac{X_i^{estimated} - X_i^{measured}}{X_i^{measured}} \right|}{n} \times 100 \quad (1)$$

where $X_i^{estimated}$ are estimated data; $X_i^{measured}$ are the measured data, and n is the number of observations.

Before the validation process, the OLI images, with a 30 m spatial resolution, were scaled to the same resolution of MODIS products (500m). To demonstrate the results of this validation, four pixels of water (v1 to v4) were extracted from the region of the Doce river mouth. The locality of these points is shown in Fig. 2B and the validation results in Fig. 3.

This is a necessary procedure that aims to reduce errors in the estimated SPM concentration that arise from the use of satellite images (Bernardo et al., 2017).

4.2.4. Suspended particulate material (SPM)

The SPM concentration was estimated using the algorithm proposed by Nechad et al. (2010) and validated by several authors in different environments (e.g., Gangloff et al., 2017; Cao et al., 2017). The algorithm, designed for multi-sensor data, was applied to a series of OLI/Landsat-8 images (Eq. (2)).

$$SPM = \left(\frac{A^p \, x \, \rho w}{1 - {\rho w}/{C^p}} \right) + B^p \quad (2)$$

Where ρw corresponds to the water surface reflectance at a given wavelength, and A^p, C^p and B^p are coefficients that depend on the chosen wavelength (e.g., OLI/L8, at 654 nm: A^p = 289.29, B^p = 0, and C^p = 16.86).

The time series of SPM was evaluated based on selected pixels from areas 1, 2 and 3. In the case of area 1 (Fig. 4), 1 pixel from the mouth of the main rivers was used. The statistics of SPM samples were analyzed according to confidence intervals. For areas 2 and 3, four SPM pixels were sampled for each profile.

For Area 2, SPM data were collected for the months of January between 2015–2019, for July 2015 and July 2016. Data analysis comprised four profiles (P1 to P4). In Area 3, SPM values were analyzed for three profiles from January 2015 to 2019.

Samples from Profile 1 and Profile 2 are located, respectively, to the southwest and the east of Sudeste island. Profile 3 samples are in the central portion of the area, between the Sudeste and Santa Bárbara islands.

4.2.5. Spectral similarity

To map the similarity between the SPM-laden mud of the Fundao dam observed at the Doce river mouth and the SPM observed in the Abrolhos reefs, the Spectral Angle Mapper algorithm (SAM; Kruse et al., 1993) was used. SAM is a supervised classification algorithm that identifies similarities between the test spectra (or images) and reference spectra, whose optical properties are known. The algorithm determines the similarity between two spectra by calculating the spectral angle between them, treating them as vectors in an *n-D* space, where *nb* is the number of bands. The calculated distance between the two curves is a geometric measure given by the arc cosine value of the scalar product of the image vector and the reference spectrum; i.e., the SAM algorithm determines the similarity degree, *d*, of a given test spectrum *t*, in relation to a reference spectrum *r*, applying Eq. (3):

$$d = cos^{-1}\left(\frac{\sum_{i=1}^{nb} t_i r_i}{\left(\sum_{i=1}^{nb} t_i^2\right)^{0.5}\left(\sum_{i=1}^{nb} r_i^2\right)^{0.5}}\right) \quad (3)$$

Where i is the number of spectra in the set of samples, and nb is the number of bands.

For the supervised classification of the OLI images, the area corresponding to the Doce river sediment plume was considered as the reference. Images from January 1st 2016, and July 11th 2016, were utilized. We also obtained the spectral curves of these regions. SC-1 is the pixel representing the Doce river plume, considered as the reference spectrum (Fig. 2B). SC-2 is the pixel representing the Abrolhos Archipelago (Fig. 2C), considered as the test spectrum. The SAM was applied to identify similarities in the spectral responses between the water with tailings and the water near Abrolhos. The existence of spectral similarities between these targets can be an indicator that the water with tailings may have reached the Abrolhos coral reefs.

4.3. Results

4.3.1. Atmospheric correction

The comparison between the surface reflectance obtained from OLI data through ACOLITE and the MODIS reflectance product is shown in Fig. 3A–D. Fig. 3E presents the reflectance data correlation between the two sensors. The results show a linear coherence, with a correlation coefficient R = 0.93 and mean percentage errors (ε) of 8.08% (blue), 30.41% (green), 7.56% (red), and 11.58% (NIR).

The atmospheric correction applied to OLI data was efficient to reduce Rayleigh scattering effects at shorter wavelengths, with a slight increase towards longer wavelengths. ACOLITE produced underestimated surface reflectance values in almost all wavelengths. Considering MODIS data as the reference, ACOLITE was more restrictive in reducing the path radiance.

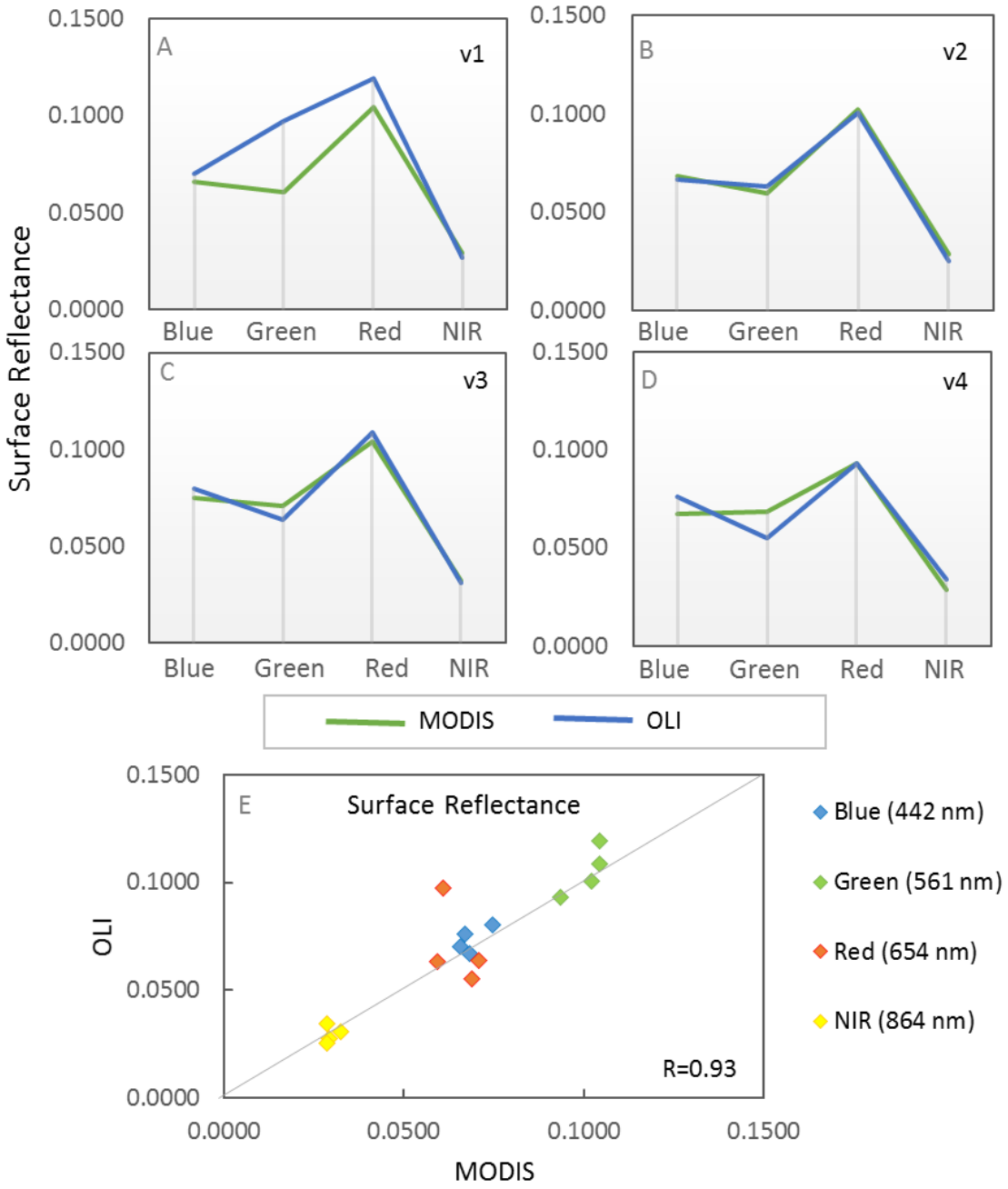

Fig.3. (A–D): Comparison between OLI surface reflectance obtained through ACOLITE and the equivalent MODIS product. For validation (v1-v4) (Fig. 2A) four pixels and their spectral signatures centered at 442 nm (Blue), 561 nm (Green), 654 nm (Red), and 864 nm (NIR) were selected. (E) Correlation of reflectance values extracted from OLI and MODIS data at equivalent sites. (For interpretation of the references to color in this figure legend, the reader is referred to the online version of this chapter).

4.3.2. Spatial and temporal analysis of rainfall and SPM

A time series of monthly rainfall was generated for all catchments into which six major rivers (i.e., Doce, Barra Nova, São Mateus, Itaúnas, Mucuri/Riacho Doce, Caravelas/Nova Viçosa) in the coastal region of Area 1 flow (Fig. 1). Fig. 4 displays the rainfall (mm/month) and the SPM time series extracted from pixels of OLI images near the mouth of major rivers in Area 1 (Fig. 2A) from January 2014 to February 2019. Cloud cover in the study area made it impossible to obtain SPM samples for all months of the series.

Statistical analysis of the confidence interval of the SPM sample group is shown in Fig. 5. Samples were divided into pre and post collapse. SPM averages are displayed on the gray bars, and the 95% confidence interval is represented by the black line. The pre-collapse averages range from 13.8 to 23.0 g/m^3 (light gray bar), and post-collapse averages range from 16.4 to 38.7 g/m^3 (dark gray bar).

Before the dam collapse, the rainfall in almost all catchments did not exceed 200mm/month, except for October 2014, when values of rainfall of 200 and 225mm/month were observed for catchments B4 and B2, respectively (Fig. 4). After the dam collapse, there was a significant increase in rain, particularly during the spring and summer months of the Southern Hemisphere.

During the 2015-2016 Austral summer, above-average regional rainfall occurred in all catchments (Fig. 4), primarily in January. During the 2016/2017 Austral spring and summer, these rainfall peaks occurred in November 2016. In the 2017/2018 Austral summer, rainfall was concentrated in two months, in December 2017 and February 2018. The 2018/2019 Austral summer received heavy rains in December 2018. Table 1 summarizes the rainfall (mm/month) for catchments B1-B6.

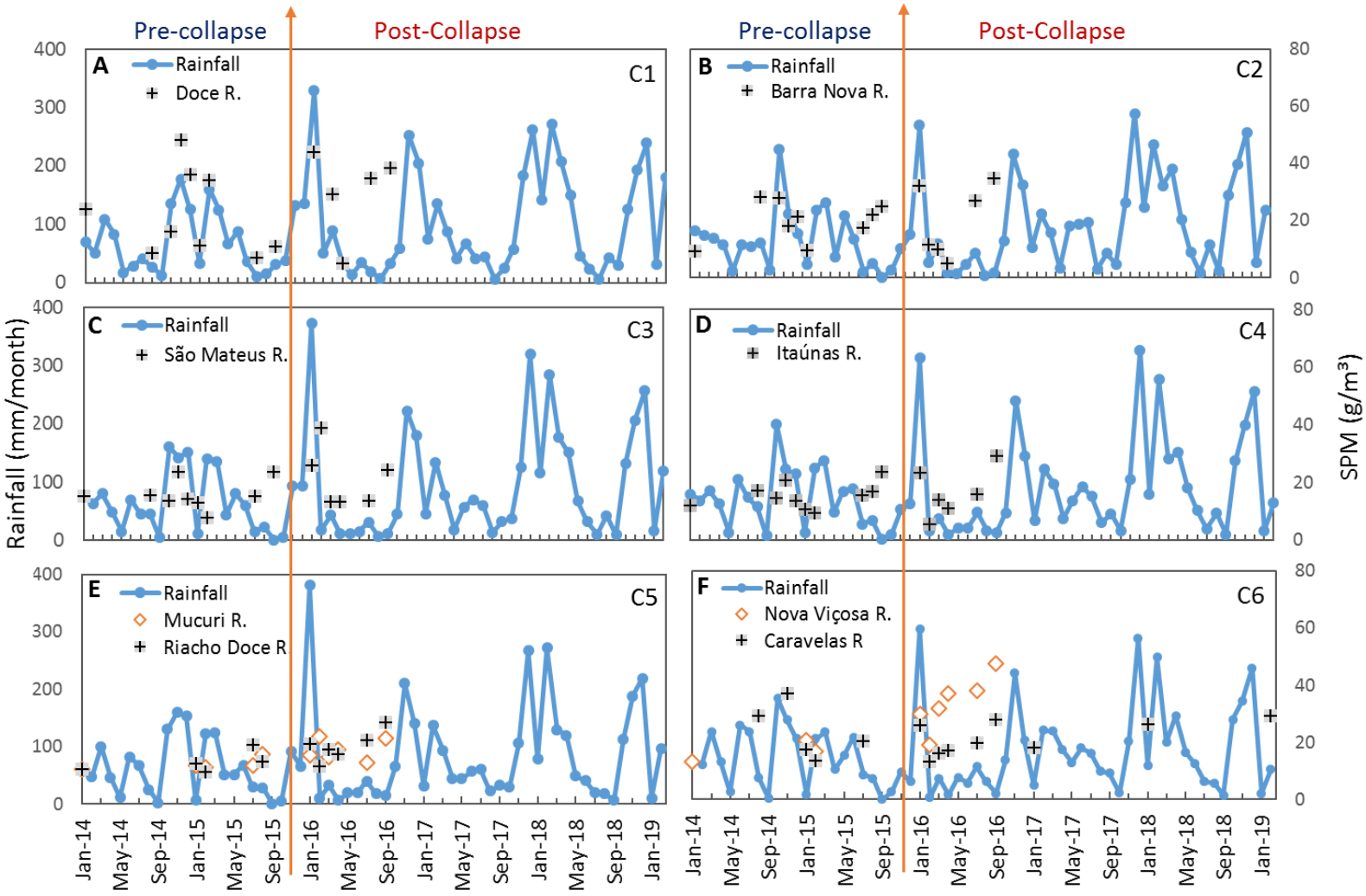

Fig.4. Temporal rainfall series (mm/month) for the six delimited catchments and SPM concentrations obtained from OLI data. (A) Doce river catchment, (B) Barra Nova river catchment, (C) São Mateus river catchment, (D) Itaúnas river catchment, (E) Mucuri and Riacho Doce river catchments, and (F) Caravelas and Nova Viçosa river catchments.

Table 1. Monthly rainfall (mm/month) in the main spring and summer months after the Fundao dam collapse; B1 to B6 catchments

	Austral summer (2015-2016)	Austral spring and summer (2016/2017)	Austral summer (2017/2018)	
	Jan-16	Nov-16	Dec-17	Feb-18
B1	329	252	261	271
B2	267	215	286	233
B3	372	221	319	284
B4	315	242	329	278
B5	380	210	267	271
B6	299	221	289	248

Coastal area SPM concentration is influenced by the rainfall pattern in the catchments because the particulate matter in the watersheds is washed into the coastal zone waters, contributing to the increasing turbidity. SPM values at the Doce river mouth (Fig. 4A) during periods before the dam collapse were typically less than 25 g/m^3, except for occasional spring and summer months in 2014/2015, namely November, December, and February, when SPM values reached 48, 37, and 35 g/m^3, respectively.

After the collapse, SPM peaks at the Doce river mouth occurred in January 2016 (SPM = 44 g/m^3) and March 2016 (SPM = 30 g/m^3). These values are linked to the heavy rain and the excessive load of sediment discharged at the river mouth after the dam collapse. The value of SPM in April 2016 was 6 g/m^3, indicating a possible sediment deposition during this month. In July and August 2016, despite the low rain volume, notable SPM increases occurred, reaching 35 and 39 g/m^3, respectively, indicating a resuspension of sediments caused by currents and wind action.

Relatively high SPM values appeared in the Barra Nova river (Fig. 4B) before the collapse in August (28 g/m^3) and October 2014 (27 g/m^3). After the collapse in 2016, SPM values were high in January (SPM = 32 g/m^3), July 2016 (SPM = 27 g/m^3), and September (SPM = 34 g/m^3).

The São Mateus and Itaúnas rivers (Fig. 4C e D), even though they are located in different catchments, reveal a similarity to the rainfall pattern and the delivery of sediments to the river mouth. In both river catchments, SPM did not exceed 24 g/m3 before the collapse. Higher SPM values are limited to the interval between January and

September 2016. Anomalous SPM values appear on January (25 g/m^3) and February (38 g/m^3) 2016 in the mouth of São Mateus river, and in September 2016 (29 g/m^3) in the mouth of the Itaúnas river.

SPM sampling near the mouths of Mucuri and Riacho Doce rivers (Fig. 4E) was quite limited before the collapse due to the presence of clouds, and SPM did not rise above 20 g/m^3. However, after the collapse, we detected two episodes: (i) the first occurred between January and March 2016 (SPM ranged from 14 to 24 g/m^3), a period with heavy rain; (ii) the second occurred between July and September 2016, when even under low rainfall conditions, SPM reached its highest value in the series, 28 g/m^3.

SPM values in the mouth of the Nova Viçosa river (Fig. 4F) were lower than 20 g/m3 before the collapse. After it, higher SPM values occurred in 2016, as follows: January (30 g/m^3), March (32 g/m^3), April (37 g/m^3), July (38 g/m^3), and September (47 g/m^3). In the mouth of the Caravelas river (Fig. 4F), before the collapse, SPM values did not exceed 20 g/m^3 , except in August and November 2014, when SPM reached 29 and 37 g/m^3 , respectively. After the collapse, the highest values in the series appeared in 2016, during January (26 g/m^3) and September (28 g/m^3), as well as in January 2018 (26 g/m^3) and January 2019 (29 g/m^3).

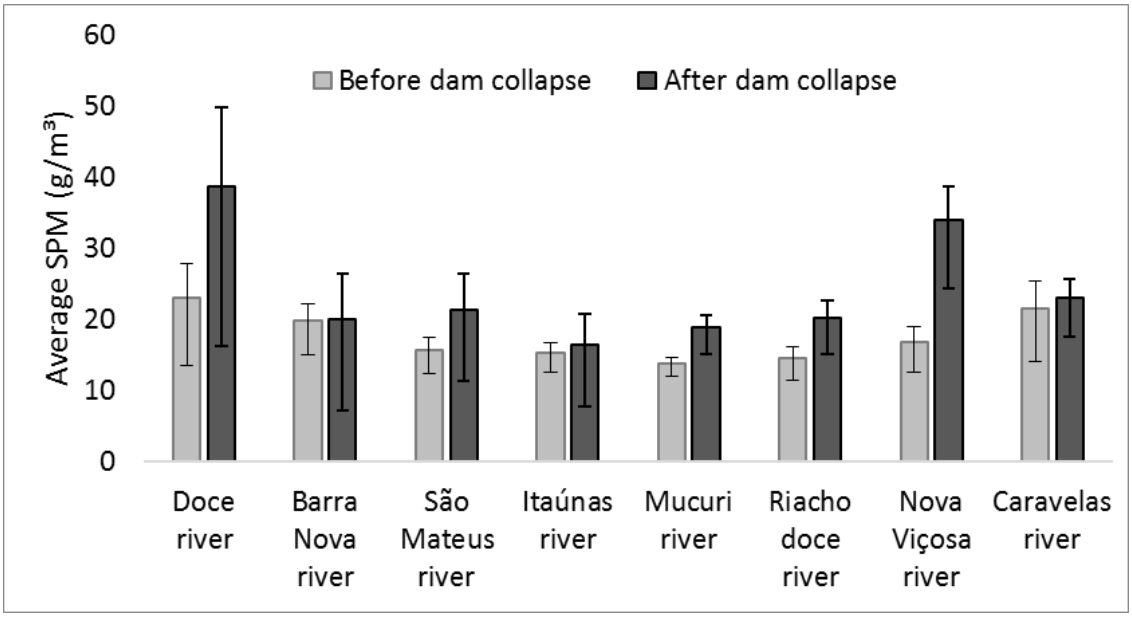

Fig.5. SPM concentrations and their confidence interval, before and after dam collapse, extracted from the mouth of the main rivers shown in Fig. 4.

4.3.3. The Doce river mud plume after dam collapse

To understand the dispersal dynamics of the Doce river plume after the collapse, we considered two evaluation periods: one representative of the Southern Hemisphere summer (January 2016) and the other of the Southern Hemisphere winter (July 2016). In both cases, the OLI images were subjected to SAM classification with training samples extracted from the Doce river mouth. Fig. 6A and D show the January 2016 OLI color composition image (RGB-432) and its SAM classification. Fig. 6B and E show the same information for July 2016. Representative spectral curves of the regions of interest are shown in Fig. 6C.

At the Doce river mouth, January 2016 data shows surface reflectance values that are relatively higher than July 2016, which is explained by considering the volume of tailings discharged into the river mouth at that time and the fact that these suspended particles promote the scattering of the incident light. For both January and July, reflectance peaks are observed at 654 nm, which indicates the presence of material with high iron oxide content at the mouth of the Doce river. Iron oxide exhibit strong reflection in the red band, with decreasing absorptions in the green and blue bands (Clark et al. 1993).

At the Abrolhos Archipelago, January 2016 data shows reflectance values higher than those for July 2016 (Fig. 6C). Reflectance in both months is higher at green and blue wavelengths. Overall, the reflectance from January 2016 is higher than July 2016. High reflectance in the near infrared is due to inorganic materials, as observed in the spectrum of January 2016. In July we observed an increase of absorption by water itself.

According to Leipe et al. (1999), the SPM from Abrolhos is dominated by carbonate shells, coral fragments, and needle-shaped biogenic opal. These materials hamper a straight comparison of other water masses with the same spectral features observed in Doce River mouth. The SAM classifier was not able to identify the river source material in the Abrolhos Archipelago region because of the distance from the coastline and the different composition of the suspended particles.

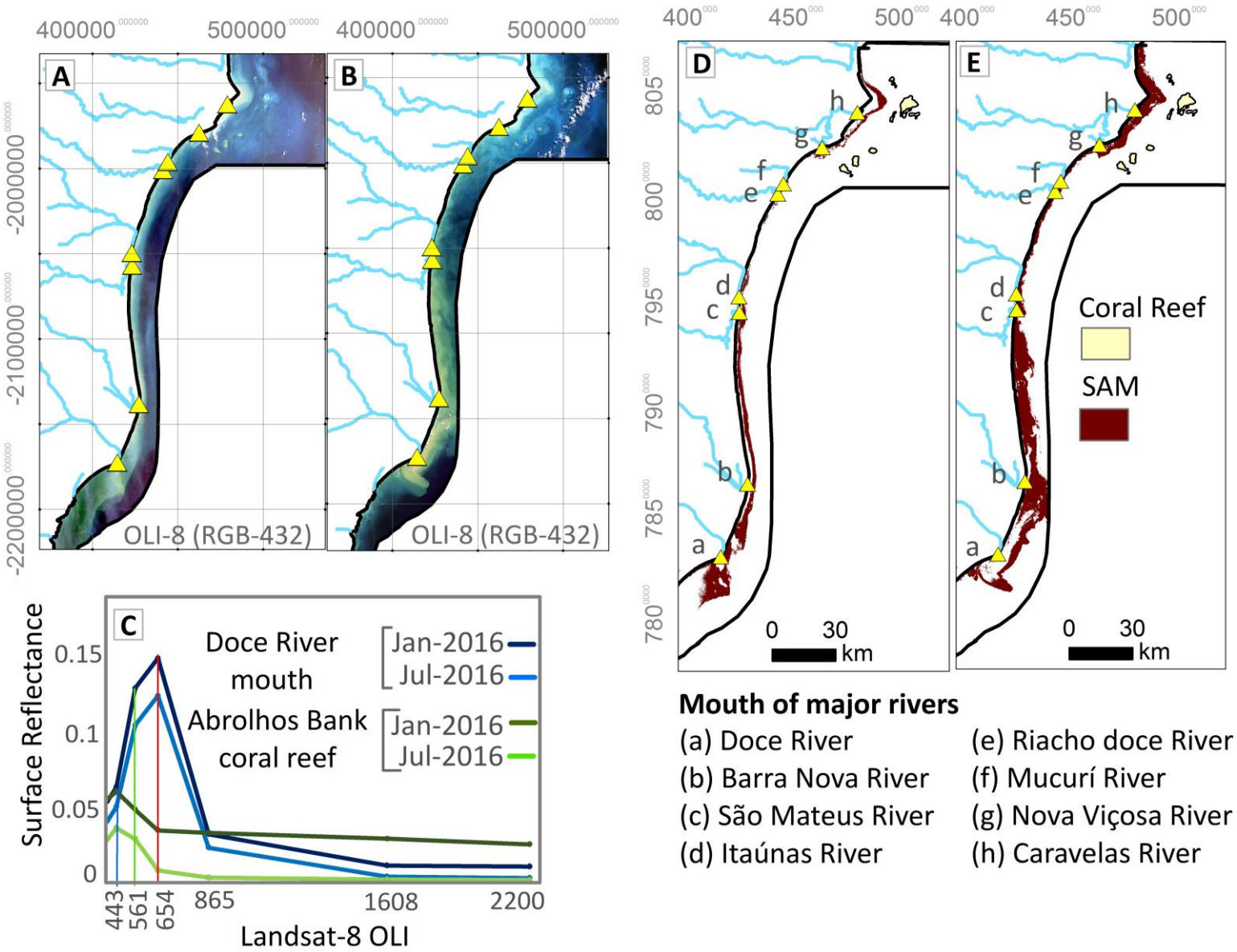

Fig .6. (A and B): True color rendition of OLI data (4R3G2B) acquired in January and July 2016. OLI bands 1, 2, 3, 4, 5, 6 and 7 centered at 443 nm, 482 nm, 561 nm, 654 nm, 865 nm, 1608 nm and 2200 nm. (C): Comparison of spectral curves extracted from 1 pixel at the Doce river mouth region and 1 pixel at the Abrolhos Archipelago. (D and E) Results of the Spectral Angle Mapper (SAM) classification of Landsat-8 OLI images taken in January and July 2016.

The classification results were compared with the L2 daily Wind METEOP products, which indicate the wind direction (Fig. 7 A and B). The wind vectors considered are comprised of data gathered up to 3 days before the date of the image obtained for SAM classification (December 30th–31th 2015 and January 1st 2016; July 9th - 11th 2016).

The Doce river plume is quite broad in January 2016 and is in line with the wind direction, which is predominantly towards the south. In July 2016, the course of the Doce river plume also coincides with the prevailing wind direction, which is northward during the winter. In this case, we notice a migration of the Doce river plume to the north. Pixels with spectral characteristics similar to those found in the Doce river mouth were mainly those from alongshore.

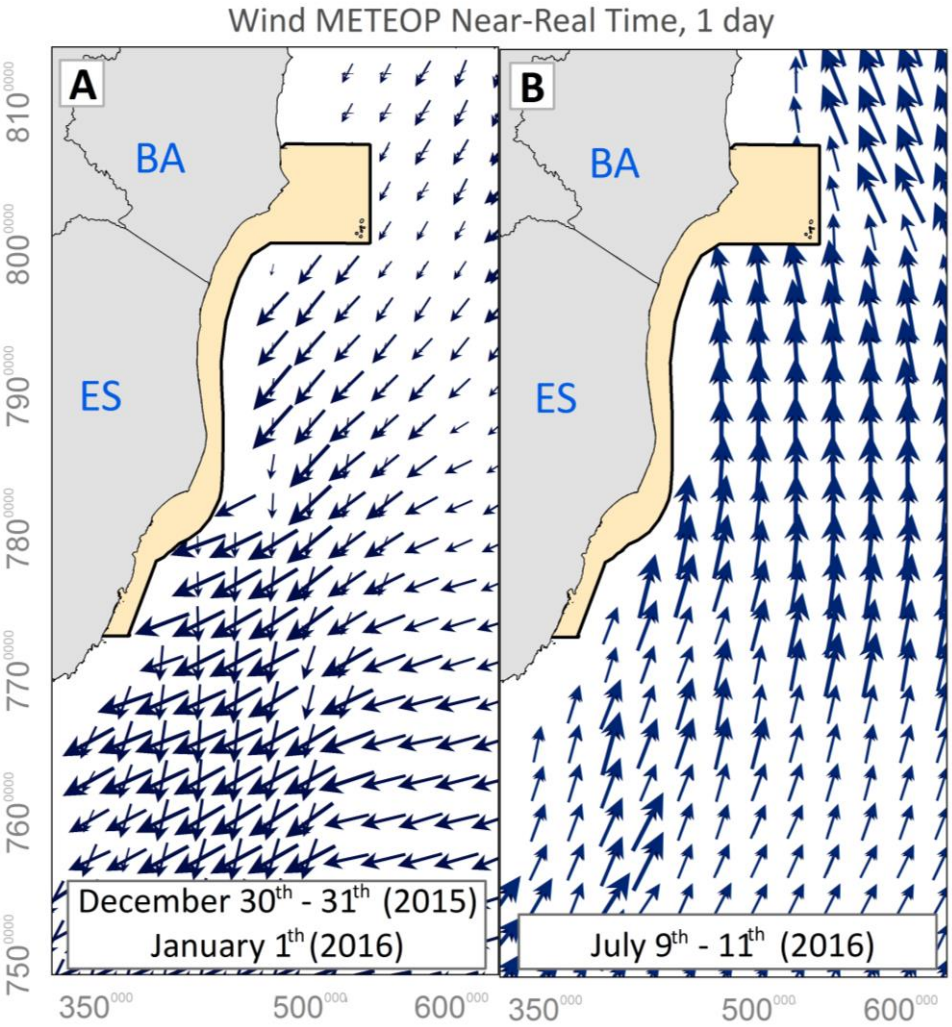

Fig. 7. (A and B): Vectors of prevailing wind direction (Wind METER Near-Real Time product), representatives of the Austral Summer and winter.

4.3.4. SPM spatial and temporal distribution

The SPM was analyzed during pre- and post-collapse periods in three predefined areas: one is more regional (Fig. 8), and two are more detailed (Figs. 9 and 10). Fig. 8 compares the estimated SPM for January and July in the years 2015 and 2016, for Area 1. In January 2015, the SPM spatial distribution was below 5.5 g/m^3. During this month, the residual direction of the Doce river sediment plume was to the south; it did not reach large proportions and the SPM did not exceed 10 g/m^3. Between the mouth of the Barra Nova river (a) and the Mucuri river (f), the SPM values were below 12 g/m^3; these values occurred alongshore. At the mouth of the Nova Viçosa (g) and Caravelas (h) rivers, the SPM values were between 20 and 40 g/m^3, respectively.

Typically, SPM concentrations are higher in January 2016 than in 2015. The Doce river plume reaches wider dimensions towards the south. The SPM values at the mouth exceed 35 g/m^3. Along the entire coast, extending from the mouth of the Doce river to the mouth of Caravelas river, the interconnected sediment plume exhibit a peculiar feature with SPM spreading to large dimensions, with values ranging from 10 to 35 g/m^3.

High SPM values appear continuously across the coast in July 2015 and 2016. In both months, the Doce river plume was directed towards the north. In 2015, between the mouths of the Barra Nova and Nova Viçosa rivers, SPM ranged from 15 to 25 g/m^3. At the mouth of the Caravelas river, SPM reached 30 g/m^3. In 2016, SPM reached higher values compared to those seen in 2015, which could highlight the possible dispersion of mud from the dam.

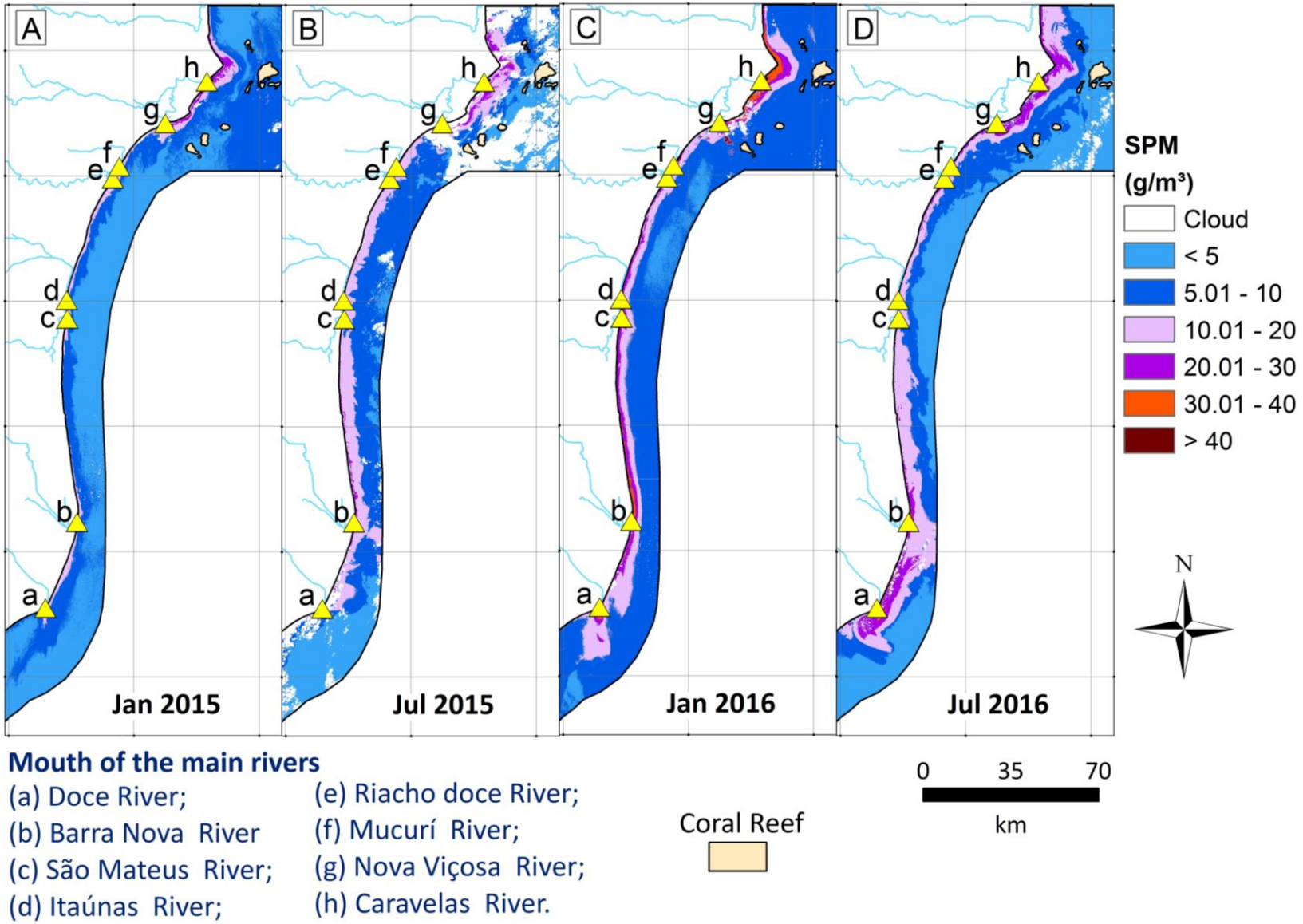

Fig.8. Distribution of SPM for Area 1. (A and B): Comparison between January 2015 and 2016; (C and D): Comparison between July 2015 and 2016.

SPM concentrations higher than 25 g/m^3 occurred in Area 1, including Doce river mouth up to Barra de Caravelas. In CER, the SPM ranged from 5 to 10 g/m^3. SPM changes over time for Areas 2 and 3 were verified based on systematic pixel sampling and spatial distribution maps, as displayed in Figs. 9 and 10. The maps show that in January 2015 and 2017, there is a smaller difference between SPM values throughout Area 2, indicating a high degree of similarity in both years (Fig. 9A and C). SPM values generally range from 4 to 7 g/m^3. In the region closest to the mouth of the Caravelas river, SPM values are higher than 20 g/m^3.

In January 2016, 2018, and 2019, relatively high SPM values are distributed throughout Area 2 (Fig. 9B, D, and E). Under these conditions, most SPM values are higher than 8 g/m^3. In the region adjacent to the Caravelas bar, the sediment plume is broader than in 2015 and 2017, with SPM values reaching 40 g/m^3. In July 2015, Area 2 had extensive cloud cover; therefore, a detailed analysis of the SPM distribution was not possible (Fig. 9F). However, in July 2016, higher SPM values occur primarily near Caravelas, some exceeding 20 g/m^3. SPM values higher than 8 g/m^3 occur in regions encompassing the CER and surrounding the coral reefs (Fig. 9G).

The boxplots produced for Area 2, profiles P1-P4 for January and July (Fig. 9 H and I), reveal a trend of increasing SPM concentrations in 2016, 2018, and 2019 relative to those in 2015 and 2017. In January 2015 and 2017, the SPM values range from 4.5 to 6 g/m^3. In January 2016, 2018, and 2019, the minimum SPM value is 7 g/m^3, and the maximum is 10 g/m^3. An oscillation between 2 and 5 g/m^3 occurred in July 2015; in 2016, this oscillation was between 5 and 9 g/m^3.

The spatial distribution of SPM for Area 3 shows an increasing trend from 2015 to 2019, which is evident in the corresponding boxplots. In January 2015, SPM values in the entire area do not exceed 10 g/m^3 (Fig. 10A). In contrast, from January 2016 to 2019, the SPM values range from 4 to 13 g/m^3 (Fig. 10B to E).

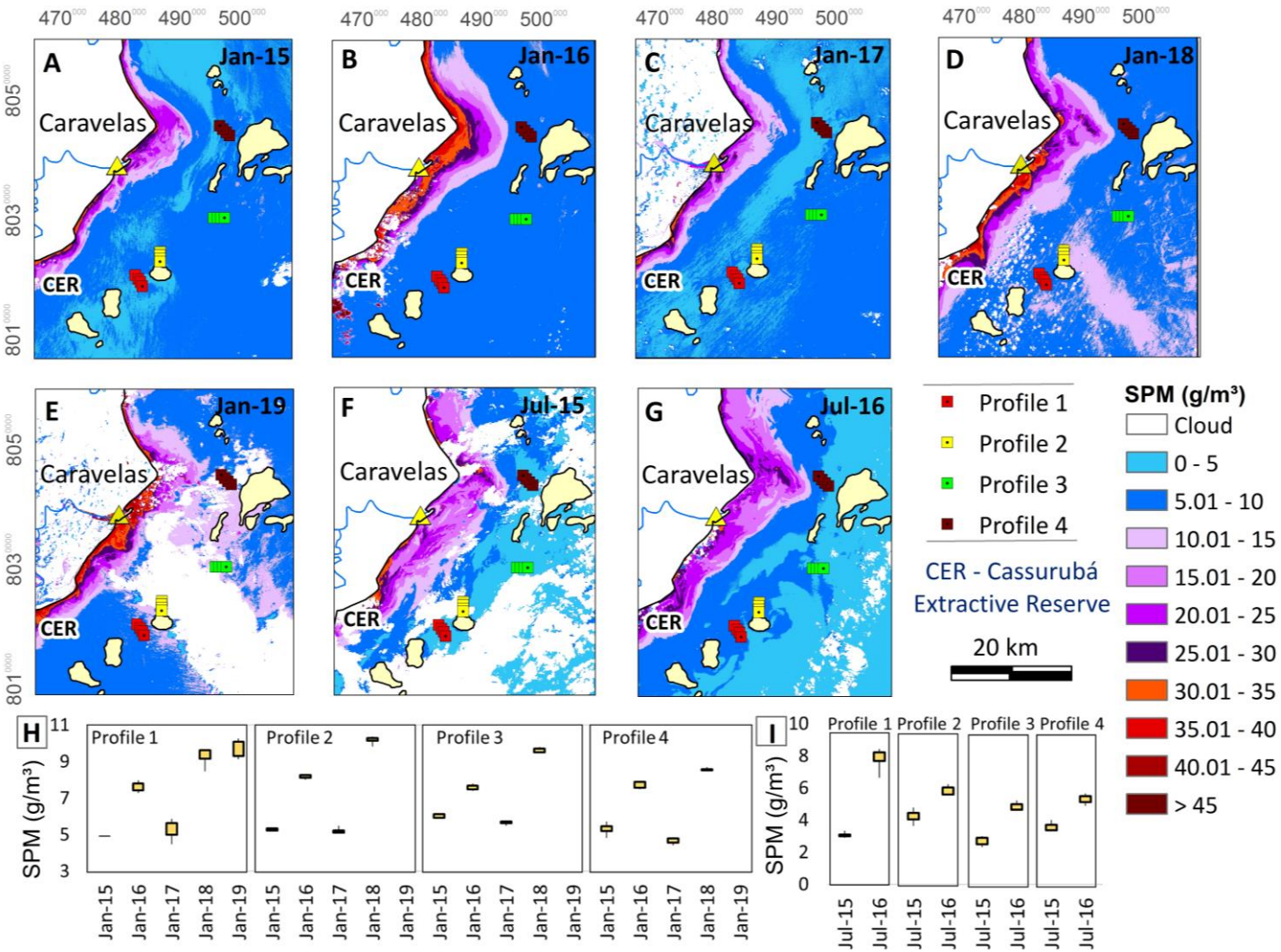

Fig.9. Distribution of SPM values for Area 2. (A to E): January 2015 to 2019. (F and G): July 2015 and 2016. (H and I): Boxplots representing SPM values of the four profiles (P1-P4), for January and July, respectively. In the case of January, it is observed that in 2015 and 2017, SPM values are lower in Area 2 compared with 2016, 2018, and 2019, when the SPM concentration rose to 110 g/m^3 in the regions nearest the coast. The contrast between 2015 and 2016 is also evident in July. The graphs indicate an increase in SPM for all explored profiles. The boxplots obtained for Area 3 reveal a trend of increasing SPM values between January 2015 and 2019 (Fig. 10F). In January 2015, the SPM concentrations of the three groups had values between 6 and 7.6 g/m^3, which are lower than the concentrations seen from January 2016 to 2019, when the SPM varies between 9 and 13 g/m^3.

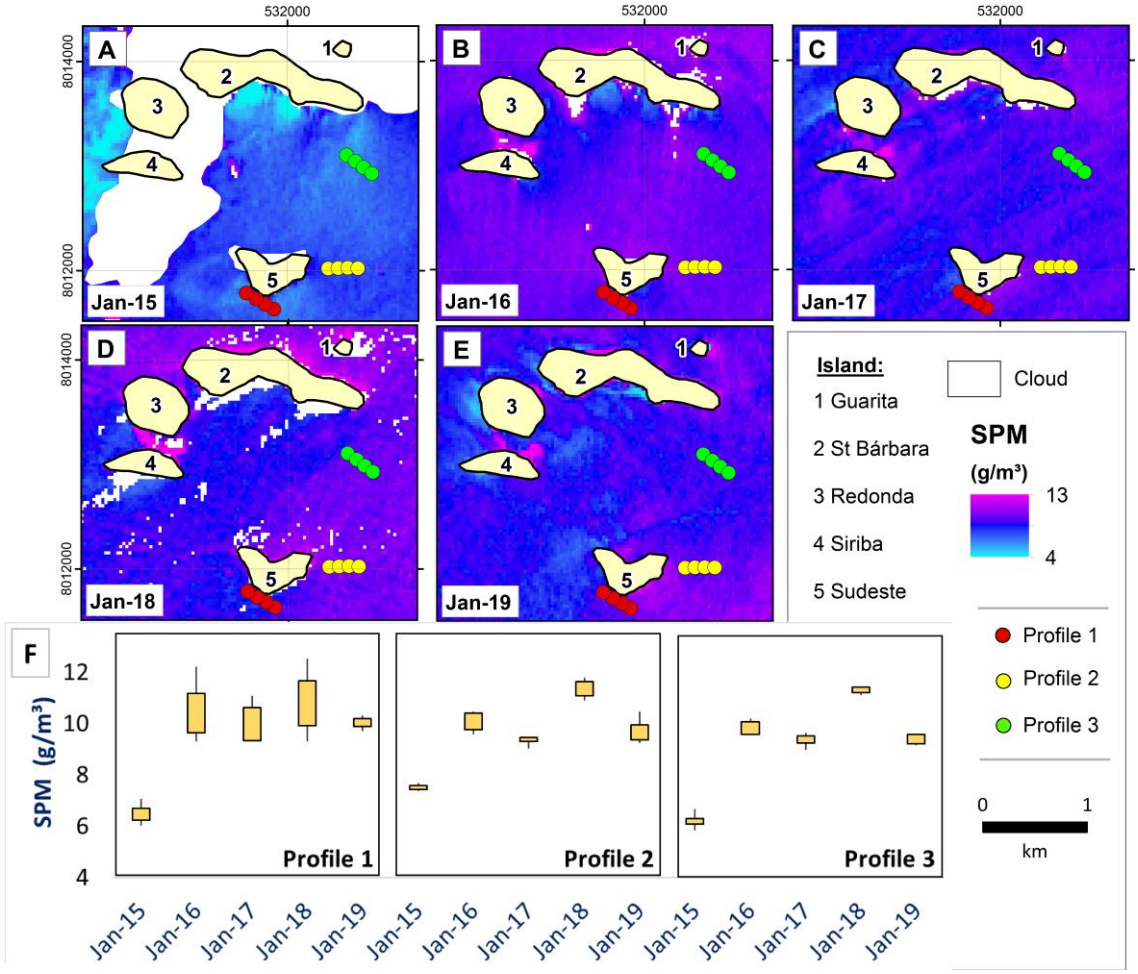

Fig.10. Distribution of SPM for Area 3. (A to E): January 2015 to 2019. (F): Boxplot representing the three sampling profiles from January 2015 to 2019. The SPM space distribution, along with the boxplots, disclose an increasing trend in SPM values between 2015 and 2019, with the highest values appearing in January 2018.

4.4. Discussion

There was a considerable increase in rainfall in the six studied river catchments from 2016 onwards, especially during the summer months in the Southern Hemisphere. This increase is influenced by synoptic scale weather systems such as frontal systems, which can produce intense precipitation that can cause flood and landslides near the southeastern coastal regions of Brazil (Oliveira and Quaresma, 2017).

Long-term time variations for flow and load of suspended sediment at the mouth of the Doce river are driven by climate and human activities, such as deforestation, urbanization, and soil degradation (Oliveira and Quaresma, 2017). These

factors intensify the magnitude of flood events and, consequently, the amount of sediment discharged along the coast. The spatiotemporal analysis showed a considerable increase in SPM from 2016 onwards, primarily near the mouths of the major rivers in Area 1 (see Fig. 1). This increase was revealed in the statistical analyses, in which the SPM averages before the collapse was relatively lower than after collapse (Fig. 5). The direct consequence of the increased SPM concentrations in the coastal zone is a decrease in light penetration into the water column, reducing the euphotic zone and marine photosynthesis activity, which in turn inhibits fauna and flora growth. In addition, the increase in turbidity reduces the aesthetic quality of water, negatively affecting recreation and tourism.

The detailed evaluation of Areas 2 (CER region) and 3 (Abrolhos Archipelago) also reveals an increasing trend in SPM concentrations between 2015 and 2019. The most significant differences between pre and post-collapse values were observed near the mouth of the Doce river. In the CER region, the sediments supplied by the Nova Viçosa and Caravelas rivers stand out. Suspended sediments, particularly fine sediments, reduce the quality and quantity of light penetrating the water column. This leads to a decline in the production of zooxanthellae, which are single-cell algae that live in symbiosis with the corals, supplying them the required energy through photosynthesis (Glynn, 1993). Therefore, an increase in SPM concentration and sedimentation can lead to coral extinction (Erftemeijer et al., 2012). Deposition of particulate matter on the coral causes shadowing and suffocation, which contributes an additional source of decreased photosynthesis activity by the zooxanthellae and may cause coral bleaching (Dikou and van Woesik, 2006).

SAM imagery classification, using pixel reference spectra sampled from waters loaded with sediment (sediment-laden water) after the dam rupture in January and July 2016, indicates that water bodies similar to those with tailings were more concentrated in the shallow regions near the coast. Such a phenomenon was caused primarily by the Brazilian current and the force exerted by wind.

During the summer of 2016 in the Southern Hemisphere, the sediment plume was directed southwards - a direction influenced primarily by the wind, as shown in Fig. 5F. Therefore, the distribution of sediments may have possibly reached across a large area, involving the protected marine areas of Rio de Janeiro (Magris et al., 2019).

According to Rudorff et al. (2018), ocean dynamics in the study area is volatile. In the summer, the ocean currents are often directed to the south but, eventually, the currents can be inverted. These authors also pointed out that changes on the dominant wind pattern from NE to S reversed the Doce river plume direction towards the northern shelf, causing an increase of the turbidity.

In July 2015 and 2016, the Doce river plume was directed to the north. This occurred because the preferential wind path was in the same direction, carrying the suspended particles to the north and, in this case, these particles could reach areas near the Abrolhos reef. Analysis of Sr and Nd radiogenic isotopes confirmed that the Abrolhos sediments mixed with those released from the Doce river mouth after the dam rupture (Evangelista and Valeriano, 2017).

In July 2016, the month that marks the post-collapse event, the northward migration of the plume represented a threat to the equilibrium of the coastal system, especially for protected areas, such as the CER and the Abrolhos Archipelago. This threat is primarily due to the composition of iron tailings discharged at the mouth of the Doce river, which contains potentially toxic metals, according to Queiroz et al. (2018) and Gomes et al. (2017). Geochemical studies conducted in different colonies show that anomalous incorporation of Zn and Cu into coral skeletons occurred after the arrival of the Fundão sediment plume. Besides, anomalous contents of P, As and Ba was observed in the Abrolhos National Park (i.e., https://www.hakaimagazine.com/news/research-unveils-new-damage-caused-brazils-failed-fundaodam/). Chronic and delayed effects due to contamination by these elements can cause significant changes in estuarine benthic communities, affecting overall biodiversity and population dynamics (Gomes et al., 2017).

4.5. Conclusions

The increase of rainfalls during the Austral spring and summer of 2016 intensified sediment discharge in the coastal region of the entire Area 1, resulting in a higher concentration of SPM near the mouth of major rivers. The Austral winter is a season when rainfall is relatively low. The observed rise of SPM during the winter of 2016 is possibly related to bottom sediment resuspension.

The seasonal wind pattern is one of the determining factors that direct sediments from rivers. In January, the specific direction of Austral summer winds is predominantly to the south, and products obtained from OLI/Landsat-8 in 2016 show that the path of the Doce river plume is aligned with the wind direction. Therefore, the increase in SPM observed in the Abrolhos Archipelago and CER during this period is associated with the basins in the region, such as Barra de Caravelas, and other northern catchments.

In July 2016, the direction of Austral winter winds was predominantly to the north. In such conditions, the plume of sediments from the Doce river is coincident with wind direction and possibly may have migrated to the north, as suggested by analysis of the imagery investigated here. However, we are unable to fully prove the origin of suspended sediments along the coast based solely on the interpretation of satellite images and spectral signatures derived from them. Nevertheless, admitting that muddy plumes from the Doce river reached the coast of the Bahia state and mixed with local sediments, it could have reached the Abrolhos archipelago, as already indicated by independent work based on sediment geochemistry.

4.6. References

Bernardo, N., Watanabe, F., Rodrigues, T., Alcântara, E., 2017. Atmospheric correction issues for retrieving total suspended matter concentrations in inland waters using OLI/Landsat-8 image. Adv. Space Res. 59, 2335–2348.

Cao, Z., Dua, H., Feng, L., Ma, R., Xue, K., 2017. Climate and human induced changes in suspended particulate matter over Lake Hongze on short and long timescales. Remote Sens. Environ. 192, 98–113.

Carmo, F.F., Kamino, L.H.Y., Tobias Júnior, R., Campos, I.C., Carmo, F.F., Silvino, G., Castro, K.J.S.X., Mauro, M.L., Rodrigues, N.U.A., Miranda, Pinto, C.E.F., 2017. Fundão tailings dam failures: the environment tragedy of the largest technological disaster of Brazilian mining in global context. Perspectives in Ecology and Conservation 15, 145–151.

Clark, R.N., Swayze, G.A., Gallagher, A., 1993. Mapping Minerals with Imaging Spectroscopy, U.S. Geological Survey, Office of Mineral Resources Bulletin 2039. pp. 141–150.

Coimbra, K.T.O., Alcântara, E.H., Souza Filho, C.R., 2019. An assessment of natural and manmade 1 hazard effects on the underwater 2 light field of the Doce river continental shelf. Sci. Total Environ. 685, 1087–1096. https://doi.org/10.1016/j.scitotenv.2019.06.127c.

Curtarelli, M., Rennó, C.D., Alcântara, E., 2014. Evaluation of the Tropical Rainfall Measuring Mission 3B43 product over an inland area in Brazil and the effects of satellite boost on rainfall estimates. J. Appl. Remote. Sens. 8, 83589–83589–14.

Dikou, A., vanWoesik, R., 2006. Survival under chronic stress from sediment load: spatial patterns of hard coral communities in the southern islands of Singapore. Mar. Pollut. Bull. 52, 7–21.

Erftemeijer, P.L.A., Riegl, B., Hoeksema, B.W., Todd, P.A., 2012. Environmental impacts of dredging and other sediment disturbances on corals: a review. Mar. Pollut. Bull. 64, 1737–1765.

Evangelista, H., Valeriano, C., 2017. Sumário das Análises de Isótopos Radiogênicos de Sr e Nd em sedimentos da foz do rio Doce-ES e do Parque Nacional dos Abrolhos-BA (antes e depois do rompimento da barragem de rejeitos da Samarco em Mariana-MG). DOI.http://www.consultaesic.cgu.gov.br/busca/dados/Lists/Pedido/Attachments/612349/RESPOSTA_PEDIDO_02680002082201705%20-%20sumario_de_analises_UERJ_21Set2017.pdf.

Evangelista, H., Valeriano, C.M., Santos, E.A., Vaz, G., Neto, Carla., Nogueira, J.S., Licinio, M.V., Ribeiro, J.N., Pereira, M.G., Ribeiro, A.V.F.N., Caldero, E.N., Castro, C.B., Guebert, F., Jerozolimski, R., Cruz, E., Cajueiro, L.M., Rodrigues, A., 2016. Estudo preliminar sobre a detecção da pluma de sedimentos do Rio Doce sobre o Parque Nacional dos Abrolhos-BA, para o evento de 5-6 de Janeiro 2016. DOI. http://www.icmbio.gov.br/portal/images/stories/comunicacao/publicacoes/Documentos/DCOM_relatorio_UERJ_versao_final.pdf.

Fernandes, G.W., Goulart, F.F., Ranierid, B.D., Coelho, M.S., Dalesf, K., Boescheg, N., Bustamanteh, M., Carvalho, F.A., Carvalho, D.C., Dirzob, R., Fernandes, S., Galetti Jr., P.M., Millang, V.E.G., Mielkeg, C., Ramirezk, J.L., Nevesa, A., Rogassg, C.,

Ribeirol, S.P.,Sariotm, A., Filho, B.S., 2016. Deep into the mud: ecological and socio economic impacts of the dam breach in Mariana, Brazil. Natureza & Conservação https://doi.org/10.1016/j.ncon.2016.10.003.

Gangloff, A., Verney, R., Doxaran, D., Ody, A., Estournel, C., 2017. Investigating Rhône river plume (Gulf of Lions, France) dynamics using metrics analysis from the MERIS 300m Ocean Color archive (2002−2012). Cont. Shelf Res. 144, 98–111.

Garcia, L.C., Ribeiro, D.B., Roque, F.O., Quintero, J.M.O., Laurance,W.F., 2017. Brazil's worst mining disaster: corporations must be compelled to pay the actual environmental costs. Ecol. Appl. 27, 5–9.Glynn, P.W., 1993. Coral Reefs 12 (1). https://doi.org/10.1007/BF00303779.

Gomes, L.E.O., Correa, L.B., Sáb, F., Neto, R.R., Bernardino, A.F., 2017. The impacts of the Samarco mine tailing spill on the Rio Doce estuary, eastern Brazil. Mar. Pollut. Bull. https://doi.org/10.1016/j.marpolbul.2017.04.056.

Guerra, M.B.B., Teaney, B.T., Mount, B.J., Asunskis, D.J., Jordan, B.T., Barker, R.J., Santos, E.E., Schaefer, C.E.G.R., 2017. Post-catastrophe analysis of the Fundão tailings dam failure in the Doce river system, Southeast Brazil: potentially toxic elements in affected soils. Water Air Soil Pollut. 228–252.

Hatje, V., Pedreira, R.M.A., Rezende, C.E., Schettini, C.A.F.S., Souza, G.C., Marin, D.C., Hackspacher, P.C., 2017. The environmental impacts of one of the largest tailing dam failures worldwide. Sci. Rep. 7, 10706. https://doi.org/10.1038/s41598-017-11143-x.

Kruse, F.A., Lefkoff, A.B., Boardman, J.B., Heidebrecht, K.B., Shapiro, A.T., Barloon, P.J., Goetz, A.F.H., 1993. The spectral image processing system (SIPS) - interactive visualization and analysis of imaging spectrometer data. Remote Sens. Environ. 44, 145–163.

Lee, Z., Weidemann, A., Kindle, J., Arnone, R., Carder, K.L., Davis, C., 2007. Euphotic zone depth: its derivation and implication to ocean-color remote sensing. J. Geophys. Res. 112, C03009. https://doi.org/10.1029/2006JC003802.

Leipe, T., Knoppers, B., Marone, E., et al., 1999. Geo-Mar. Lett. 19, 186. https://doi.org/10.1007/s003670050108.

Magris, R.A., Marta-Almeida, M.,Monteiro, J.A.F., Ban, N.C., 2019. A modelling approach to assess the impact of landmining onmarine biodiversity: assessment in coastal catchments experiencing catastrophic events (SWBrazil). Sci. Total Environ. 659, 828–840. https://doi.org/10.1016/j.scitotenv.2018.12.238.

Marta-Almeida, M.M., Mendes, R., Amorim, F.N., Cirano, M., Dias, J.M., 2016. Fundão dam collapse: oceanic dispersion of river Doce after the greatest Brazilian environmental accident. Mar. Pollut. Bull. https://doi.org/10.1016/j.marpolbul.2016.07.039.

Mazzei, E.F., Bertoncini, A.A., Pinheiro, H.T., Machado, L.F., Vilar, C.C., Guabiroba, H.C., Costa, T.J.F., Bueno, L.S., Santos, L.N., Francini-Filho, R.B., Hostim-Silva, M., 2017. Newly discovered reefs in the southern Abrolhos Bank, Brazil: anthropogenic impacts and urgent conservation needs. Joyeux Marine Pollution Bulletin 114, 123–133. https://doi.org/10.1016/j.marpolbul.2016.08.059.

Miranda, L.S.,Marques, A.C., 2016. Hidden impacts of the Samarcomining waste dam collapse to Brazilian marine fauna – an example from the staurozoans (Cnidaria). Biota Neotropica 16 (2), e20160169.

Nechad, B., Ruddick, K.G., Park, Y., 2010. Calibration and validation of a generic multisensor algorithm for mapping of total suspended matter in turbid waters. Remote Sens. Environ. 114, 854–866. https://doi.org/10.1016/j.rse.2009.11.022.

Nobre, D.M., Alarconc, D.T., Cintid, A., Schiavettie, A., 2017. Governance of the Cassurubá Extractive Reserve, Bahia State, Brazil: an analysis of strengths and weaknesses to inform policy. 77, 44–45.

Oliveira, K.S.S., Quaresma, V.S., 2017. Temporal variability in the suspended sediment load and streamflow of the Doce river. J. S. Am. Earth Sci. 78, 101–115. https://doi.org/10.1016/j.jsames.2017.06.009.

Omachi, C.Y., Siani, S.M.O., Chagas, F.M., Mascagni, M.L., Cordeiro, M., Garcia, G.D., Thompson, C.C., Siegle, E., Thompson, F.L., 2018. Atlantic Forest loss caused by the world's largest tailing dam colapse (Fundão Dam, Mariana, Brazil). Remote Sensing Applications: Society and Environment 12, 30–134.

Queiroz, H.M., Nóbrega, G.N., Ferreira, T.O., Almeida, L.S., Romero, T.B., Santaella, S.T., Bernadinho, A.F., Otero, X.L., 2018. The Samarco mine tailing disaster: a possible time-bomb for heavy metals contamination? Sci. Total Environ. 637–638, 498–506.

Rudorff, N., Rudorff, C.M., Kampel, M., Ortiz, G., 2018. Remote sensing monitoring of the impact of a major mining wastewater disaster on the turbidity of the Doce river plume off the eastern Brazilian coast. ISPRS J. Photogramm. Remote Sens. https://doi.org/10.1016/j.isprsjprs.2018.02.013.

Sánchez, L.E., Alger, K., Alonso, L., Barbosa, F.A.R., Brito, M.C.W., Laureano, F.V., May, P., Roeser, H., Kakabadse, Y., 2018. Impacts of the Fundão DamFailure. A Pathway to Sustainable and ResilientMitigation. Rio Doce Panel Thematic Report No. 1. IUCN, Gland, Switzerland https://doi.org/10.2305/IUCN.CH.2018.18.en.

Segura, F.R., Nunes, E.A., Paniz, F.P., Paulelli, A.C.C., Rodrigues, G.B., Braga, G.U.L., Pedreira Filho,W.R., Barbosa Jr., F., Cerchiaro, G., Silva, F.F., Batista, B.L., 2016. Potential risks of the residue fromSamarco'smine damburst (Bento Rodrigues, Brazil). Environ. Pollut. 218, 813–825.

Silva, A.C., Cavalcante, C.D., Fabris, J.D., Franco Junior, R., Barral, U.M., Farnezi, M.M.M., Viana, A.J.S., Ardisson, J.D., Outon, L.E.F., Lara, L.R.S., Stumpf, H.O., Barbosa, J.B.S., Silva, L.C., 2016. Chemical,mineralogical and physical characteristics of a material accumulated on the river margin from mud flowing from the collapse of the iron ore tailings damin Bento Rodrigues,Minas Gerais, Brazil. Revista Espinhaço. 5 (2), 44–53.

Valeriano, C.M., Neumann, R., Alkimim, A.R., Evangelista, H., Heilbron, M., Neto, C.C.A., Souza, G.P., 2019. Sm–Nd and Sr isotope fingerprinting of iron mining tailing deposits spilled from the failed SAMARCO Fundão dam 2015 accident at Mariana, SE-Brazil. Appl. Geochem. 106, 34–44.

Vanhellemont, Q., Ruddick, K., 2014. Turbidwakes associated with offshorewind turbines observed with Landsat 8. Remote Sens. Environ. 145, 105–115.

Vanhellemont, Q., Ruddick, K., 2015. Advantages of high quality SWIR bands for ocean colour processing: examples from Landsat-8. Remote Sens. Environ. 161, 89–106. Werner, T.B., Pinto, L.P., Dutra, G.F., Pereira, P.G.P., 2000. Abrolhos 2000: conserving the southern Atlantic's richest coastal biodiversity into the next century.

CAPÍTULO 5

Satellite Evidence for Pervasive Water Eutrophication in the Doce River Reservoirs following the Fundao Dam Failure, Brazil

K.T.O. Coimbra, E. Alcântara, C.R. Souza Filho

Published in the Environmental Pollution Journal, available online 9 November 2020, Page 116014. DOI: https://doi.org/10.1016/j.envpol.2020.116014

One of the worst socio-environmental disasters to mark the history of Brazil and the world occurred in November 2015 and involved the mining sector. The collapse of the Fundao dam released approximately 43 million m³ of iron ore tailings, which moved downstream to reach the Doce River. This resulted in the contamination of water, soil, and sediments along the entire course of the river, which also affected its mouth in the Atlantic Ocean. Four years after the disaster, several socio-environmental problems continue to persist in the affected areas. In this context, the reservoirs built along the Doce River deserve special attention as they are artificial environments that are highly vulnerable to changes in water parameters. This study aims to determine water quality indicators of these reservoirs using remote sensing data and image processing methods, including semi-analytical algorithms, to comprehend the progress of eutrophication processes. Operational land imager /Landsat-8 data (from 2013 to 2019) were used to map the suspended particulate matter (SPM), euphotic zone (Z_{eu}) and chlorophyll-*a* (Chl-*a*) before and after the collapse. The results showed significant changes in SPM and Z_{eu} in the reservoirs after the collapse. Non-conformity of these parameters is observed even now, and they tend to intensify during rainy periods when resuspension processes of sediments occur. Moreover, there has been an increase in the eutrophication of reservoirs as noticed by the significant increase in Chl-*a* after the disaster, especially in January, July, and August.

5.1. Introduction

Four years after one of the world's largest environmental disasters involving mining tailings dams, its effects on the ecosystem and biodiversity of the affected areas continue to be of great concern. The collapse of the Fundao dam in November 2015 released approximately 43 million m³ of iron ore tailings and formed a 10 m high wave with high-speed flow. Before reaching the Doce River, this wave destroyed the district of Bento Rodrigues and buried parts of the Gualaxo do Norte and Carmo rivers, leading to the loss of 19 lives (Samarco, 2016).

The consequences of the collapse extended along 670 km² of the Doce River, where tailings sludge led to the pollution of water, sediments, and soils, thereby affecting the aquatic and terrestrial biodiversity that depended on water resources. Furthermore, ecosystem

services were compromised due to the destruction of agricultural areas, pastures, and permanent preservation areas. This led to water and energy supply crisis, as well as the suspension of fishing and tourism activities (IBAMA, 2015; Fernandes et al., 2016; Omachi et al., 2018)

The causal link of the impacts of the dam collapse on the sediments and water quality of the Doce River has been the subject of numerous studies (eg. Carmo et al., 2017; Hatje et al., 2017). Reports issued by SAMARCO, the mining company responsible for the Fundao mine, indicated that the water quality of the Doce River was not ideal before the dam collapse due to discharge of pollutants from different sources (IBAMA, 2015). Conversely, the tailings wave excavated and eroded the banks of the Doce River and its tributaries, allowing the remobilization of sediments that contained heavy metals and pre-existing contaminants. This material was spread throughout the river and coastal region (Carmo et al., 2017; Hatje et al., 2017).

There is growing concern regarding the water quality of the reservoirs in the Doce River, as they have been heavily impacted by tailings sludge. In general, such environments are overly sensitive to physico-chemical changes in water and sediments. Moreover, they are vulnerable to the eutrophication process, which is the natural or artificial discharge of nutritional elements to a body of water, resulting in increased primary productivity of the aquatic environment and consequent phytoplankton proliferation (Wetzel, 2001). Some species of phytoplankton, such as cyanobacteria, have toxic potential. Water contaminated by these organisms is a threat to public health and biodiversity. Thus, it is important to systematically monitor reservoirs by analyzing its physical, chemical, and biological parameters.

Suspended particulate matter (SPM) is a key physical parameter related to mining tailings pollution and other effluents. Clay particles suspended in water can potentially adsorb toxic metals and macronutrients, such as phosphorus and nitrogen, and eventually, help transport these elements over large distances (Segura et al., 2016; Silva et al., 2016). Excess SPM may also reduce the penetration of light through water, thereby limiting the depth of the euphotic zone (Z_{eu}), which is defined as the depth at which the photosynthetically active radiation (PAR) corresponds to 1% of its surface value. The penetration and availability of light in water control phytoplankton photosynthesis, nutrient cycling, and physical processes, by means of heat transfer (Kirk, 1994). Chlorophyll-*a* (Chl-*a*) is another biological parameter that is essential for monitoring the quality of water in reservoirs. Chlorophyll pigments are

found in all groups of plants and autotrophic organisms; therefore, its determination is important in studying primary productivity, analyzing the physiological state of phytoplankton, and assessing the degree of eutrophication in an aquatic environment (Watanabe et al. 2019).

Studies conducted in different environments reported the presence of heavy metals due to the increased eutrophication of aquatic ecosystems under the influence of mine drainage and other effluents (Fielding et al., 2020; Gomes et al., 2020; Nwankwegu et al., 2020). After the collapse, there was a significant increase in dissolved metals in the water column of the Doce River, as well as an increase in potentially toxic metals in sediments and soils of the impacted areas. Several studies have researched this pollution scenario and its effects on the biodiversity of the Doce River and its coastal regions (Segura et al., 2016, Hatje et al., 2017, Gomes et al., 2017, Botino et al., 2017; Queiroz et al., 2018; Weber et al., 2020; Fernandes et al., 2020; Passos et al., 2020).

Evidence on the possible increase of phytoplankton biomass in the Doce River reservoirs after the collapse exits but is poorly documented (**Fernandes et al., 2020**). It is yet unclear whether this escalation in phytoplankton content is local or widespread and justifiably associated with physicochemical changes in sediments and water caused by tailings sludge. One of the difficulties in establishing criteria for environmental assessment of areas impacted by disasters of this magnitude is the lack of information on the pre-disaster state. To this end, satellite images can provide useful information for multitemporal analysis of the affected areas (Coimbra et al., 2019; 2020).

The objective of this study is to investigate, with unprecedented detail, the concentration and spatial distribution of Chl-*a* in the reservoirs of the Doce River, pre and after the Fundao dam collapse, to determine possible variations in the trophic state of the water bodies and to define whether changes can be possibly related to the tailing dam spill.

5.1.1. Study Area

The onshore region affected by the Fundao Dam collapse encompassed three main reservoirs of the Doce River (Fig. 1) built for power generation: Risoleta Neves Power Plant (RNPP), Baguari Power Plant (BPP), and Eliezer Batista Power Plant (EBPP).

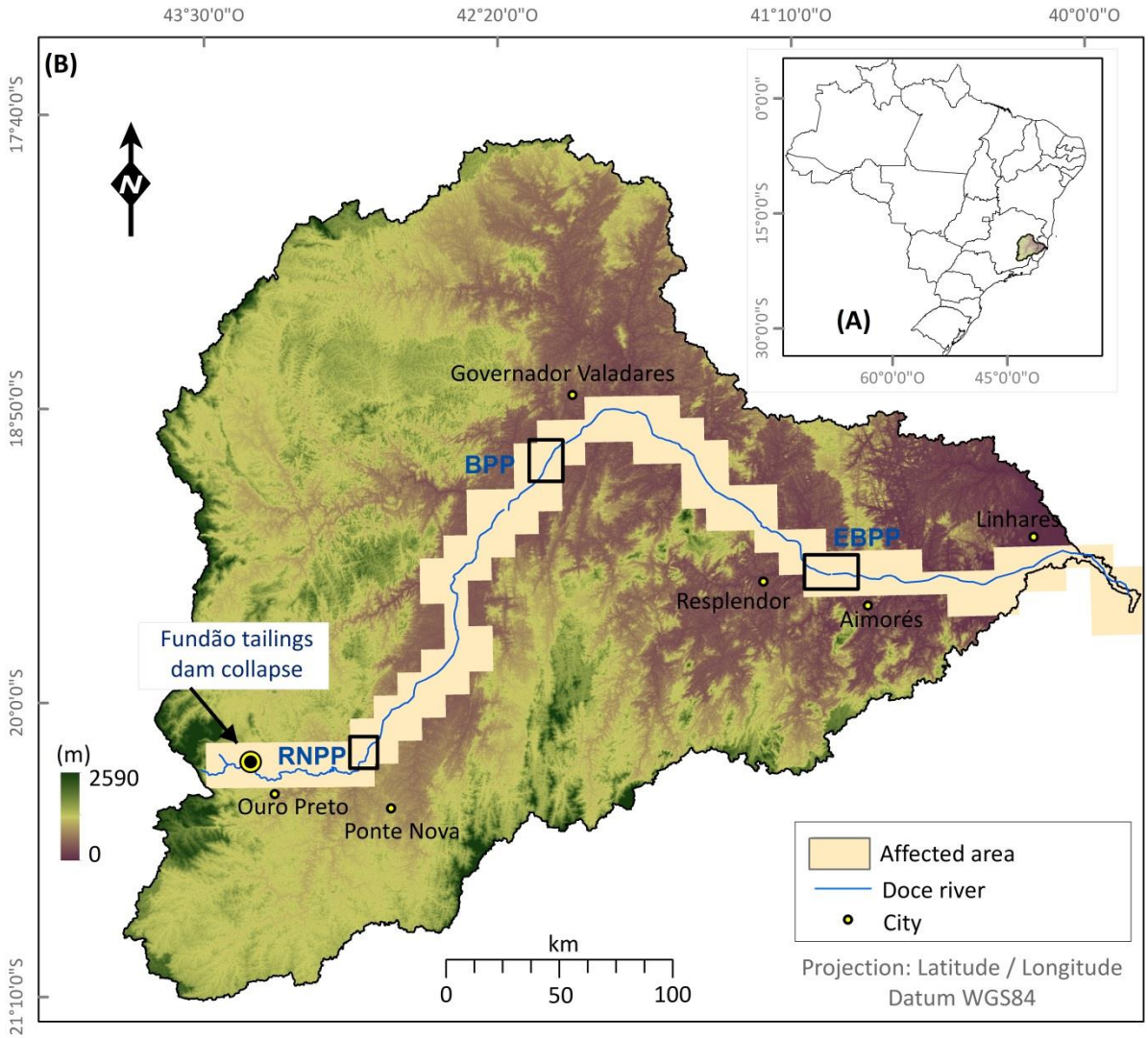

Fig. 1. Location of the study area. (A) Location of the Doce River Basin in Brazil. (B) Emphasis on the area affected by the Fundao dam collapse. The general course of the Doce River is highlighted in yellow, including three reservoirs studied here, namely Risoleta Neves Power Plant (RNPP), Baguari Power Plant (BPP), and Eliezer Batista Power Plant (EBPP).

RNPP is located between the municipalities of Rio Doce and Santa Cruz do Escalvado, in Minas Gerais, which is near the headwaters of the Doce River. This hydroelectric power plant began operations in 2004, with a flooded area of approximately 2.84 km². RNPP was the most affected by the collapse (ANA, 2015; Sanches et al., 2018), as its dam was the first obstacle encountered by the tailings wave. A large amount of the tailings was retained in this area and was deposited along the floodplain of the reservoir. Bathymetric surveys of RNPP conducted in 2014 showed that the service life of this plant is 180 years (LACTEC, 2018). However, after the collapse of the dam, its functioning was compromised due to siltation of the reservoir and a decrease in water levels.

BPP is located on the Doce riverbed in Governador Valadares. It covers the municipalities of Periquito, Alpercata, Fernandes Tourinho, Sobrália, and Lapu. The plant

began operations in 2010 and supplies water to a city consisting of 450 thousand inhabitants. The BPP reservoir has a flooded area of 16 km² and a water volume of 43.562 x 10^6 m³, of which 22 km are in the Doce River and 5 km are in the Corrente Grande River (http://www.uhebaguari.com.br/quem-somos/).

EBPP is in the middle of the Doce River and covers the municipalities of Aimorés, Ituêta, and Resplendor in Minas Gerais as well as Baixas Gandu in Espirito Santo. EBPP has been operating since 2005, with a 30.9 km² reservoir area, an average depth of 16 m, and a maximum quota of 92 m (https://ejatlas.org/conflict/aimores-hydroelectric-power-plant-brazil)

5.2. Materials and methods

5.2.1. Meteorological data

Data on the monthly average rainfall from 2014 to 2020 were obtained from the Tropical Rainfall Measuring Mission's (TRMM) product 3B43 (Curtarelli et al., 2014) of the GIOVANNI-NASA platform: Geospatial Interactive Online Visualization and Analysis Infrastructure (https://giovanni.gsfc.nasa.gov/giovanni/). Rainfall data refer to the average rainfall at the limits of the Doce River basin (Fig. 1).

5.2.2. Satellite image processing

Level 1 OLI/Landsat-8 images, from 2013 to 2019, were obtained from the USGS Earth Explorer (https://earthexplorer.usgs.gov). Given the persistent presence of clouds, it was not possible to obtain images for all the months of the time series. Thus, a total of 23 images were used, of which 9 were of RNPP, 4 of BPP, and 10 of EBPP. The Level 1 product is an image with geometric and radiometric correction, having a spatial resolution of 15–30 m.

The OLI images were atmospherically-compensated using the ACOLITE software (https://odnature.naturalsciences.be/remsem/software-and-data/acolite). The surface reflectance (SR) product was used to calculate SPM and Chl-*a* concentrations. ACOLITE also helped in obtaining the products of diffused attenuation coefficient of water at 490 nm (K_d490), which were used to estimate the depth of the euphotic zone, Z_{eu}. These products underwent processes to remove clouds, soil, and sandbank from the river to avoid spectral contamination of the water pixels that were analyzed. To compare scenarios before and after the dam collapse, images from the WorldView-2 satellite sensor were used. These images

were made available by the Brazilian Institute of the Environment and Renewable Natural Resources – IBAMA (https://www.gov.br/ibama/pt-br).

5.2.3. Suspended Particulate Matter (SPM) and Euphotic Zone (Zeu)

The model proposed by Nechad et al. (2010) was used to estimate SPM in the three reservoirs chosen in this study (Eq. 1). The algorithm was calibrated with different sensors and *in situ* data on turbid waters from the Belgica and Zeeleeuw campaigns over the Southern North Sea. It is currently used in various environments (Gangloff et al., 2017).

$$\mathrm{SPM} = \left(\frac{A^p x\, \rho w}{1 - \frac{\rho w}{C^p}}\right) \qquad \text{Eq (1)}$$

where ρw corresponds to the Surface Reflectance (SR) of water at a 877 nm; A^p, C^p, and B^p are the coefficients dependent on the chosen wavelength (e.g., OLI / L8 at 877 nm: A^p = 3199.96, B^p = 0, and C^p = 0.2101).

Z_{eu} (Eq. 2) was estimated using the algorithm developed by Zhao et al. (2013) whose variable is the diffuse attenuation coefficient of water (K_d490). This model has been successfully implemented in Brazil and other parts of the world (Gomes et al., 2020).

$$Z_{eu} = 0.28 + \left(\frac{395.92 \text{ x } 0.0092}{0.0092 + K_d490}\right) \qquad \text{Eq (2)}$$

5.2.4. Chl-*a* and trophic state (TS) classification

To estimate the Chl-*a* concentration (Eq. 3), we used the model proposed by Mishra and Mishra (2012) based on the normalized difference chlorophyll-*a* index (NDCI, Eq. 4). The NDCI has been used as a proxy for Chl-*a* concentration with relative success around the world (e.g. Caballero et al. 2020; Pahlevan et al. 2020; Watanabe et al. 2019).

$$\mathrm{Chl} - a = A + B \text{ x } \mathrm{NDCI} + C \text{ x } \mathrm{NDCI}^2 \qquad \text{Eq (3)}$$

Where: A = 14.039; B = 86.115; C = 194.325. The NDCI is calculated as:

$$\mathrm{NDCI} = \frac{R_{rs}\,(\lambda 2) - R_{rs}\,(\lambda 1)}{R_{rs}\,(\lambda 2) + R_{rs}\,(\lambda 1)} \qquad \text{Eq (4)}$$

where R_{rs} corresponds to remote sensing reflectance at wavelengths: λ1 = 655 nm; λ2 = 865 nm.

The original work from Mishra and Mishra (2012) uses λ1 = 665 nm; λ2 = 708 nm. They used these wavelengths because the NDCI was first developed to be applied to MERIS (MEdium Resolution Imaging Spectrometer) images. Since we used OLI/Landsat-8 images, the wavelengths were adapted.

Chl-*a* maps were used to classify the trophic state of water according to the intervals indicated in Table 1.

Table 1: Trophic state classification for reservoirs, adapted from CETESB (2017).

Trophic state classification	**Chl-*a* (mg/m^{-3})**
Ultraoligotrophic	Chl-*a* ≤ 1.17
Oligotrophic	1.17 < Chl-*a* ≤ 3.24
Mesotrophic	3.24 < Chl-*a* ≤ 11.03
Eutrophic	11.03 < Chl-*a* ≤ 30.55
Supertrophic	30.55 < Chl-*a* ≤ 69.05
Hypereutrophic	69.05 < Chl-*a*

5.2.5. Time series analysis of SPM, Zeu, and Chl-*a*

Time series maps of SPM, Z_{eu}, Chl-*a* concentration and trophic status (TS) were produced for three reservoirs: RNPP, BPP and EBPP using OLI/Landsat-8 images. Boxplots were drawn using a sample of 20 pixels extracted from each map of the time series. The sampling spots were carefully selected to avoid spectral mixture with land in the pixels. A background threshold (BG) was plotted in the boxplot, corresponding to the average reference values before the tailings dam collapse.

In the RNPP area, the pixels were sampled for July to determine the results in 2014, 2016, 2017, and 2019. The BG was positioned in the graph according to the median of the year before the collapse (2014), such that BG_{SPM} = 45.76 g/m³, BG_{Zeu} = 4.57 m, and $BG_{Chl\text{-}a}$ = 5.19 mg/m^{-3} (Figs. 3A, H and N). Additionally, the pixels were sampled for August to calculate the results in 2013, 2014, 2016, 2017, and 2019. In this case, the BG used comprised the average of the two years preceding the collapse (2013 and 2014), wherein BG_{SPM} = 48.90 g/m³, BG_{Zeu} = 5.11 m, and $BG_{Chl\text{-}a}$ = 5.01 mg/m^{-3} (Figs.3B, J, and O).

In the BPP area, the pixels were sampled for August to determine the results in 2015, 2016, 2017, and 2019. BG values were observed to be close to the 2015 median, which corresponds to pre-collapse level, such that BG_{SPM} = 67.47 g/m³, BG_{Zeu} = 3.40 m, and $BG_{Chl\text{-}a}$ = 5.64 mg/m^{-3} (Figs. 3C, I, and P).

In EBPP, the sampled pixels were extracted for January, June, and September. For January, the years 2014, 2015, and 2017 were considered. January 2014 is the month following the natural flooding of the Doce River (DR-Flooding), which occurred due to high rainfall in December 2013. This event caused substantial changes in bio-optical water parameters due to large amount of sediments, carried from the DR watershed. Therefore, 2015 was selected as the reference year for the BG values, as it had a rainfall similar to the historical average; thus, BG_{SPM} = 43.10 g/m³, BG_{Zeu} = 3.31 m, and $BG_{Chl\text{-}a}$ = 27.49 mg/m^{-3} (Figs. 3D, K, and Q). In June and September, BG was within the 2015 reference range (before-DC), that is BG_{SPM} = 38.24 g/m³, BG_{Zeu} = 2.65 m, and $BG_{Chl\text{-}a}$ = 42.54 mg/m^{-3} for June (Figs. 3F, L, R); and BG_{SPM} = 99.90 g/m³, BG_{Zeu} = 4.48 m, and $BG_{Chl\text{-}a}$ = 19.98 mg/m^{-3} for September (Figs. 3G, M, and S).

5.2.6. Statistical analysis

The SPM, Z_{eu}, and Chl-*a* parameters were analyzed with 95% confidence interval. The sample groups were systematically separated according to the month/year under analysis, considering the average of the three reservoirs, including January, June, July, August, and September. Moreover, paired Student's t-test was used to determine whether the difference in pre- and post-collapse averages were statistically equal or different.

5.3. Results

5.3.1. Time series analysis

The sampled pixels of SPM, Z_{eu}, and Chl-*a* were analyzed according to the profiles of each reservoir (Fig. 2). After the collapse, the highest SPM values were observed in the RNPP reservoir in 2016 (July and August) and 2017 (July), reaching up to ~1300 g/m³. Although the values decreased in 2017 (August) and 2019 (July and August), they remained above BG values, varying between 29 and 191 g/m³ (Figs. 2A and B).

Greater Z_{eu} values were observed before-DC, varying between 3.22 and 8.44 m. In contrast, critical values of Z_{eu} were observed after-DC, that is in July and August (2016 and 2017), with Z_{eu} varying between 0.48 and 3.01 m (Figs. 3G and H). Chl-*a* concentration after-DC increased in July and August, reaching 48 mg/m^{-3}. In both cases, the values remained above BG (Figs. 2M and N).

In the BPP reservoir, SPM values were above BG values in August 2016, varying from 105 to 135 g/m³ (Fig. 2C). The remaining years analyzed were within BG range.

However, after-DC, Z_{eu} values were away from BG range, ranging from 0.91 to 3.35 m (Fig. 2I). The Chl-*a* of the BPP area, in turn, increased after-DC (Fig. 2O). In 2016, 2017 and 2019, the minimum values sampled were above BG (> 20 mg/m^{-3}).

In the EBPP reservoir, during DR-flooding and after-DC, the SPM values significantly exceed BG values, ranging from 102 to 410 g/m^3 (Fig. 2D). Z_{eu} was not within the BG range for both; it did not exceed 0.88 m (Fig. 2J). In January 2014 (DR-flooding), Chl-*a* showed the lowest values in the series, with the median being just below the BG value (Chl-*a* = 15–23 mg/m^{-3}). Conversely, in January 2017, Chl-*a* concentration increased significantly after-DC, reaching values well above BG (Chl-*a* = 38–51 mg/m^{-3}; Fig. 2P).

In June, after the collapse, SPM and Z_{eu} values were not within the BG range only in 2016 (Figs. 2E and K). Moreover, before-DC and after-DC showed significantly high Chl-*a* values. These values were different from the median and were extracted from sampled pixels in sites also characterized by greenish spots in the water, occurring in a widespread manner. In general, no significant changes of Chl-*a* were observed over time, except in 2016, when the average values were slightly above the BG value and Chl-*a* reached up to 176 mg/m^{-3} (Fig. 2Q).

In September, SPM and Z_{eu} showed a median value that was marginally away from the BG values only in 2017. In the other years, these parameters are in accordance with the BG (Figs. 2F and L). Within the time series, Chl-*a* differed from the BG during two events: (i) after-DC, when it reached up to 44 mg/m^{-3} in 2017 and, (ii) when Chl-*a* was far below the BG line in 2019, with values below 6 mg/m^{-3} (Fig. 2R).

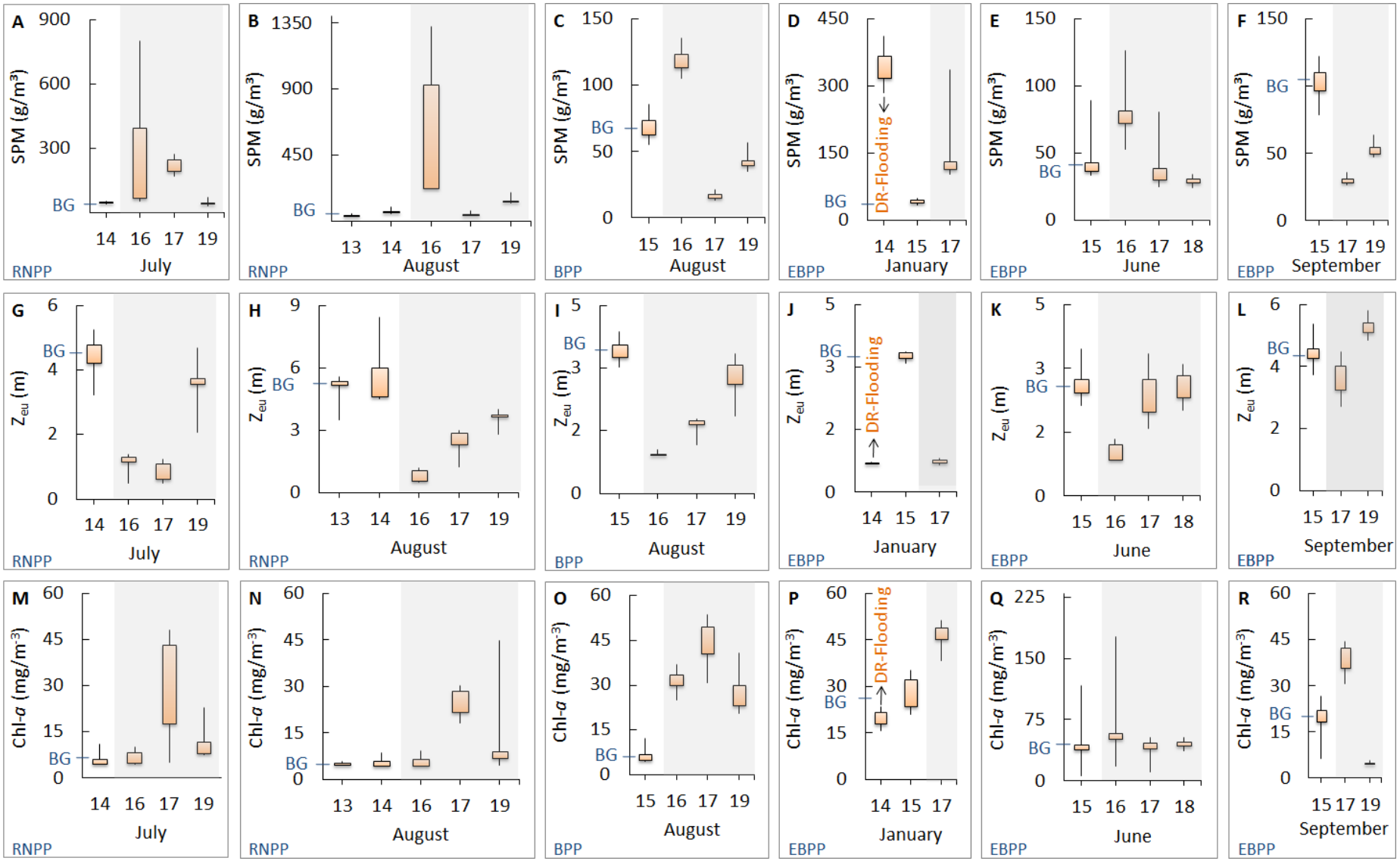

Fig. 2. Boxplots representing the SPM, Z_{eu}, and Chl-*a* values of each reservoir. The months of July and August (RNPP), August (BPP), and June and September (EBPP) are under analysis here. (A to F) SPM, (G to L) Z_{eu}, and (M to R) Chl-*a*. *BG: Background; After-DC is indicated in gray.

The rainfall time series in mm/month, as well as the statistical analysis of SPM, Z_{eu}, and Chl-*a* with 95% confidence interval (considering the average of the three reservoirs), are illustrated in Fig. 3.

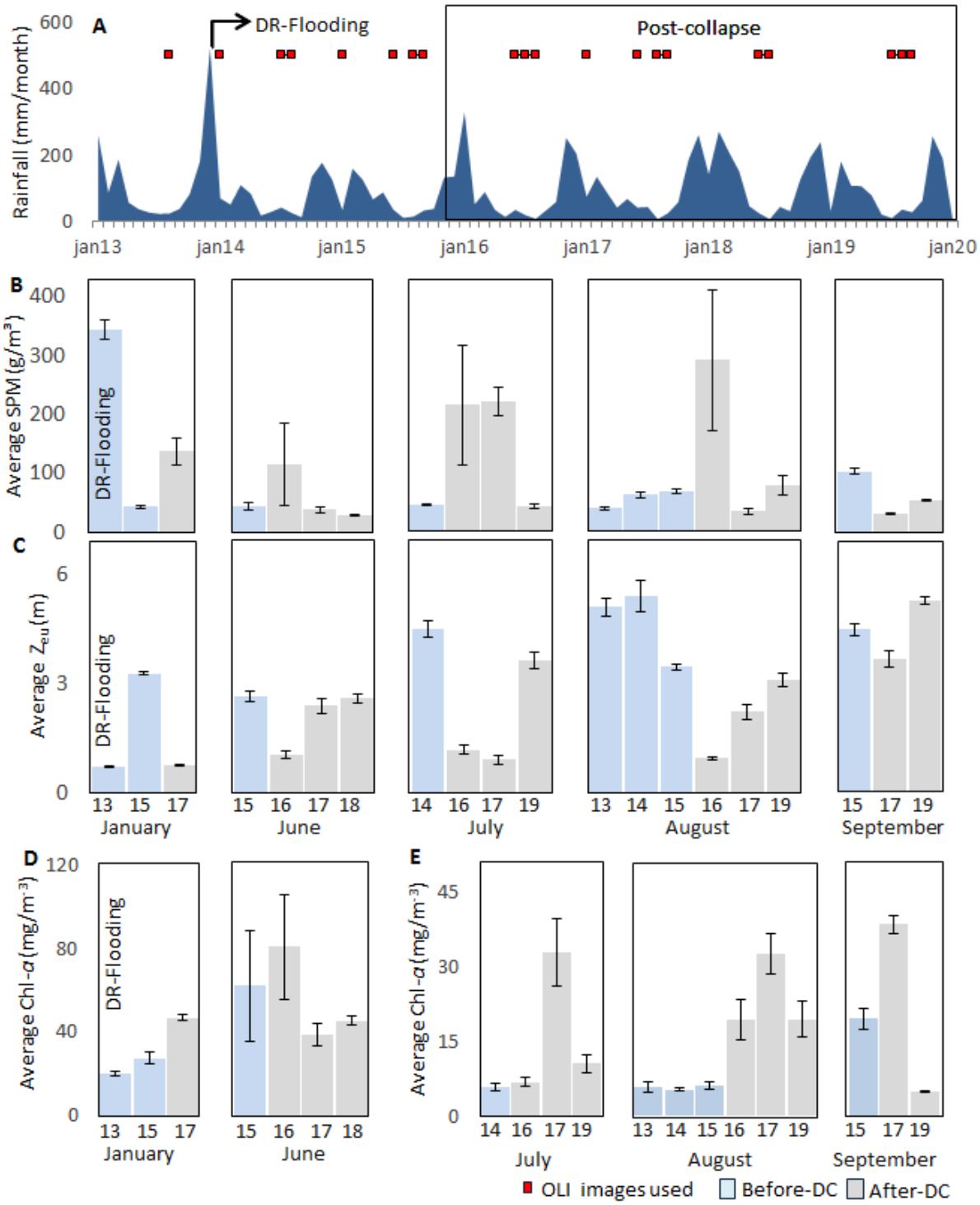

Fig. 3. (A) Monthly rainfall series for the Doce River basin from January 2013 to January 2020, with emphasis on the time of flooding of the Doce River (DRF), in December 2013. OLI/Landsat-8 images used to obtain the products are highlighted in orange boxes. (B) SPM,

(C) Z_{eu}, and (D and E) Chl-*a* averages and their respective confidence intervals, before and after dam collapse, according to the points extracted from the three reservoirs.

The graph of rainfall also indicates the OLI images used to obtain the products for this study (red boxes in Fig. 3A). All the acquired images represent the periods of drought, where rainfall is between 6 and 74 mm/month. The January 2014 image, despite showing low monthly rainfall, represents the period after the Doce River flooding (DR-flooding) that occurred in December 2013, when rainfall exceeded 520 mm/month; therefore, it is representative of this event.

The blue bars in the statistical graphs represent the averages before dam collapse (before-DC), the gray bars represent the averages after dam collapse (after-DC), and the black lines indicate the errors (Figs. 3B, C, D and E). The highest SPM values are observed in DR-flooding and after-DC in January (Fig. 3B). In this case, SPM varies between 136 e 343 g/m³. Between June and September, before-DC, SPM averages vary between 39 and 103 g/m³; with episodic concentrations reaching up to 291 g/m³.

Zeu in January also differs from the other months; it is highly limited in both DR-flooding and after-DC and it does not exceed 0.74 m. Before-DC, between June-September, the averages of Z_{eu} are relatively high, between 2.64 and 5.39 m. Statistical analysis of after-DC data allows for the identification of two distinct behaviors of Z_{eu}: (i) months with a significant decrease in Z_{eu} values, which are equal to those before-DC, as in June and September (Z_{eu} = 0,88 to 5.28 m); (ii) months whose values do not return to those before-DC, as in July and August (Z_{eu} = 0.86 to 3.63 m; Fig. 3C). Statistical graphs show that there is an increase in Chl-*a* concentration after-DC, mainly in January, July, and August and September (Figs. 3D and E).

The results of the paired t-test for SPM, Z_{eu}, and Chl-*a* showed that in the RNPP and BPP reservoirs, the *p*-value is below the 5% significance level for almost every month analyzed. The exception is for SPM concentrations from August in the BPP reservoir, which confirmed that there is a significant statistical difference between the averages before-DC and after-DC (Table 2). In EBPP, there is statistically significant difference between SPM, $Z_{eu,}$ and Chl-*a* for DR-flooding and after-DC (*p*-value < 0.002), besides Z_{eu} of June and SPM of September (before and after-DC).

Table 2: Paired Student's t-test among maps of SPM, Zeu, and Chl-a before and after the dam collapse for all reservoirs.

		95% conf		Avereage		T-value	*p*-value
	July	before-DC	after-DC	before-DC	after-DC		
	SPM	1,69	48,73	46,64	138,01	-3,92	0,001
	Zeu	0,23	0,14	4,48	1,94	19,66	0,000
RNPP	Chl-*a*	0,90	2,69	5,90	17,06	-8,24	0,000
	August	before-DC	after-DC	before-DC	after-DC		
	SPM	3,32	95,44	51,39	230,09	-4,04	0,001
	Z_{eu}	0,28	0,27	5,24	2,19	16,39	0,000
	Chl-*a*	0,64	2,17	5,60	14,53	-8,28	0,000
	August	before-DC	after-DC	before-DC	after-DC		
BPP	SPM	4,76	5,43	68,97	66,75	0,644	0,407
	Z_{eu}	0,10	0,11	3,44	1,80	23,461	0,000
	Chl-*a*	0,72	1,86	6,13	32,40	-27,347	0,000
	January	DR-flooding	after-DC	DR-flooding	after-DC		
	SPM	17,61	24,03	343,03	136,45	14,407	0,000
	Z_{eu}	0,00	0,02	0,69	0,74	-3,879	0,000
	Chl-*a*	1,08	1,48	20,01	47,00	-31,051	0,000
EBPP	**June**	before-DC	after-DC	before-DC	after-DC		
	SPM	7,11	18,52	42,62	51,99	-0,905	0,417
	Z_{eu}	0,16	0,19	2,64	2,17	3,886	0,000
	Chl-*a*	28,31	9,29	62,37	55,08	0,524	0,680
	September	before-DC	after-DC	before-DC	after-DC		
	SPM	5,23	1,23	103,18	41,30	24,114	0,000
	Z_{eu}	0,17	0,16	4,48	4,47	0,038	0,964
	Chl-*a*	2,31	1,01	19,65	21,77	-1,760	0,140

*before-DC: Before dam collapse. After-DC: after dam collapse. DR-flooding: Doce River flooding

5.3.2. Spatiotemporal analysis

After the Fundao dam collapse, the three reservoirs were impacted in different ways. In the RNPP, where a large amount of tailings sludge was retained by the dam, in addition to the changes in bio-optical water parameters, siltation of drainage and changes in the water level of the reservoir were observed, which is demonstrated by the WorldView-2 true-color images with 1.84 m spatial resolution (Figs. 4A and B).

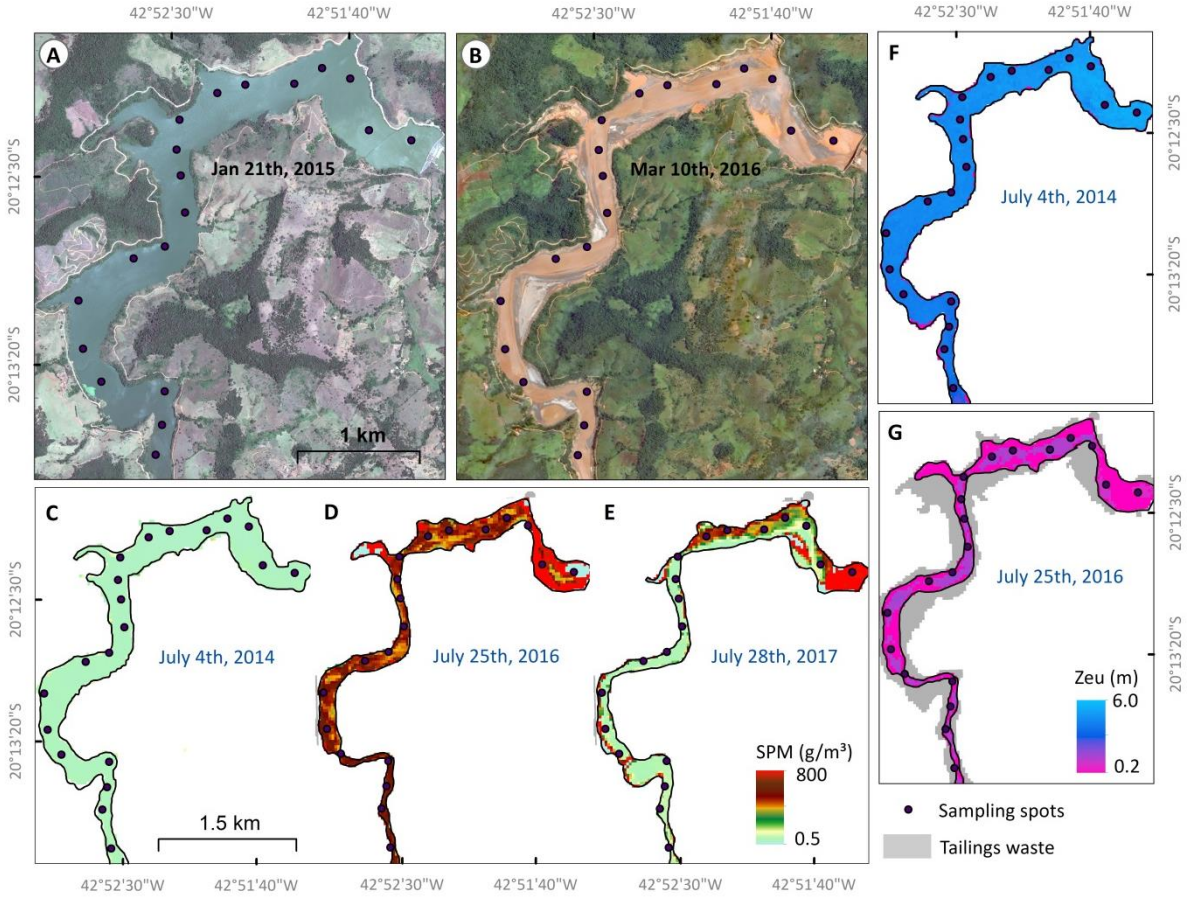

Fig. 4. RNPP reservoir, before and after dam collapse. (A and B) WorldView-2 true-color images obtained 11 months before-DC and 4 months after-DC. The contrast between the two images is striking. It is clear that after the collapse there is a decrease in the volume of water, with tailings causing siltation thorough the reservoir. (C, D, and E) SPM spatial distribution estimated using OLI data for July 2014, 2016, and 2017, respectively. In July 2014, SPM was relatively low compared to the years after the collapse. In 2016 and 2017, high SPM values were observed throughout the reservoir, mainly in the region near the dam. (F and G) Z_{eu} spatial distribution estimated via OLI for July 2014 and 2016. The contrasting values can be observed before-DC and after-DC, with relatively higher values in 2016.

July was chosen to demonstrate the spatial distribution of the products obtained from RNPP using OLI data, considering that significant statistical changes between the averages of before-DC and after-DC were observed in this month. Before-DC, SPM spatial distribution showed extremely low values throughout the reservoir area, hardly exceeding 40 g/m³ (Fig. 4C). However, in 2016 and 2017, SPM values above 80 mg/m^{-3} were recurrent, reaching up to 800 g/m³ in regions near the dam (Figs. 4D and E). Z_{eu} spatial distribution showed high depths throughout the reservoir in July 2014, generally above 4 m (Fig. 4F). In 2016, these values decreased significantly; however, it did not go below 1 m (Fig. 4G).

Chl-*a* spatial analysis and trophic state (TS) classification for July 2014, 2016, 2017, and 2019 can be seen in Fig. 5. In general, in 2014, Chl-*a* values were below 5 mg/m^{-3} throughout the area. After-DC, there was an increase of Chl-*a* for all the years analyzed, mainly in 2017, when values above 50 g/m³ were distributed throughout the reservoir, reaching up to 160 mg/m-3 in some sites. Consequently, there was an increase in the degree of eutrophication, going from mesotrophic (before-DC) to eutrophic/hypertrophic (after-DC).

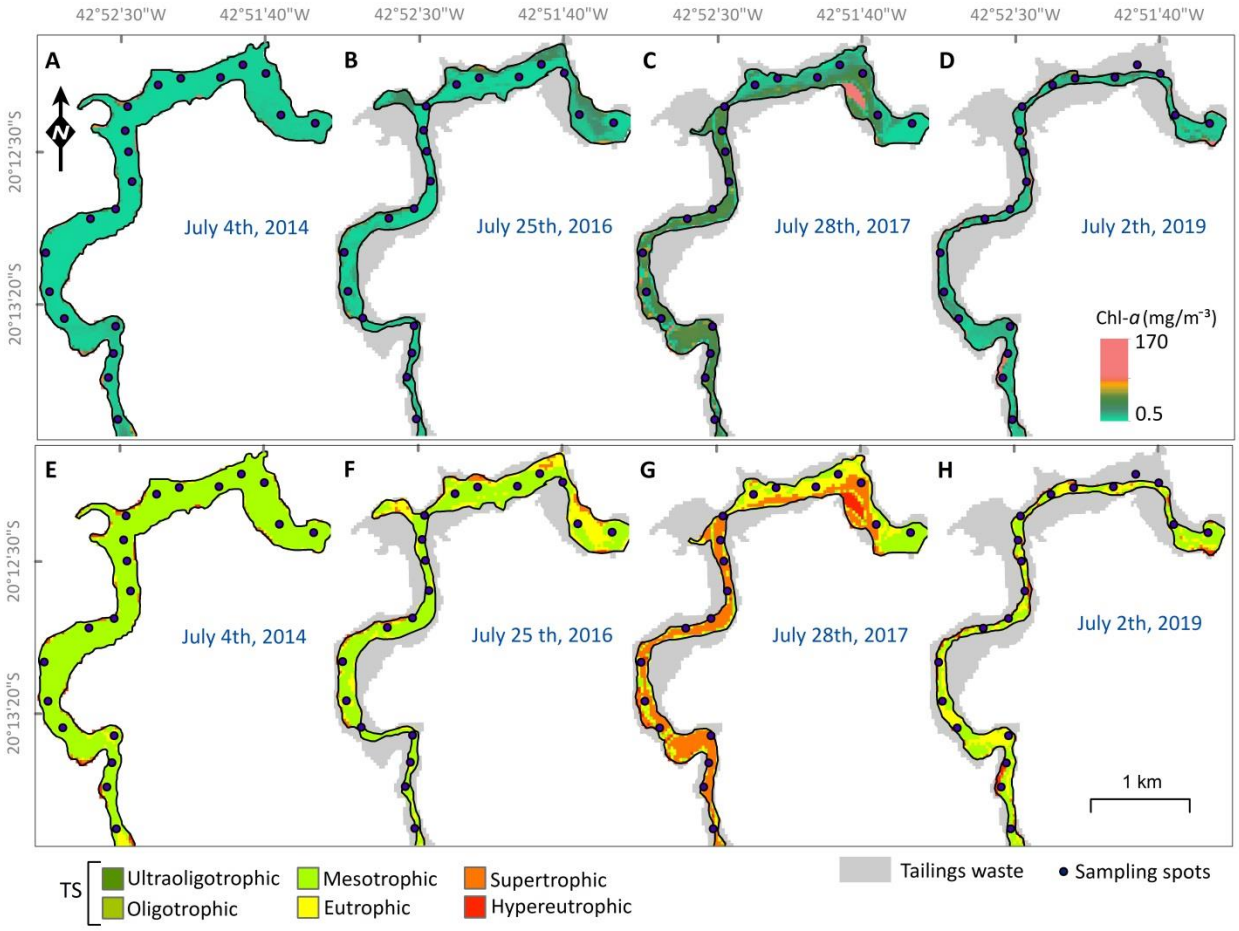

Fig. 5. RNPP reservoir showing Chl-*a* spatial distribution and trophic state (TS) classification before-DC and after-DC. (A and E) Chl-*a* and TS for July 2014. In this year, Chl-*a* values do not exceed 5 g/m³ and the reservoir is classified as mesotrophic. (B, C, D) Chl-*a* for July 2016, 2017, and 2019 and their respective TS classifications (F, G, and H). High values of Chl-*a* are observed after-DC in all reservoirs, with 2017 being the most critical moment, classified as eutrophic to hypereutrophic.

Analysis of the OLI time series of the BPP reservoir showed a significant increase in Chl-*a* after the collapse, which became clear by the spatial distribution maps of Chl-*a* and TS classification (Fig. 6). Generally, near the dam, high chlorophyll values occur every year (Chl-*a* > 180 mg/m^{-3}) and these sites are classified as hypertrophic. In

2015, overall Chl-*a* did not exceed 9 mg/m^{-3} (Fig. 6C). After the collapse, higher concentrations of Chl-*a* that were distributed throughout the area (28 < Chl-*a* < 40) were observed in 2016 and in 2019 (Figs. 6D and E). Therefore, the TS classification changed from mesotrophic (before-DC) to eutrophic/supertrophic (after-DC) (Figs. 6F, G, and H).

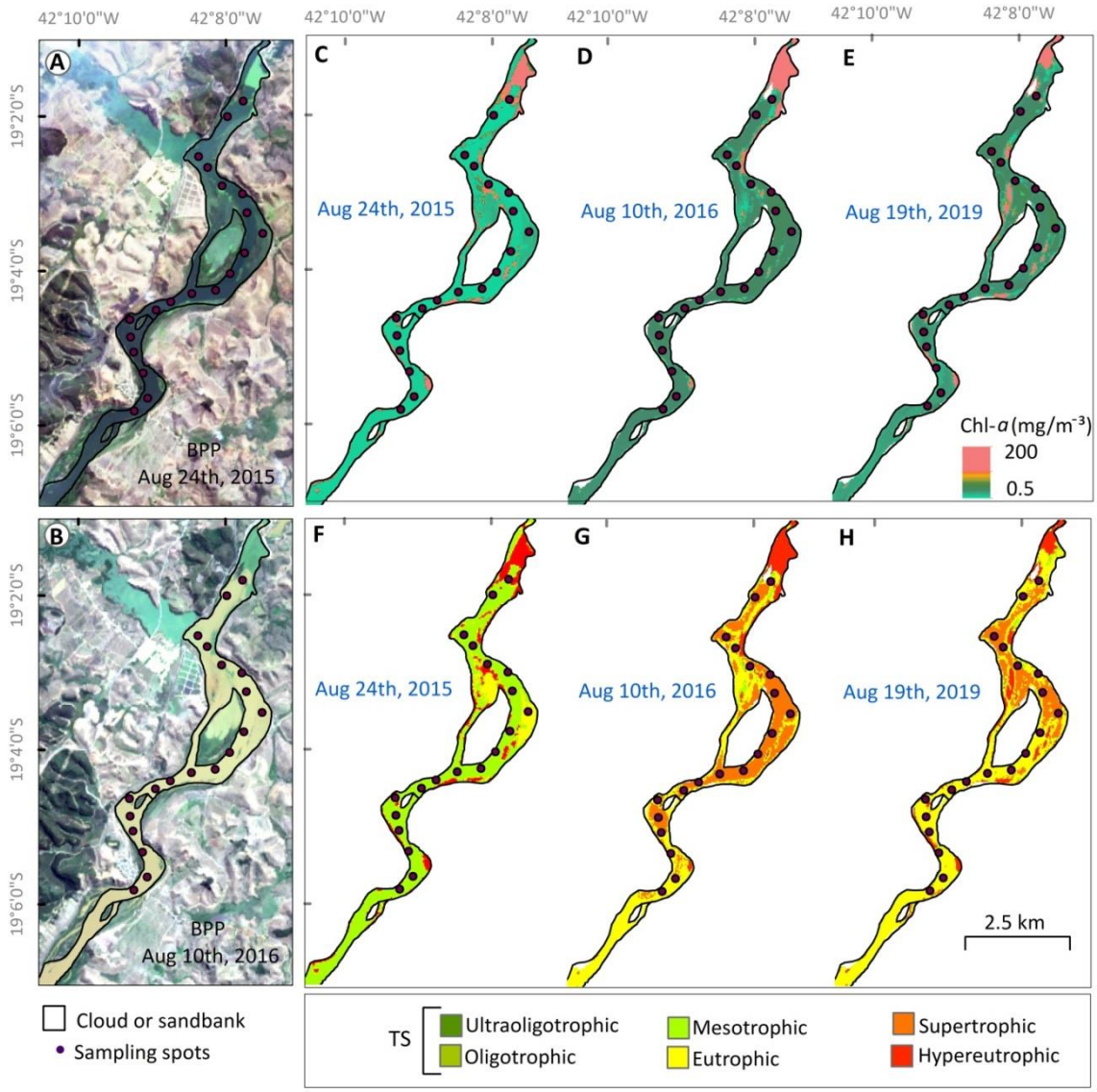

Fig.6. BPP reservoir, before and after collapse. (A and B): OLI true color image for August 2015 and 2016, respectively. The images show the contrast of the color of the water before-DC and after-DC, with emphasis on the region near the dam, with greenish spots in the water observed in both situations. (C, D, E): Chl-*a* in August 2015, 2016 and 2019 and respective classifications of the reservoir TS (F, G, and H). Sites with greenish spots near the dam show high values of Chl-*a* and are classified as hypereutrophic. By August 2015, Chl-*a* concentration is relatively lower throughout the area. Eutrophic to hypertrophic portions are observed in a few sites, with mesotrophic being predominant. Conversely, in August 2016 and 2019, there is a significant increase in Chl-*a* thorough the reservoir, changing it to eutrophic/supertrophic.

The results of the spatial distribution of Chl-*a* and TS are presented in Fig. 7, together with the OLI true-color image of the EBPP area. The products obtained from January 2014 and 2017 were selected because they represented DR-flooding and after-DC, respectively. The SPM and Z_{eu} historical series values showed great similarity with respect to DR-flooding and after-DC, because of the greater number of suspended particles in the water. SPM spatial distribution reveals slightly higher values upstream of the reservoir, mainly in 2014. Still, there is a predominance of SPM pixels above 103 g/m³ in both DR-flooding and after-DC (Figs. 7B and C).

The EBPP historical series showed a marked difference among the respective chlorophyll concentrations, which were much higher after-DC. Chl-*a* spatial distribution in Fig. 7 revealed that by 2014, it was below 23 mg/m^{-3} throughout EBPP (Fig. 7D). In contrast, in 2017, most concentrations above mg/m^{-3} were upstream and downstream of the EBPP dam (Fig. 7E). Thus, the reservoir TS classification (Figs. 7F and G) changed from eutrophic (DRF) to supertrophic (after-DC).

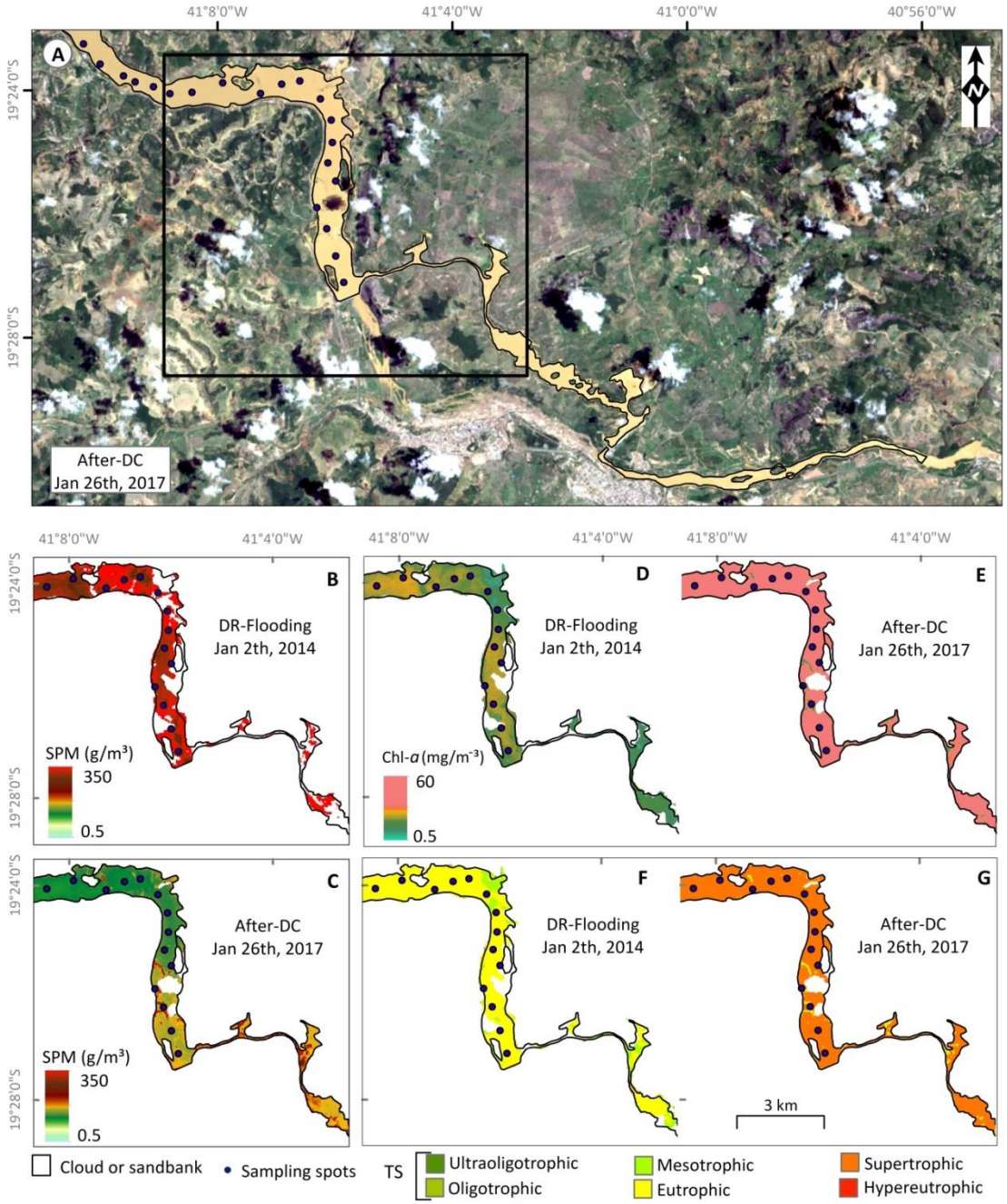

Fig. 7. EBPP reservoir, with emphasis on DR-flooding and after-DC episodes. (A) True color OLI image illustrating the cloudy appearance of the water three years after the collapse. (B and C) comparison of SPM in DR-flooding and after-DC. In both situations, SPM is high throughout the area. (D and F) Chl-*a* for DR-flooding and after-DC and the respective trophic state classifications (F and G).

5.4. Discussion

The results of this study refer to the temporal analysis of products obtained via remote sensing from areas of the Doce River that were affected by the tailings sludge of the Fundao dam. The SPM, Z_{eu}, Chl-*a* concentration and TS classification of the reservoirs of the RNPP, BPP, and EBPP plants were analyzed.

RNPP was the plant most affected by sludge. It has been the scene of numerous environmental problems after the collapse, mainly related to siltation of the drainage and lowering of the water level. Moreover, there were changes in the parameters of water and sediment quality thorough the Doce River and its mouth (Hadtje et al., 2016). Decreasing water levels and increasing water residence time in a reservoir can favor an increase in phytoplankton biomass and, consequently, lead to the advancement of eutrophication (Agostinho et al., 1999).

The results obtained in this study show an increase in Chl-*a* in the RNPP reservoir during July and August, after the collapse, when the trophic state went from mesotrophic (before DC) to supertrophic (after-DC). This increase is also observed in the BPP and EBPP reservoirs. In EBPP, in January, TS changed from eutrophic (before-DC) to supertrophic (after-DC). In BPP, in August, TS also changed from mesotrophic (before DC) to supertrophic (after-DC).

Previous studies conducted with samples of sediments, soils, water, and aquatic species collected in the Doce River, tributaries, and coastal region, clearly showed an increase in the concentration of metals in the ecosystem, after the dam collapse (Segura et al., 2016, Hatje et al., 2017, Gomes et al., 2017, Botino et al., 2017; Queiroz et al., 2018; Weber et al., 2020; Fernandes et al., 2020; Passos et al., 2020)). Therefore, it is suggested that an increase in Chl-*a* in the reservoirs may have been triggered by physico-chemical changes in the water and sediments generated by the tailings sludge.

Statistical analyses also showed significant changes in SPM and Z_{eu} for the pre- and post- collapse averages of the three reservoirs. In the RNPP and BPP areas, these changes occur mainly in 2016, when a high SPM value and Z_{eu} value below the BG are observed. The results showed that, by 2019, the situation had not been resolved in July and August. In EBPP, non-conformity of Z_{eu} and SPM was observed in June and September of 2016 and 2017. In 2018 and 2019, the values were within the BG range. In EBPP, DR-flooding and after-DC were compared and high SPM values and low Z_{eu} values were observed.

Although the color of Doce River's water is normal during some months, changes in SPM are possible. This was observed in the EBPP reservoir, especially

during heavy rainfall, when the tailings deposited on the riverbank were carried to the gutter, favoring resuspension processes (Hatje et al., 2017).

These resuspension processes can be a threat to ecosystem services. Tailings sludge changes the chemical characteristics of the sediments of affected areas from kaolinitic to hematite-rich sediments. Such materials have low adsorption capacity of cationic heavy metals, thus allowing the presence of these elements in the aquatic environment and making it vulnerable to contamination (Segura et al., 2016; Silva et al., 2016; LACTEC, 2018)

Furthermore, hematite can adsorb metals, such as arsenic, which can decrease the availability of this element in water and increase its absorption by species (Quadra et al., 2019). Moreover, contaminated suspended sediments can function as a source of oligoelements, keeping the organisms that inhabit the ecosystem of the Doce River in contact with these pollutants for a long time (Quadra et al., 2019).

Another concern is that these sediments may continue to be loaded and discharged into the mouth of the Doce River for an indefinite period, exposing the organisms to the cytogenotoxic effects of the tailings sludge, as the particles suspended in water may reach important marine areas of environmental preservation (Marta Almeida et al 2016; Valeriano et al., 2019; Francini-Filho et al., 2019; Gomes et al., 2017; Coimbra et al., 2019; Quadra et al., 2019, Coimbra et al., 2020).

Thus, monitoring of water quality of the Doce River and its reservoirs deserves special attention as the results of this study indicate non-conformity of SPM, Z_{eu}, and Chl-*a* after the dam collapse. The trophic state of the reservoirs chosen for this study may be related to the water pollution caused by tailings sludge.

5.5. Conclusions

After the collapse of the Fundao dam, there was a significant increase in Chl-*a* concentration in the three reservoirs selected for this study. The TS of the RNPP and BPP reservoirs changed from mesotrophic (before-DC) to supertrophic (after-DC). The EBPP reservoir changed from eutrophic (before-DC) to supertrophic (after-DC).

The SPM and Z_{eu} parameters were not within the BG range in any of the analyzed reservoirs. In RNN and BPP, these parameters had not returned to their reference values even by 2019.

Two scenarios of EBPP were compared, namely the DR-flooding (January 2013) and after-DC (January 2017). High SPM and low Z_{eu} values were observed in both cases. However, the Chl-*a* concentration in DR-flooding was relatively low compared to after-DC. Furthermore, the TS changed from mesotrophic (DR-flooding) to supertrophic (after-DC). This suggests that the changes in sediments and water composition caused by tailings may have contributed to this increase in Chl-*a* and the increase in the TS of the reservoirs.

Monitoring of water quality of the Doce River and its reservoirs deserves special attention as the results of this study indicate non-conformity of SPM, Z_{eu}, and Chl-*a* after the dam collapse. In situ periodic monitoring of water quality is also important as the presence of clouds tend to limit the use of remote sensing images, and it is not possible to analyze every month of the time series.

5.6. Acknowledgements

K.T.O.C. thanks the Coordination for the Improvement of Higher Education Personnel (CAPES) for the scholarship. C.R.S.F. (88882.329731/2019-01) and E.A. acknowledge the Brazilian National Council for Scientific and Technological Development (CNPq) for research grants 309712/2017-3 and 303169/2018-4, respectively.

5.7. References

Agostinho, A.A., Miranda, L.E. Bini, L.M., Gomes, L.C., Thomaz, S.M., Suzuki, H.I., 1999. Patterns of colonization in Neotropical Reservoirs, and Prognoses on aging. In: Tundisi, J.G., Straskraba, M., 1999. Theoretical Reservoir Ecology. 227-265.

ANA, Agência Nacional das Águas., 2015. Encarte Especial sobre a Bacia do Rio Doce, Rompimento da Barragem em Mariana/MG. Conjuntura dos Recursos Hídricos do Brasil. 50p.

Bottino, F., Milan, J.A.M., Cunha-Santino, M.B., Bianchini-Jr, I., 2017. Influence of the residue from an iron mining dam in the growth of two macrophyte species. Chemosphere 186, 488-494.

Caballero, I., Fernández, R., Escalante, O.M. et al. New capabilities of Sentinel-2A/B satellites combined with in situ data for monitoring small harmful algal blooms in complex coastal waters. Sci Rep 10, 8743 (2020). https://doi.org/10.1038/s41598-020-65600-1

Carmo, F.F., Kamino, L.H.Y., Tobias Júnior, R., Campos, I.C., Carmo, F.F., Silvino, G., Castro, K.J.S.X., Mauro, M.L., Rodrigues, N.U.A., Miranda, Pinto, C.E.F., 2017. Fundao tailings dam failures: the environment tragedy of the largest technological disaster of Brazilian mining in global context. Perspectives in Ecology and Conservation 15, 145–151

CETESB - Companhia Ambiental do Estado de São Paulo, 2017. Qualidade das águas interiores no estado de São Paulo - 2016. https://cetesb.sp.gov.br/aguas-interiores/publicacoes-e-relatorios/ (accessed: june 11th, 2020).

Coimbra, K.T.O., Alcântara, E.H., Souza Filho, C.R., 2019. An assessment of natural and manmade 1 hazard effects on the underwater 2 light field of the Doce river continental shelf. Science of the Total Environment. 685, 1087–1096.

Coimbra, K.T.O., Alcântara, E.H., Souza Filho, C.R., 2020. Possible contamination of the Abrolhos reefs by Fundao dam tailings, Brazil – New constraints based on satellite data. Science of the Total Environment. 733, 138101.

Curtarelli, M., Rennó, C.D., Alcântara, E., 2014. Evaluation of the Tropical Rainfall Measuring Mission 3B43 product over an inland area in Brazil and the effects of satellite boost on rainfall estimates. Journal Applied to Remote. Sensing. 8, 83589–83589–14.

Fernandes, G.W., Goulart, F.F., Ranierid, B.D., Coelho, M.S., Dalesf, K., Boescheg, N., Bustamanteh, M., Carvalho, F.A., Carvalho, D.C., Dirzob, R., Fernandes, S., Galetti Jr., P.M., Millang, V.E.G., Mielkeg, C., Ramirezk, J.L., Nevesa, A., Rogassg, C., Ribeirol, S.P.,Sariotm, A., Filho, B.S., 2016. Deep into the mud: ecological and socioeconomicimpacts of the dam breach in Mariana, Brazil. Natureza & Conservação.

Fernandes, L.F.L., Paiva, T.R., Longhini, C. M., Pereira, J. B., Ghisolfi, R.D., Lázaro, G.C.S., Demoner, L.E., Laino, P.S., Conceição, L.R., Sá, F., Neto, R.R., Dias-Jr, C., Lemos, K.N., Quaresma, V.S., Oliveira, K.S., Grilo, C.F., Rocha, G.M., 2020. Marine zooplankton dynamics after a major mining dam rupture in the Doce River, southeastern Brazil: Rapid response to a changing environment. Science of the Total Environment. 736, 139621.

Francini-Filho, R.B., Cordeiro, M.C., Omachi, C.Y., Rocha, A.M., Bahiense, L., Garcia, G.D., Tschoeke, D., Almeida, M.G., Rangel, T.P., Oliveira, B.C.V., Almeida, D.Q.R., Menezes, R., Mazzei, E.F., Joyeux, J.C., Rezende, C.E., Thompson, C.C., Thompson, F.L., 2019. Remote sensing, isotopic composition and metagenomics analyses revealed Doce River ore plume reached the southern Abrolhos Bank Reefs. Science of the Total Environment. 697, 134038.

Fielding, J., Croudace, I.W., Alan E.S. Kemp, A.E.S., Pearce, R.B., Cotterill, C.J., Langdon, P.,Avery, R., 2020. Tracing lake pollution, eutrophication and partial recovery from the sediments of Windermere, UK, using geochemistry and sediment microfabrics. Science of the Total Environment. 722, 137745.

Gangloffa, A., Verneya, R., Doxaran, D., Ody, A., Estournel, C., 2017. Investigating Rhône River plume (Gulf of Lions, France) dynamics using metrics analysis from the MERIS 300m Ocean Color archive (2002–2012). Continental Shelf Research. 144, 98–111.

Gomes, L.E.O., Correa, L.B., Sá, F., Neto, R.R., Bernadinho, A.F., 2017. The impacts of the Samarco mine tailing spill on the Rio Doce estuary, Eastern Brazil. Marine Pollution Bulletin. 120, 28–36.

Gomes, A.C., Alcântara, E., Rodrigues, T., Bernado, N., 2020. Satellite estimates of euphotic zone and Secchi disk depths in a colored dissolved organic matter-dominated inland water. Ecological Indicators. 110, 105848.

Gomes, P., Valente, T., Geraldo, T., Ribeiro, C., 2020. Photosynthetic pigments in acid mine drainage: Seasonal patterns and associations with stressful abiotic characteristics. Chemosphere. 239, 124774.

Hatje, V., Pedreira, R.M.A., Rezende, C.E., Schettini, C.A.F.S., Souza, G.C., Marin, D.C., Hackspacher, P.C., 2017. The environmental impacts of one of the largest tailing dam failures worldwide. Scientific Reports. 7, 10706.

IBAMA, Instituto Brasileiro do Meio Ambiente e dos Recursos Naturais Renováveis., 2015. Impactos ambientais decorrentes do desastre envolvendo o rompimento da barragem de Fundao, em Mariana, Minas Gerais. Laudo Técnico Preliminar. 74p.

Kirk, J.T.O., 1994. Light & Photosynthesis in Aquatic Ecosystems, second ed. Cambridge University Press, Melbourne.

LACTEC., 2018. Diagnóstico socioambiental dos danos decorrentes do rompimento da barragem de Fundao na bacia do rio Doce. Relatório Pós-Desastre 2: Meios Físico e Biótico. http://www.mpf.mp.br/grandes-casos/caso-samarco/documentos/relatorios-lactec/lactec_relatorio-pos-desastre-grupo-02 (acessed: june 11th, 2020)

Marta-Almeida, M.M., Mendes, R., Amorim, F.N., Cirano, M., Dias, J.M., 2016. Fundao Dam collapse: oceanic dispersion of River Doce after the greatest Brazilian environmental accident. Marine Pollution Bulletin. 112, 359–364.

Mishra, S., Mishra, D.R., 2012. Normalized difference chlorophyll index: a novel model for remote estimation of chlorophyll-a concentration in turbid productive waters. Remote Sens. Environ. 117, 394–406.

Nechad, B., Ruddick, K.G., Park, Y., 2010. Calibration and validation of a generic multisensor algorithm for mapping of total suspended matter in turbid waters. Remote Sensing of Environment. 114, 854–866

Nwankwegu, A.S., Li, Y., Huang, Y., Wei, J., Norgbey, E., Lai, Q., Sarpong, L., Wang, K., Ji, D., Yang, Z., Paerl, H.W., 2020. Nutrient addition bioassay and phytoplankton community structure monitored during autumn in Xiangxi Bay of Three Gorges Reservoir, China. Chemosphere. 247, 125960.

Omachi, C.Y., Siani, S.M.O., Chagas, F.M., Mascagni, M.L., Cordeiro, M., Garcia, G.D., Thompson, C.C., Siegle, E., Thompson, F.L., 2018. Atlantic Forest loss caused by the world's largest tailing dam colapse (Fundao Dam, Mariana, Brazil). Remote Sensing Applications: Society and Environment 12, 30–134.

Pahlevana, N., Smitha, B., Schalles, J., Binding, C., Cao, Z., Ma, R., Alikas, K., Kangro, K., Gurlin, D., Hà, N., Matsushita, B., Moses, W., Greb, S., Lehmann, M.K., Ondrusek, M., Oppelt, N., Stumpf, R., 2020. Seamless retrievals of chlorophyll-a from Sentinel-2 (MSI) and Sentinel-3 (OLCI) in inland and coastal waters: A machine-learning approach. Remote Sensing of Environment. 240, 111604.

Passos, L.S., Gnocchi, K.G., Pereira, T.M., Coppo, G.C., Cabral, D.S., Gomes, L.C., 2020. Is the Doce River elutriate or its water toxic to Astyanax lacustris (Teleostei: Characidae) three years after the Samarco mining dam collapse?. Science of the Total Environment. 736, 139644.

Quadra, G.R., Roland, F., Barros, N., Malm, O., Lino, A.S., Azevedo, G.M., Thomaz, J.R., Vieira, L.F.A., Fontes, M.M.P., Almeida, R.M., Mendonça, R.F., Cardoso, S.J., Guida, Y.S., Campos, J.M.S., 2019. Far-reaching cytogenotoxic effects of mine waste from the Fundao dam disaster in Brazil. Chemosphere. 215, 753-757.

Queiroz, H.M., Nóbrega, G.N., Ferreira, T.O., Almeida, L.S., Romero, T.B., Santaella, S.T., Bernadinho, A.F., Otero, X.L., 2018. The Samarco mine tailing disaster: a possible time-bomb for heavy metals contamination? Science of the Total Environment. 637–638, 498–506.

Samarco, 2016. Balanço de ações: um ano do rompimento de Fundao, Available in: http://www.samarco.com/wp-content/uploads/2016/11/Dossiee um-ano03-11 v4.pdf.

Sánchez, L.E., Alger, K., Alonso, L., Barbosa, F.A.R., Brito, M.C.W., Laureano, F.V., May, P., Roeser, H., Kakabadse, Y., 2018. Os impactos do rompimento da Barragem de Fundao. O caminho para uma mitigação sustentável e resiliente. Relatório Temático no 1 do Painel do Rio Doce. Gland, Suíça: UICN.

Segura, F.R., Nunes, E.A., Paniz, F.P., Paulelli, A.C.C., Rodrigues, G.B., Braga, G.U.L., Pedreira Filho,W.R., Barbosa Jr., F., Cerchiaro, G., Silva, F.F., Batista, B.L., 2016. Potential risks of the residue fromSamarco'smine damburst (Bento Rodrigues, Brazil). Environmental Pollution. 218, 813–825.

Silva, A.C., Cavalcante, C.D., Fabris, J.D., Franco Junior, R., Barral, U.M., Farnezi, M.M.M., Viana, A.J.S., Ardisson, J.D., Outon, L.E.F., Lara, L.R.S., Stumpf, H.O., Barbosa, J.B.S., Silva, L.C., 2016. Chemical, mineralogical and physical characteristics of a material accumulated on the river margin from mud flowing from the collapse of the iron ore tailings damin Bento Rodrigues, Minas Gerais, Brazil. Revista Espinhaço. 5 (2), 44–53.

Valeriano, C.M., Neumann, R., Alkimim, A.R., Evangelista, H., Heilbron, M., Neto, C.C.A., Souza, G.P., 2019. Sm–Nd and Sr isotope fingerprinting of iron mining tailing deposits spilled from the failed SAMARCO Fundao dam 2015 accident at Mariana, SE-Brazil. Applied Geochemistry. 106, 34–44.

Watanabe, F., Alcântara, E., Bernardo, N., Andrade, C., Gomes, A.C., Carmo, A., Rodrigues, T., Rotta, L., 2019. Mapping the chlorophyll-a horizontal gradiente in a cascading reservoirs system using MSI Sentinel-2A images. Advances in Space Research. 64, 581-590.

Weber, A, A., Sales, C.F., Faria, F.S., Melo, R.M.C., Bazzoli, N., Rizzo, E., 2020. Effects of metal contamination on liver in two fish species from a highly impacted neotropical river: A case study of the Fundao dam, Brazil. Ecotoxicology and Environmental Safety. 190,110165.

Wetzel. R.G., 2001. Limnology: lake and river ecosystems. San Diego, Academic Press.

Zhao, J., Barnes, B., Melo, N., English, D., Lapointe, B., Karger, F.M., Schaeffer, B., Hu, C., 2013. Assessment of satellite-derived diffuse attenuation coefficients and euphotic depths in south Florida coastal waters. Remote Sensing Environment. 131, 38–50.

CONCLUSÕES

O colapso da barragem de Fundão marcou a história do Brasil e do mundo, trazendo consequências imensuráveis à sociedade e ao meio ambiente, muitas das quais são irreparáveis, como a morte de pessoas e de animais.

Os resultados dos indicadores de qualidade da água obtidos via sensoriamento remoto foi uma das contribuições dessa tese de doutorado e podem auxiliar no entendimento dos efeitos da contaminação do ecossistema aquático do rio Doce após o colapso, em diferentes escalas.

Na Bacia do rio Doce, na escala microrregional, foi revelado o avanço da eutrofização no reservatório da Usina Hidrelétrica Risoleta Neves, em que o estado trófico passou de mesotrófico (antes do colapso) para supertrófico (após o colapso). Analisando o histórico de acontecimentos pós-colapso, pode-se afirmar que, além da presença de contaminantes no ecossistema trazidos pela lama, houve o aumento do tempo de residência da água no reservatório da usina, em momentos que as comportas foram mantidas fechadas para dragagem do rejeito. Tais motivos somados contribuíram para uma maior disseminação de fitoplâncton na água.

Na escala macrorregional, foi também verificado um aumento do estado trófico da água de reservatórios. A análise multitemporal da região da Usina Hidrelétrica Eliezer Batista contemplou o período de inundação da bacia do rio Doce (dezembro de 2013 e janeiro de 2014) e anos posteriores ao colapso. Nos dois casos, foram constatados altos valores de SPM e baixos de Z_{eu}. Porém, na inundação de 2013, a concentração de Chl-*a* estava abaixo das médias observadas, diferente dos anos pós-colapso, em que os valores de Chl-*a* extrapolaram os limites da série histórica. Esses resultados suportam a hipótese de que o avanço da eutrofização dos reservatórios foi influenciado pelo aumento de poluentes trazidos pela lama.

As consequências do colapso da barragem de Fundão sobre os ecossistemas aquáticos se estenderam além da região *onshore* da Bacia do rio Doce, alcançando a região costeira adjacente, que engloba toda costa do Espírito Santo até o Sul da Bahia. Na região *offshore,* as principais conclusões da pesquisa são as seguintes:

- O Evento de inundação de dezembro de 2013 causou alterações nos parâmentos bio-ópticos da água assim como a chegada da lama na foz do rio Doce, após o colapso. Nos dois casos, houve grande aporte de sedimentos na pluma do rio Doce, onde a profundidade da Z_{eu} ficou limitada. Paralelamente, altas concentrações de SPM foram observadas. No entanto, na inundação a situação se normalizou dentro de poucos meses, ao contrário do caso do colapso, em que os efeitos foram mais persistentes no meio. Dentro do prazo de oito meses da chegada da lama na foz do rio Doce, processos de ressuspensão de sedimentos de fundo provocaram novamente as alterações dos parâmetros investigados.
- A pluma de sedimentos do rio Doce mostrou concordância com os vetores de direção do vento, onde em janeiro de 2016 (verão) teve direção preferencial para o sul, e em julho de 2016 (inverno) para o norte.
- O aumento de SPM foi observado em toda região costeira estudada após o colapso, incluindo a foz dos principais rios, desde o rio Doce (ES) até a Barra de Caravelas (BA). Em relação ao verão, esse aumento foi associado à elevada precipitação da chuva nas bacias. No inverno, como é uma época de estiagem, foi relacionado com processo de ressuspensão dos sedimentos de Fundo.
- No Arquipélago dos Abrolhos e entorno, essas altas concentrações de SPM também foram observadas após o colapso. No momento em que a pluma de sedimentos do rio Doce estava direcionada para o norte, as partículas mais finas suspensas na água foram carregadas por longas distâncias, até o sul da Bahia. Nesse episódio, é possível que o material da barragem tenha alcançado o Arquipélago dos Abrolhos.

SUGESTÕES PARA FUTURAS PESQUISAS

Apesar de o rio Doce ser considerado um dos rios mais monitorados do Brasil, as consequências do colapso da barragem na vida das pessoas, biodiversidade e ecossistema, tendem a persistir ainda por muitos anos. Há muitas lacunas no conhecimento, principalmente no que se refere às questões ambientais, considerando a dimensão da área atingida pela lama, tanto na parte *offshore* quanto *onshore,* e a complexidade da dinâmica fluvial e marinha. Diante das principais conclusões da tese de doutorado, seguem algumas sugestões para futuros trabalhos com abordagens de sensoriamento remoto:

- Para os reservatórios estudados sugere-se que o monitoramento dos parâmetros bio-ópticos e dos indicadores de qualidade da água continue sendo realizado mensalmente e em longo prazo.
- A validação dos modelos usados tanto pra região *offshore* quanto *onshore* pode ser feita, considerando-se dados coletados em campo;
- Pesquisas limnológicas podem ser realizadas em escala micro e macrorregional para esclarecer a relação do rejeito e dos contaminantes trazidos pela lama com o aumento de clorofila dos reservatórios após o colapso;
- Os estudos dos indicadores de qualidade da água podem ser expandidos para os afluentes do rio Doce, os rios Gualaxo do norte e do Carmo, que foram intensamente impactados. Nesses locais, imagens de alta resolução espacial podem trazer bons resultados, considerando que são rios menores.
- O monitoramento dos parâmetros bio-ópticos da água da foz do rio Doce também deve se estender ao longo de anos, podendo incluir também análise de clorofila e temperatura de superfície do mar.
- Estudos adicionais podem ser feitos para verificar o quanto períodos chuvosos podem impactar a qualidade da água do rio e da foz após o colapso. Nessa perspectiva sugere-se comparar o evento de inundação (2013), o colapso da barragem (2015) e uma inundação recente que aconteceu no rio Doce, em janeiro de 2020.

REFERÊNCIAS BIBLIOGRÁFICAS

Agostinho, A.A., Miranda, L.E. Bini, L.M., Gomes, L.C., Thomaz, S.M., Suzuki, H.I., 1999. Patterns of colonization in Neotropical Reservoirs, and Prognoses on aging. In: Tundisi, J.G., Straskraba, M., 1999. Theoretical Reservoir Ecology. 227-265.

Agurto-Detzel, H., Bianchi, M., Assumpção, M., Schimmel, M., Collaço, B., Ciardelli, C., Barbosa, J.R., Calhau, J., 2016. The tailings dam failure of 5 November 2015 in SE Brazil and its preceding seismic sequence, Geophysical Research Letter. 43, 4929-4936.

Alcântara, E., Novo, E., Stech, J., Lorenzzetti, J., Barbosa, C., Assireu, A., Souza, A., 2010. A contribution to understanding the turbidity behaviour in an Amazon floodplain. Hydrology and Earth System Sciences. Sci. 14, 351–364.

Alcântara, E., Nascimento, R., Kampel, M., Stech, J.L., 2013. Uso de propriedades ópticas aparentes e inerentes para a classificação da massa d'água do reservatório hidrelétrico de Itumbiara (GO). Anais XVI Simpósio Brasileiro de sensoriamento remoto – SBSR.

ANA – Agência Nacional de Águas., 2016. Encarte Especial sobre a Bacia do Rio Doce, Rompimento da Barragem em Mariana/MG. https://www.ana.gov.br/noticias-antigas/encarte-da-ana-reaone-informaassaues-sobre-rio.2019-03-15.9924387769. Acessado em 16 de agosto de 2020.

Augusto-Silva, P.B., Ogashawara, I., Barbosa, C.C.F., Carvalho, LA.S., Jorge, .S.F., Fornari, C.I., Stech, J.L., 2016. Analysis of MERIS Reflectance Algorithms for Estimating Chlorophyll-*a* Concentration in a Brazilian Reservoir. Remote Sensing. *6*, 11689-11707.

Babin,M., Stramski, M., Ferrari, G.M., Claustre, H., Bricaud, A., Obolensky, G., Hoepffner, N., 2003. Variations in the light absorption coefficients of phytoplankton, nonalgal particles, and dissolved organic matter in coastal waters around Europe. ournal of Geophysical Research. 108, 3211.

Baum, A., Fleming, R., Davidson, A. M. 1983. Natural disaster and technological catastrophe. Environment and behavior. 333-354.

Bernardino, A.F., Netto, S.A., Pagliosa, P.R., Barros, F., Christofoletti, R.A, Rosa Filho, J.S., Colling, A., Lana, P.C., 2015. Predicting ecological changes on benthic estuarine assemblages through decadal climate trends along Brazilian Marine Ecoregions. Estuarine, Coastal and Shelf Science. 166, 74-82.

Bernardo, N., Watanabe, F., Rodrigues, T., Alcântara, E., 2017. Atmospheric correction issues for retrieving total suspended matter concentrations in inland waters using OLI/Landsat-8 image. Advances in Space Research. 59, 2335–2348

Bonecker, A.C.T., Castro, M.S., Costa, P.G., Bianchini, A., Bonecker, S.L.C., 2017. Larval fish assemblages of the coastal area affected by the tailings of the collapsed dam in southeast Brazil. Regional Studies in Marine Science. 32, 100848.

Booth, J.G., Miller, R.L., McKee, B.A., Leathers, R.A., 2000. Wind-induced bottom sediment resuspension in a microtidal coastal environment. Continental Shelf Research - Journal. 20, 785–806.

.

Bottino, F., Milan, J.A.M., Cunha-Santino, M.B., Bianchini-Jr, I., 2017. Influence of the residue from an iron mining dam in the growth of two macrophyte species. Chemosphere. 186, 488-494.

Caballero, I., Fernández, R., Escalante, O.M. et al. 2020. New capabilities of Sentinel-2A/B satellites combined with in situ data for monitoring small harmful algal blooms in complex coastal waters. Scientific Reports. 10, 8743.

Cao, Z., Dua, H., Feng, L., Ma, R., Xue, K., 2017. Climate and human induced changes in suspended particulate matter over Lake Hongze on short and long timescales. Remote Sensing of Environment. 192, 98–113.

Carmo, F.F., Kamino, L.H.Y., Tobias Júnior, R., Campos, I.C., Carmo, F.F., Silvino, G., Castro, K.J.S.X., Mauro, M.L., Rodrigues, N.U.A., Miranda, Pinto, C.E.F., 2017. Fundão tailings dam failures: the environment tragedy of the largest technological disaster of Brazilian mining in global context. Perspectives in Ecology and Conservation. 15, 145–151.

Carswell, T., Costa, M., Young, E., Komick, N., Gower, J., Sweeting, R., 2017. Evaluation of MODIS-Aqua Atmospheric Correction and Chlorophyll Products of Western North American Coastal Waters Based on 13 Years of Data. Remote Sensing of Environment. 9, 1063.

CETESB - Companhia Ambiental do Estado de São Paulo, 2017. Qualidade das águas interiores no estado de São Paulo - 2016. https://cetesb.sp.gov.br/aguas-interiores/publicacoes-e-relatorios/ (accessed: june 11th, 2020).

Chang, G., Whitmire, A.L., 2009. Effects of bulk particle characteristics on backscattering and optical closure. Optics Express. 17, 2131–2142.

Chen, S.L., Zhang, G.A., Yang, S.L., Shi, J.Z., 2006. Temporal variations of fine suspended sediment concentration in the Changjiang River Estuary and adjacent coastal waters. China Journal Hydrogeologic. 331 (1-2): 137-145.

Clark, R.N., Swayze, G.A., Gallagher, A., 1993. Mapping Minerals with Imaging Spectroscopy, U.S. Geological Survey, Office of Mineral Resources Bulletin. 2039, 141–150.

Cloern, J.E., Foster, S.Q., Kleckner, A.E., 2014. Phytoplankton primary production in the world's estuarine-coastal ecosystems. Biogeosciences. 11, 2477–2501.

Coimbra, K.T.O., Alcântara, E.H., Souza Filho, C.R., 2019. An assessment of natural and manmade 1 hazard effects on the underwater 2 light field of the Doce river continental shelf. Science of the Total Environment. 685, 1087–1096.

Coimbra, K.T.O., Alcântara, E.H., Souza Filho, C.R., 2020. Possible contamination of the Abrolhos reefs by Fundao dam tailings, Brazil – New constraints based on satellite data. Science of the Total Environment. 733, 138101.

CPRM – Serviço Geológico do Brasil. Monitoramento especial da bacia do rio Doce: Acompanhamento da onda de cheia. Relatório 1, 2015a.

CPRM – Serviço Geológico do Brasil, 2014. Sistema de alerta de enchentes da bacia do rio Doce. Relatório Técnico do Período Crítico de Dezembro de 2013.

CRH-ANA - Conjuntura dos recursos hídricos no Brasil, Agência Nacional das Águas. Encarte Especial sobre a Bacia do Rio Doce: Rompimento da Barragem em Mariana/MG. Relatório final, 2015.

Curtarelli, M., Rennó, C.D., Alcântara, E., 2014. Evaluation of the Tropical Rainfall Measuring Mission 3B43 product over an inland area in Brazil and the effects of satellite boost on rainfall estimates. Journal of Applied Remote Sensing. 8 (083589-083589-14).

Dagg,M., Benner, R., Lohrenz, S., Lawrence, D., 2004. Transformation of dissolved and particulate materials on continental shelves influenced by large rivers: plume processes. Continental Shelf Research. (ISSN: 0278-4343) 24 (7–8), 833–858.

Dikou, A., vanWoesik, R., 2006. Survival under chronic stress from sediment load: spatial patterns of hard coral communities in the southern islands of Singapore. Marine Pollution Bulletin. 52, 7–21.

Dominguez J.M.L. 2004. The coastal zone of Brazil: an overview. Journal of Coastal Research. SI39:16-20.

Dominguez J.M.L. & Wanless H.R. 1991. Facies architecture of a falling sealevel, Doce river coast, Brazil. International Association of Sedimentologists Special Publication. 14:259-281.

Dominguez J.M.L., Bittencourt A.C.S.P., Martin L. 1983. O papel da deriva litorânea de sedimentos arenosos na construção das planícies costeiras associadas a desembocaduras dos rios São Francisco (SE/AL0), Jequitinhonha (BA), Doce (ES) e Paraíba do Sul (RJ). Revista Brasileira de Geociências, 13(4):93-105.

Dorji, P., Fearns, P., 2017. Impact of the spatial resolution of satellite remote sensing sensors in the quantification of total suspended sediment concentration: a case study in turbid waters of Northern Western Australia. PLOS ONE. 12, e0175042.

Duarte, E.B., Neves, M.A., Oliveira, F.B., Martins, M.E., Oliveira, C.H.R., Burak, D.L., Orlando, M.T.D.A., Rangel, C.V.G.T., 2020. Trace metals in Rio Doce sediments before and after the collapse of the Fundão iron ore tailing dam, Southeastern Brazil. Chemosphere. 262, 127879.

EMBRAPA - Empresa Brasileira de Pesquisa Agropecuária, Ministério da Agricultura, Pecuária e Abastecimento., 2015. Tragédia em Mariana: produção agropecuária em áreas atingidas está comprometida. https://www.embrapa.br/busca-de-noticias/-/noticia/8410974/tragedia-em-mariana-producao-agropecuaria-em-areas-atingidas-esta-comprometida (Acessado em 17 de agosto de 2020).

Erftemeijer, P.L.A., Riegl, B., Hoeksema, B.W., Todd, P.A., 2012. Environmental impacts of dredging and other sediment disturbances on corals: a review. Marine Pollution Bulletin. 64, 1737–1765.

Evangelista, H., Valeriano, C.M., Santos, E.A., Vaz, G., Neto, Carla., Nogueira, J.S., Licinio, M.V., Ribeiro, J.N., Pereira, M.G., Ribeiro, A.V.F.N., Caldero, E.N., Castro, C.B., Guebert, F., Jerozolimski, R., Cruz, E., Cajueiro, L.M., Rodrigues, A., 2016. Estudo preliminar sobre a detecção da pluma de sedimentos do Rio Doce sobre o Parque Nacional dos Abrolhos-BA, para o evento de 5-6 de Janeiro 2016.

Evangelista, H., Valeriano, C., 2017. Sumário das análises de isótopos radiogênicos de Sr e Nd em sedimentos da foz do rio Doce-ES e do Parque Nacional dos Abrolhos-BA (Antes e depois do rompimento da barragem de rejeitos da Samarco em Mariana-

MG. Relatório. Laboratório de radioecologia e Mudanças Globais. Disponível em: http://www.consultaesic.cgu.gov.br/busca/dados/Lists/Pedido/Attachments/612349/RESPOSTA_PEDIDO_02680002082201705%20-%20sumario_de_analises_UERJ_21Set2017.pdf (Acessado em julho de 2020).

Fernandes, G.W., Goulart, F.F., Ranierid, B.D., Coelho, M.S., Dalesf, K., Boescheg, N., Bustamanteh, M., Carvalho, F.A., Carvalho, D.C., Dirzob, R., Fernandes, S., Galetti Jr., P.M., Millang, V.E.G., Mielkeg, C., Ramirezk, J.L., Nevesa, A., Rogassg, C., Ribeirol, S.P., Sariotm, A., Filho, B.S., 2016. Deep into the mud: ecological and socioeconomicimpacts of the dam breach in Mariana, Brazil. Natureza & Conservação.

Fernandes, L.F.L., Paiva, T.R., Longhini, C. M., Pereira, J. B., Ghisolfi, R.D., Lázaro, G.C.S., Demoner, L.E., Laino, P.S., Conceição, L.R., Sá, F., Neto, R.R., Dias-Jr, C., Lemos, K.N., Quaresma, V.S., Oliveira, K.S., Grilo, C.F., Rocha, G.M., 2020. Marine zooplankton dynamics after a major mining dam rupture in the Doce River, southeastern Brazil: Rapid response to a changing environment. Science of the Total Environment. 736, 139621.

Fielding, J., Croudace, I.W., Alan E.S. Kemp, A.E.S., Pearce, R.B., Cotterill, C.J., Langdon, P.,Avery, R., 2020. Tracing lake pollution, eutrophication and partial recovery from the sediments of Windermere, UK, using geochemistry and sediment microfabrics. Science of the Total Environment. 722, 137745.

Franchito, S.H., Rao, V.B., Vasques, A.C., Santo, C.M.E., Conforte, J.C., 2009. Validation of TRMM precipitation radar monthly rainfall estimates over Brazil. Journal of Geophysical Research. 114, D02105.

Francini-Filho, R.B., Cordeiro, M.C., Omachi, C.Y., Rocha, A.M., Bahiense, L., Garcia, G.D., Tschoeke, D., Almeida, M.G., Rangel, T.P., Oliveira, B.C.V., Almeida, D.Q.R., Menezes, R., Mazzei, E.F., Joyeux, J.C., Rezende, C.E., Thompson, C.C., Thompson, F.L., 2019. Remote sensing, isotopic composition and metagenomics analyses revealed Doce River ore plume reached the southern Abrolhos Bank Reefs. Science of the Total Environment. 697, 134038.

Gangloffa, A., Verneya, R., Doxaran, D., Ody, A., Estournel, C., 2017. Investigating Rhône River plume (Gulf of Lions, France) dynamics using metrics analysis from the MERIS 300m Ocean Color archive (2002–2012). Continental Shelf Research. 144, 98–111.

Garcia, L.C.; Ribeiro, D.B.; Roque, F.O.; Ochoa-Quintero, J.M.; Laurance, W.F. Brazil's worst mining disaster: corporations must be compelled to pay actual environmental costs. Ecological Applications. 27:5-9. 2017.

Gelaro, et al., 2017. The modern-era retrospective analysis for research and applications, version 2 (MERRA-2). J. Clim. 30, 5419–5454. Gomes, L.E.O., Correa, L.B., Sá, F., Neto, R.R., Bernadinho, A.F., 2017. The impacts of the Samarco mine tailing spill on the Rio Doce estuary, Eastern Brazil. Marine Pollution Bulletin. 120, 28–36.

Gomes, L.E.O., Correa, L.B., Sá, F., Neto, R.R., Bernadinho, A.F., 2017. The impacts of the Samarco mine tailing spill on the Rio Doce estuary, Eastern Brazil. Marine Pollution Bulletin. 120, 28–36.

Gomes, A.C., Alcântara, E., Rodrigues, T., Bernado, N., 2020. Satellite estimates of euphotic zone and Secchi disk depths in a colored dissolved organic matter-dominated inland water. Ecological Indicators. 110, 105848.

Gomes, P., Valente, T., Geraldo, T., Ribeiro, C., 2020. Photosynthetic pigments in acid mine drainage: Seasonal patterns and associations with stressful abiotic characteristics. Chemosphere. 239, 124774.

Gordon, H.R., Wang,W., 1994. Influence of oceanic whitecaps on atmospheric correction of SeaWiFS. Applied Optics. 33, 7754–7763.

Goyens, C., Jamet, C., Ruddick, K.G., 2013. Spectral relationships for atmospheric correction. II. ImprovingNASA's standard and MUMM near infra-red modeling schemes. Optics Express. 21 (18), 21176–21187.

Guerra, M.B.B., Teaney, B.T., Mount, B.J., Asunskis, D.J., Jordan, B.T., Barker, R.J., Santos, E.E., Schaefer, C.E.G.R., 2017. Post-catastrophe analysis of the Fundão tailings dam failure in the Doce river system, Southeast Brazil: potentially toxic elements in affected soils. Water, Air, & Soil Pollution. 228–252.

Hatje, V., Pedreira, R.M.A., Rezende, C.E., Schettini, C.A.F.S., Souza, G.C., Marin, D.C., Hackspacher, P.C., 2017. The environmental impacts of one of the largest tailing dam failures worldwide. Scientific Reports. 7, 10706.

IBAMA, Instituto Brasileiro do Meio Ambiente e dos Recursos Naturais Renováveis., 1991. Plano de Manejo do Parque Nacional Marinho dos Abrolhos. https://www1.icmbio.gov.br/parnaabrolhos/ (Acessado em julho de 2020).

IBAMA - Instituto Brasileiro do Meio Ambiente e dos Recursos Naturais Renováveis., 2015. Laudo Técnico Preliminar dos Impactos ambientais decorrentes do desastre envolvendo o rompimento da barragem de Fundão, em Mariana, Minas Gerais. 38 p.

ICMBio – Instituto Chico Mendes de Conservação da Biodiversidade., 2017. Monitoramento da Pluma de Sedimentos Proveniente da Barragem de Fundão. Nota Técnica nº 23/2017/TAMAR. 44p.

ICOLD, International Commission on Large Dams. 2001. Tailings dams: risk of dangerous occurrences, lessons learnt from practical experiences. Paris: ICOLD, 144 p. 2001. (Bulletin, 121).

IGAM - Instituto Mineiro de Gestão das Águas Gerência de Monitoramento de Qualidade das Águas., 2018. Acompanhamento da Qualidade das Águas do Rio Doce Após o Rompimento da Barragem da Samarco no distrito de Bento Rodrigues – Mariana/MG. Relatório técnico. 27 p.

Joyce, K.E., Belliss, S.E., Samsonov, S.V., McNeill, S.J., Glassey, P.J., 2009. A reviewof the status of satellite remote sensing and image processing techniques for mapping natural hazards and disasters. Progress in Physical Geography. 33, 183–207.

Karki, S., French, K., McCarthy, V., Hanafin, J., Jennings, E., Delaney, C., Veerkamp, V., Golden, A., McKinstry, A., Ahmed, M., 2020. In-Situ Validation of Water Quality Algorithms and Monitoring of Irish Lakes using Sentinel 2 Imagery. Presentation at European Geophysical Meeting – EGU. 2020-2223.

Kirk, J.T.O., 1994. Light and Photosynthesis in Aquatic Ecosystems. Cambridge University Press, New York.

Kruse, F.A., Lefkoff, A.B., Boardman, J.B., Heidebrecht, K.B., Shapiro, A.T., Barloon, P.J., Goetz, A.F.H., 1993. The spectral image processing system (SIPS) - interactive visualization and analysis of imaging spectrometer data. Remote Sensing of Environment. 44, 145–163.

LACTEC., 2018. Diagnóstico socioambiental dos danos decorrentes do rompimento da barragem de Fundão na bacia do rio Doce. Relatório Pós-Desastre 2: Meios Físico e Biótico. http://www.mpf.mp.br/grandes-casos/caso-samarco/documentos/relatorios-lactec/lactec_relatorio-pos-desastre-grupo-02 (acessado em julho de 2020).

LACTEC., 2019. Diagnóstico socioambiental dos danos decorrentes do rompimento da barragem de Fundão na bacia do rio Doce: Atualização Linha-Base Ambientes Costeiros. http://www.mpf.mp.br/grandes-casos/caso-samarco/documentos/relatorios-lactec/ (Acessado em julho de 2020).

Lahet, F., Stramski, D. 2010. MODIS imagery of turbid plumes in San Diego coastal waters during rainstorm events. Remote Sensing of Environment. 114 (2010), 332–344.

Lari, S., Frattini, P., Crosta, G.B. 2009. Integration of natural and technological risks in Lombardy, Italy. Natural Hazards and Earth System Sciences. 9:2085-2106.

Le, C., Lehrter, J.C., Schaeffer, B.A., Hu, C., Murrell, M.C., Hagy, J.D., Greene, R.M., Beck, M., 2016. Bio-optical water quality dynamics observed from MERIS in Pensacola Bay, Florida. Estuarine, Coastal and Shelf Science. 173, 26–38.

Lee, Z., Weidemann, A., Kindle, J., Arnone, R., Carder, K.L., Davis, C., 2007. Euphotic zone depth: its derivation and implication to ocean-color remote sensing. Journal of Geophysical Research. 112, C03009.

Lee, Z.P, Hu, C., Shang, S., Du, K., Lewis,M., Arnone, R., Brewin, R., 2013. Penetration of UV visible solar radiation in the global oceans: insights from ocean color remote sensing. Journal of Geophysical Research. 118 (9), 4241–4255.

Leipe, T., Knoppers, B., Marone, E., et al., 1999. Geo-Marine. Letters. 19, 186.

Magris, R.A., Marta-Almeida, M.,Monteiro, J.A.F., Ban, N.C., 2019. A modelling approach to assess the impact of landmining onmarine biodiversity: assessment in coastal catchments experiencing catastrophic events (SWBrazil). Science of the Total Environment. 659, 828–840.

Marta-Almeida, M.M., Mendes, R., Amorim, F.N., Cirano, M., Dias, J.M., 2016. Fundao Dam collapse: oceanic dispersion of River Doce after the greatest Brazilian environmental accident. Marine Pollution Bulletin. 112, 359–364.

Mazzei, E.F., Bertoncini, A.A., Pinheiro, H.T., Machado, L.F., Vilar, C.C., Guabiroba, H.C., Costa, T.J.F., Bueno, L.S., Santos, L.N., Francini-Filho, R.B., Hostim-Silva, M., 2017. Newly discovered reefs in the southern Abrolhos Bank, Brazil: anthropogenic impacts and urgent conservation needs. Joyeux Marine Pollution Bulletin 114. 123–133.

Miller, R. L., Mckee, A. B. 2004. Using MODIS Terra 250 m imagery to map concentrations of total suspended matter in coastal waters. Remote Sensing of Environment. 93: 259-266.

Miranda, L.S.,Marques, A.C., 2016. Hidden impacts of the Samarcomining waste dam collapse to Brazilian marine fauna – an example from the staurozoans (Cnidaria). Biota Neotropica. 16 (2), e20160169.

Mishra, S., Mishra, D.R., 2012. Normalized difference chlorophyll index: a novel model for remote estimation of chlorophyll-a concentration in turbid productive waters. Remote Sensing of Environment. 117, 394–406.

Morgenstern, N.R., Vick, S.G., Viotti, C.B., Watts, B.D., 2016. Comitê de Especialistas para Análise da Ruptura da Barragem de Rejeitos de Fundão. Relatório sobre as Causas Imediatas da Ruptura da Barragem de Fundão. 83p.

Moses,W.J., Gitelson, A.A., Perk, R.L., Gurlin, D., Rundquist, D.C., Leavitt, B.C., Barrow, T.M., Brakhage, P., 2012. Estimation of chlorophyll-a in turbid productive waters using airborne hyperspectral data. Water Research. 46, 993–1004.

Nechad, B., Ruddick, K.G., Park, Y., 2010. Calibration and validation of a generic multisensor algorithm for mapping of total suspended matter in turbid waters. Remote Sensing of Environment. 114, 854–866.

Nobre, D.M., Alarconc, D.T., Cintid, A., Schiavettie, A., 2017. Governance of the Cassurubá Extractive Reserve, Bahia State, Brazil: an analysis of strengths and weaknesses to inform policy. 77, 44–45.

Nwankwegu, A.S., Li, Y., Huang, Y., Wei, J., Norgbey, E., Lai, Q., Sarpong, L., Wang, K., Ji, D., Yang, Z., Paerl, H.W., 2020. Nutrient addition bioassay and phytoplankton community structure monitored during autumn in Xiangxi Bay of Three Gorges Reservoir, China. Chemosphere. 247, 125960.

Oliveira, K.S.S., Quaresma, V.S., 2017. Temporal variability in the suspended sediment load and streamflow of the Doce river. Journal of South American Earth Sciences. 78, 101–115.

Omachi, C.Y., Siani, S.M.O., Chagas, F.M., Mascagni, M.L., Cordeiro, M., Garcia, G.D., Thompson, C.C., Siegle, E., Thompson, F.L., 2018. Atlantic Forest loss caused by the world's largest tailing dam colapse (Fundão Dam, Mariana, Brazil). Remote Sensing Applications: Society and Environment 12, 30–134.

Orlando, M.T.A., Galvão, E.S., Cavichini, A.S.A., Rangel, C.V.G.T., Orlando, C.G.P., Grilo, C.F., Soares, J., Oliveira, K.S.S.O., Sá, F., Junior, A.S., Bastos, AC., Quaresma, V.S., 2020. Tracing iron ore tailings in the marine environment: An investigation of the Fundão dam failure. Chemosphere. 257, 127184.

PCGRSS – Programa de caracterização Geoquímica dos Rejeitos, Solos e Sedimentos, rompimento da barragem de Fundão. 2016. Rel. de monitoramento ambiental, Golder Associates.

Pahlevan, N., et al., 2017. Landsat 8 remote sensing reflectance (Rrs) products: evaluations, intercomparisons, and enhancements. Remote Sensing of Environment. 190, 289–301.

Pahlevana, N., Smitha, B., Schalles, J., Binding, C., Cao, Z., Ma, R., Alikas, K., Kangro, K., Gurlin, D., Hà, N., Matsushita, B., Moses, W., Greb, S., Lehmann, M.K., Ondrusek, M., Oppelt, N., Stumpf, R., 2020. Seamless retrievals of chlorophyll-a from Sentinel-2 (MSI) and Sentinel-3 (OLCI) in inland and coastal waters: A machine-learning approach. Remote Sensing of Environment. 240, 111604.

Passos, L.S., Gnocchi, K.G., Pereira, T.M., Coppo, G.C., Cabral, D.S., Gomes, L.C., 2020. Is the Doce River elutriate or its water toxic to Astyanax lacustris (Teleostei: Characidae) three years after the Samarco mining dam collapse?. Science of the Total Environment. 736, 139644.

Quadra, G.R., Roland, F., Barros, N., Malm, O., Lino, A.S., Azevedo, G.M., Thomaz, J.R., Vieira, L.F.A., Fontes, M.M.P., Almeida, R.M., Mendonça, R.F., Cardoso, S.J., Guida, Y.S., Campos, J.M.S., 2019. Far-reaching cytogenotoxic effects of mine waste from the Fundão dam disaster in Brazil. Chemosphere. 215, 753-757.

Quaresma, V.S., Catabriga, G., Bourguignon, S.N.,Godinho, E., Bastos, A.C., 2015. Modern sedimentary processes along the Doce river adjacent continental shelf. Brazilian Journal of Geology. 45(4), 635-644.

Queiroz, H.M., Nóbrega, G.N., Ferreira, T.O., Almeida, L.S., Romero, T.B., Santaella, S.T., Bernadinho, A.F., Otero, X.L., 2018. The Samarco mine tailing disaster: a possible time-bomb for heavy metals contamination? Science of the Total Environment. 637–638, 498–506.

RAMBOL., 2017. Avaliação do programa de reparação integral da bacia do rio Doce. http://www.mpf.mp.br/grandes-casos/caso-samarco/atuacao-do-mpf/pareceres-e-relatorios. Acessado em 16 de agosto de 2020.

RAMBOL., 2019. Relatório de monitoramento consolidado dos programas socioeconômicos e socioambientais para a restauração da bacia do rio Doce. http://www.mpf.mp.br/grandes-casos/caso-samarco/atuacao-do-mpf/pareceres-e-relatorios. Acessado em 16 de agosto de 2020.

RAMBOL, 2020a. Relatório de Monitoramento Mensal – Mês 039 – Março/2020. http://www.mpf.mp.br/grandes-casos/caso-samarco/atuacao-do-mpf/pareceres-e-relatorios (Acessado em 16 de agosto de 2020).

RAMBOL, 2020b. Parecer técnico - eixo prioritário n° 3: Sistema de abastecimento de água de gesteira (Barra Longa). http://www.mpf.mp.br/grandes-casos/caso-samarco/atuacao-do-mpf/pareceres-e-relatorios (Acessado em 16 de agosto de 2020).

Rienecker, M.M., et al., 2011. MERRA - NASA's modern-era retrospective analysis for research and applications. Journal of Climate. 24, 3624–3648.

Rudorff, N., Rudorff, C.M., Kampel, M., Ortiz, G., 2018. Remote sensing monitoring of the impact of a major mining wastewater disaster on the turbidity of the Doce river plume off the eastern Brazilian coast. ISPRS Journal of Photogrammetry and Remote Sensing.

Samarco, 2016. Balanço de ações: um ano do rompimento de Fundao, Available in: http://www.samarco.com/wp-content/uploads/2016/11/Dossiee um-ano03-11 v4.pdf.

Sánchez, L.E., Alger, K., Alonso, L., Barbosa, F.A.R., Brito, M.C.W., Laureano, F.V., May, P., Roeser, H., Kakabadse, Y., 2018. Os impactos do rompimento da Barragem de Fundao. O caminho para uma mitigação sustentável e resiliente. Relatório Temático no 1 do Painel do Rio Doce. Gland, Suíça: UICN.

SEDRU – Secretaria de Estado de desenvolvimento regional, política e urbana e gestão metropolitana., 2016. Avaliação dos efeitos e desdobramentos do rompimento da Barragem de Fundão em Mariana-MG. Relatório do Grupo da Força-Tarefa, Belo Horizonte..http://www.agenciaminas.mg.gov.br/ckeditor_assets/attachments/770/relatorio_final_ft_03_02_2016_15h5min.pdf. Acessado em 16 de agosto de 2020.

Schaefer, C.E.G.R., Santos, E.E., Fernandes-Filho, E.I., Assis, I.R., 2016. Paisagens de Lama: Os Tecnossolos para recuperação ambiental de áreas afetadas pelo desastre da barragem do Fundão, em Mariana. Boletim Informativo - SBSC. 18-23.

Segura, F.R., Nunes, E.A., Paniz, F.P., Paulelli, A.C.C., Rodrigues, G.B., Braga, G.U.L., Pedreira Filho,W.R., Barbosa Jr., F., Cerchiaro, G., Silva, F.F., Batista, B.L., 2016. Potential risks of the residue fromSamarco'smine damburst (Bento Rodrigues, Brazil). Environmental Pollution. 218, 813–825.

Shang, S., Lee, Z., Wei, G., 2011. Characterization of MODIS-derived euphotic zone depth: results for the China Sea. Remote Sensing of Environment. 115, 180–186.

Silva, A.C., Cavalcante, L.C.D., Fabris, J.D., Júnior, R.F., Barral, U.M., Farnezi, M.M.M., Viana, A.J., Ardisson, J.D., Outon, L.E.F., Lara, L.R.S., Sumpf, H.O., Barbosa, J.B.S., Silva, L.C., 2016. Chemical, mineralogical and physical characteristics of a material accumulated on the river margin from mud flowing from the collapse of the iron ore tailings dam in Bento Rodrigues, Minas Gerais, Brazil. Rev. Espinhaço 5, 44–53.

Thuillier, G., Hersé, M., Labs, D., Foujols, T., Peetermans, W., Gillotay, D., Simon, P.C., Mandel, H., 2003. The solar spectral irradiance from 200 to 2400 nm as measured by the SOLSPEC spectrometer from the ATLAS and EURECA missions. Solar Physics. 214, 1–22.

Tomasella, J., Vieira, R. M. S. P., Barbolsa, A. A., Rodriguez, D. A., Santana, M. O., Sestini, S. M. F. 2018. Desertification trends in the Northeast of Brazil over the period 2000–2016. International Journal of Applied Earth Observation and Geoinformation. (73): 197-206.

Valeriano, C.M., Neumann, R., Alkimim, A.R., Evangelista, H., Heilbron, M., Neto, C.C.A., Souza, G.P., 2019. Sm–Nd and Sr isotope fingerprinting of iron mining tailing deposits spilled from the failed SAMARCO Fundão dam 2015 accident at Mariana, SE-Brazil. Applied Geochemistry. 106, 34–44.

Vanhellemont, Q., Ruddick, K., 2014. Turbidwakes associated with offshorewind turbines observed with Landsat 8. Remote Sensing of Environment. 145, 105–115.

Vanhellemont, Q., Ruddick, K., 2015. Advantages of high quality SWIR bands for ocean colour processing: examples from Landsat-8. Remote Sens. Environ. 161, 89–106. Werner, T.B., Pinto, L.P., Dutra, G.F., Pereira, P.G.P., 2000. Abrolhos 2000: conserving the southern Atlantic's richest coastal biodiversity into the next century.

Viana, J.H.M., Costa, A.M., A Ciência do Solo como instrumento para a recuperação das áreas afetadas pelo desastre de Mariana e dos solos na Bacia do Rio Doce. Boletim Informativo - SBSC. 24-27.

Watanabe, F., Alcântara, E., Bernardo, N., Andrade, C., Gomes, A.C., Carmo, A., Rodrigues, T., Rotta, L., 2019. Mapping the chlorophyll-a horizontal gradiente in a cascading reservoirs system using MSI Sentinel-2A images. Advances in Space Research. 64, 581-590.

Weber, A, A., Sales, C.F., Faria, F.S., Melo, R.M.C., Bazzoli, N., Rizzo, E., 2020. Effects of metal contamination on liver in two fish species from a highly impacted neotropical river: A case study of the Fundão dam, Brazil. Ecotoxicology and Environmental Safety. 190,110165.

Weber, A, A., Sales, C.F., Faria, F.S., Melo, R.M.C., Bazzoli, N., Rizzo, E., 2020. Effects of metal contamination on liver in two fish species from a highly impacted neotropical river: A case study of the Fundão dam, Brazil. Ecotoxicology and Environmental Safety. 190,110165.

Werdell, P.J., 2005. Ocean Color K490 algorithm evaluation. Available at. http://oceancolor.gsfc.nasa.gov/REPROCESSING/SeaWiFS/R5.1/k490_update.html, Accessed date: 2 May 2017.

Wetzel. R.G., 2001. Limnology: lake and river ecosystems. San Diego, Academic Press.

Zhao, J., Barnes, B., Melo, N., English, D., Lapointe, B., Karger, F.M., Schaeffer, B., Hu, C., 2013. Assessment of satellite-derived diffuse attenuation coefficients and euphotic depths in south Florida coastal waters. Remote Sensing Environment. 131, 38–50.

ANEXO 1

Imagens de satélite de alta resolução espacial, mostrando a comparação pré e pós-colapso.

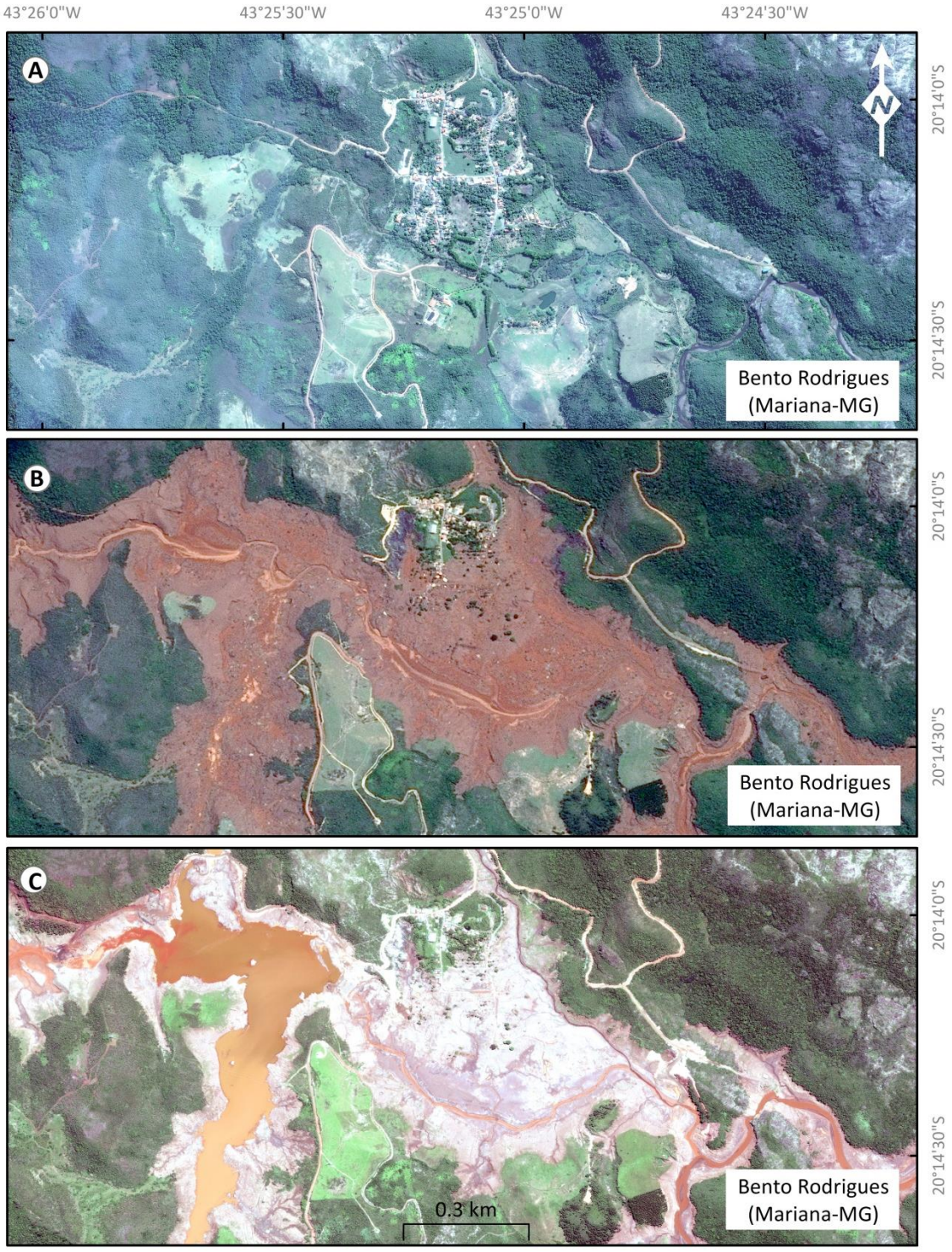

Fig. 1. Imagem do sensor WorldView-2 (composição colorida cor real (RGB-123) do distrito de Bento Rodrigues. (A) Imagem do dia 21 de julho de 2015. (B) Imagem do dia 16 de novembro de 2015. (C) Imagem do dia 20 de fevereiro de 2016.

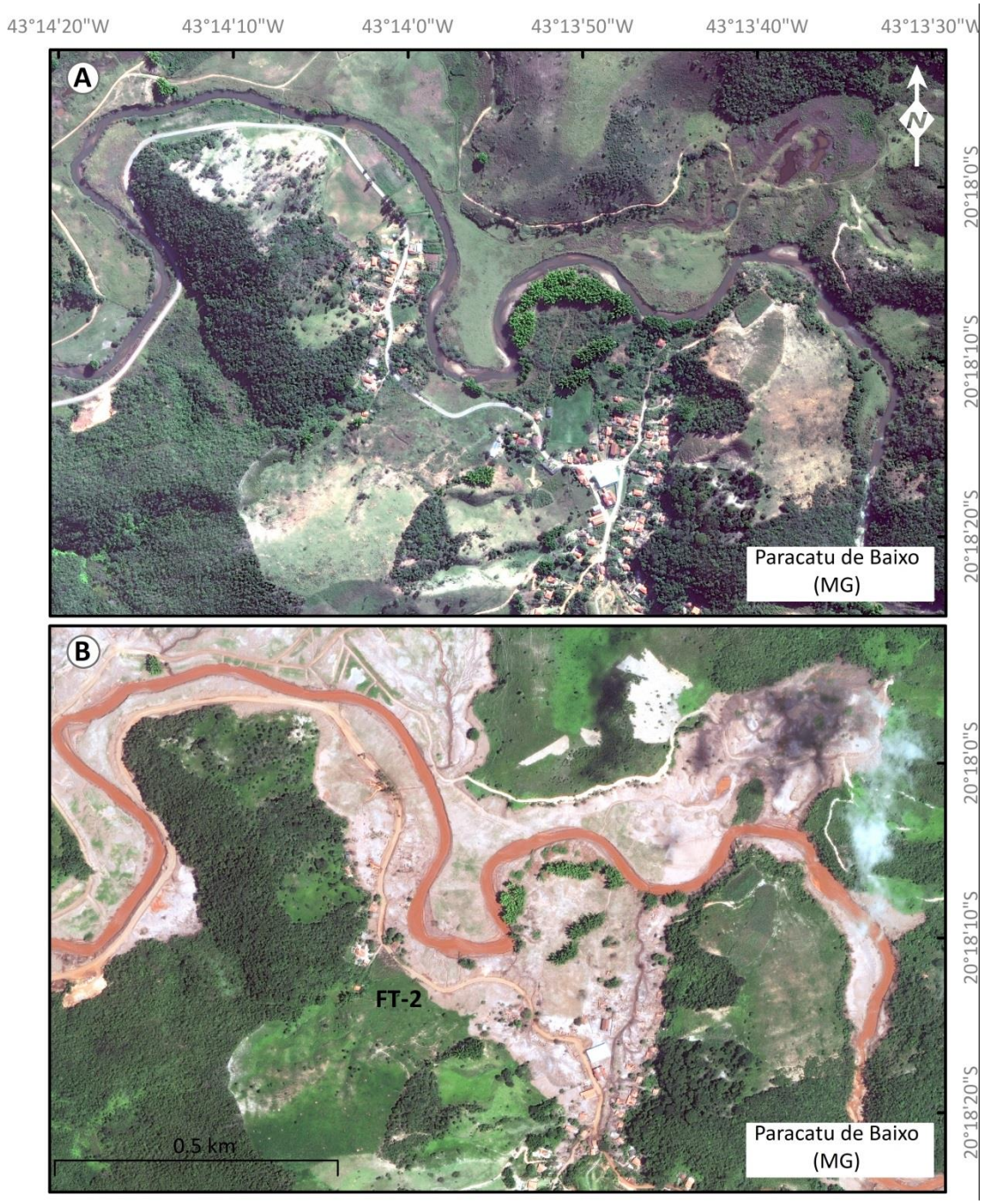

Fig. 2. Imagem do sensor World View-2 (composição colorida cor real (RGB-123)) da área urbana de Paracatu de Baixo. (A) Imagem do dia 28 de junho de 2015. (B) Imagem do dia 17 de fevereiro de 2016. Após o colapso, toda região urbana foi invadida pela lama, destruindo residências, comércios, estradas e vegetação.

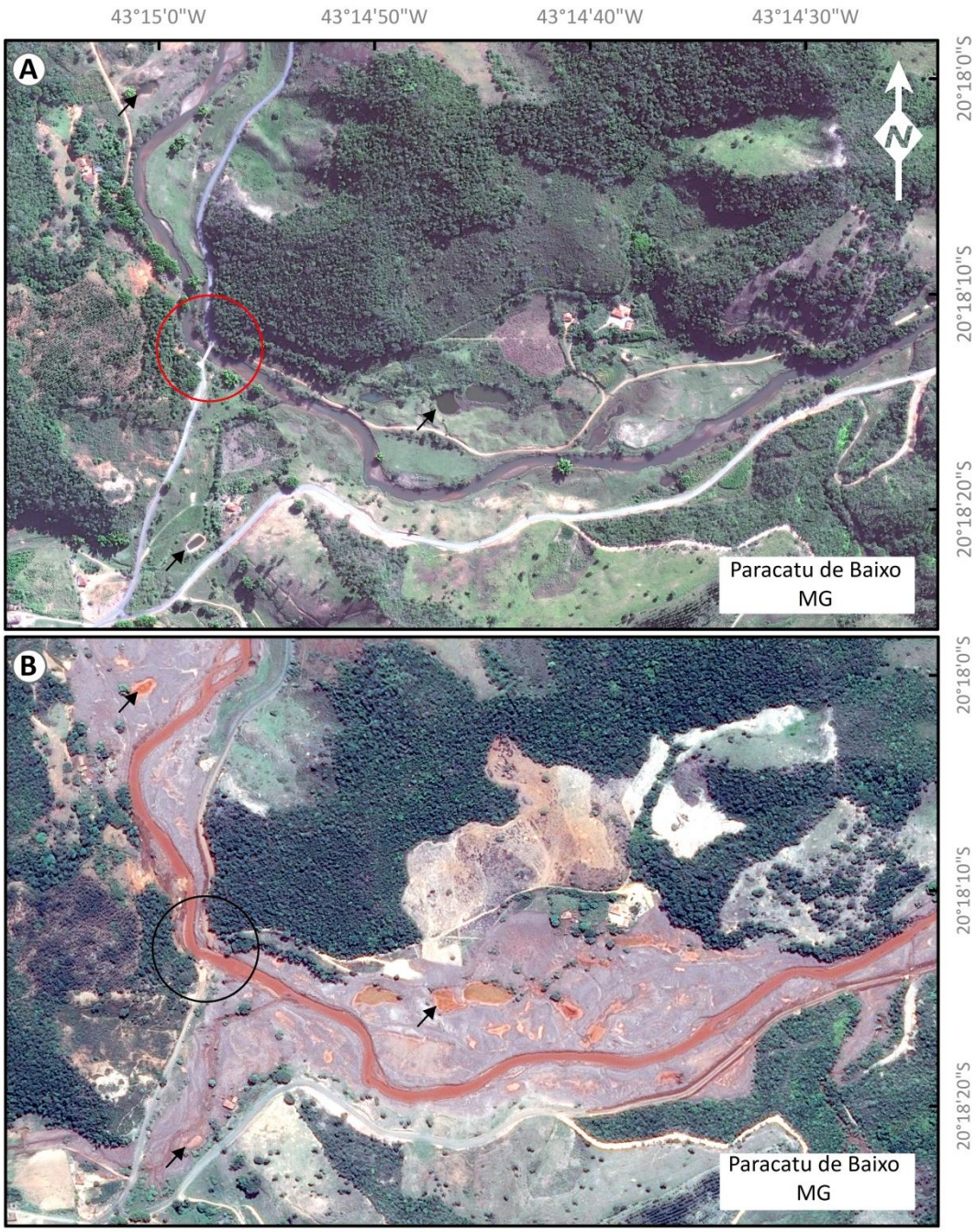

Fig. 3. Imagem do sensor World View-2 (composição colorida cor real (RGB-123)) da área rural de Paracatu de Baixo. (A) Imagem do dia 28 de junho de 2015. (B) Imagem do dia 12 de novembro de 2015. A imagem pós-colapso mostra a devastação nessa região. O círculo indica o local da ponte sobre o rio Gualaxo do Norte, que foi levada pela avalanche. As setas pretas mostram algumas lagoas que foram totalmente assoreadas. Percebe-se ainda a destruição das residências, pastagem, vegetação e solos.

ANEXO 2

Fotos obtidas nas visitas de campo, mostrando regiões atingidas pela lama, na escala microrregional: **Região de Bento Rodrigues.**

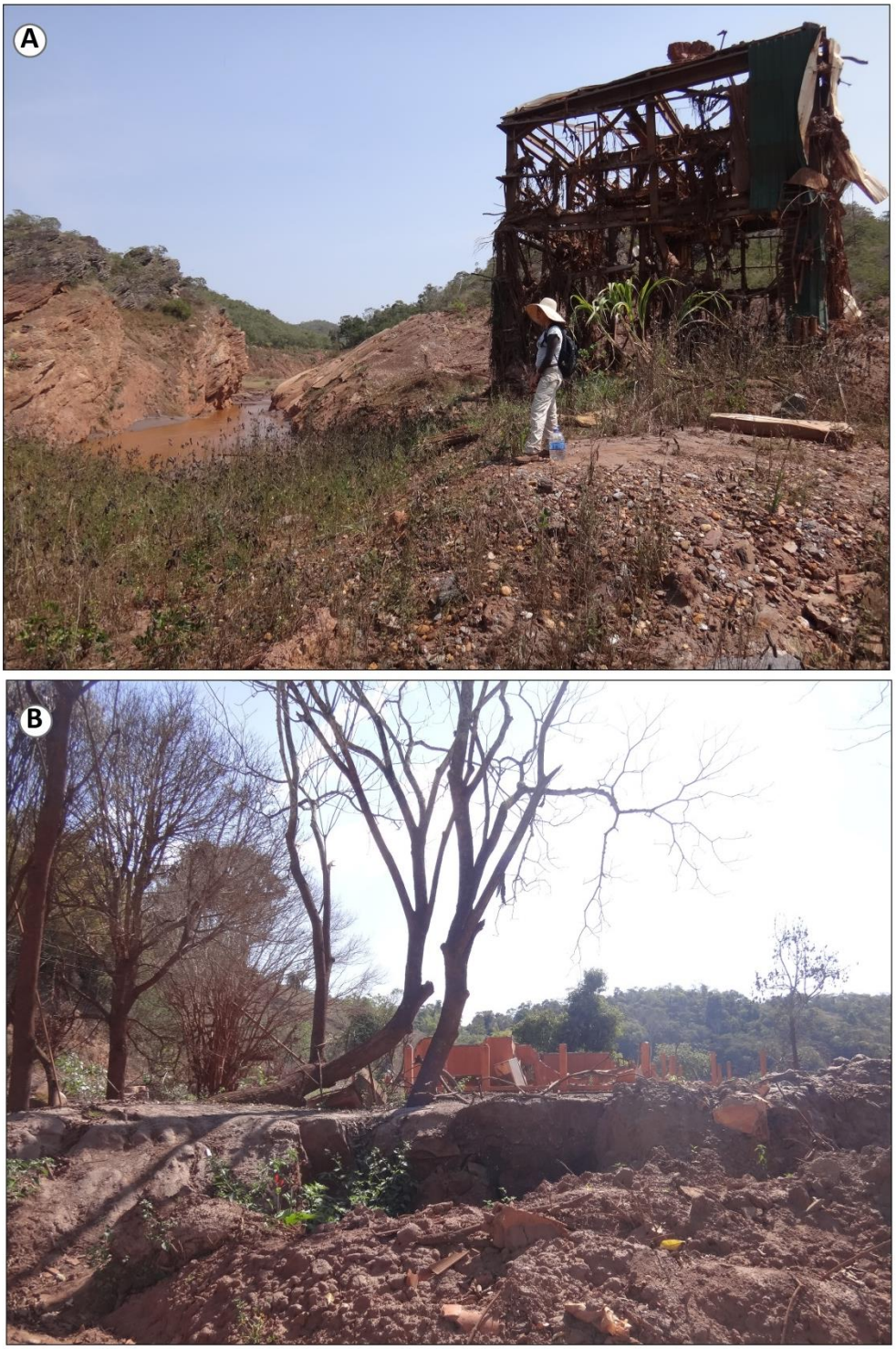

.

Fig.4. (A) Foto obtida em 14 de setembro de 2016. Galpão as margens do rio Gualaxo do Norte, que foi totalmente destruído pela avalanche. (B) Foto obtida em 13 de setembro de 2016. Vegetação de grande porte com elevado nível de stress, ao lado de residência totalmente destruída. Fonte: Acervo Pessoal.

Fig. 5. Foto obtida em 19 de setembro de 2016. Solo encoberto pelo rejeito, bastante compactado e exibindo processos erosivos iniciais. Fonte: Acervo pessoal.

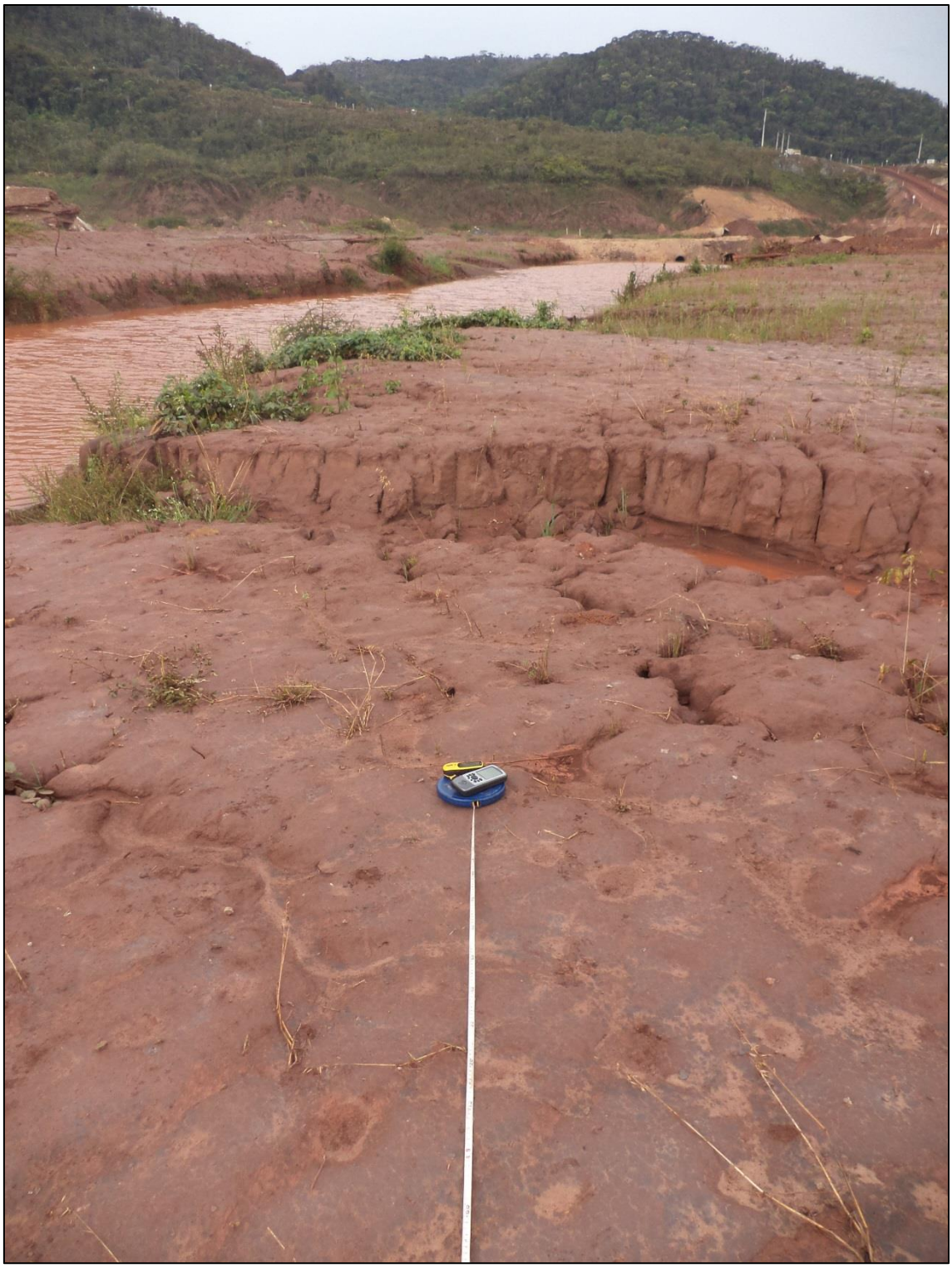

Fig. 6. Foto obtida em 19 de setembro de 2016. Planície de inundação do rio Gualaxo do Norte encoberta pelo rejeito, totalmente sem vegetação. Destaca-se na foto a elevada turbidez da água. Fonte: Acervo pessoal.

ANEXO 3

Fotos obtidas nas visitas de campo, mostrando regiões atingidas pela lama, na escala microrregional: **Região de Paracatu de Baixo**

Fig. 6. Foto obtida em 16 de setembro de 2016. Planície de inundação do rio Gualaxo do Norte. Nesse local foi plantado uma mistura de leguminosas as margens do rio para a reparação do solo, destacado com a linha tracejada. Fonte: Acervo pessoal.

ANEXO 4

Fotos obtidas nas visitas de campo, mostrando regiões atingidas pela lama, na escala microrregional: **Região da Usina Hidrelétrica Risoleta Neves (UHRN)**

Fig. 7. Foto obtida em 18 de setembro de 2016. Planície de inundação do rio Doce, a montante da UHRN. Solo totalmente compactado e sem matéria orgânica e vegetação. Fonte: Acervo pessoal.

Fig. 8. Foto obtida em 18 de setembro de 2016. Planície de inundação do rio Doce, a montante da UHRN. (A) Solo totalmente compactado e com rachaduras. (B) Trecho do rio Doce, com baixo nível d'água e o intenso assoreamento pelo rejeito depositado as margens do rio. Fonte: Acervo pessoal.